Bandwidth Considerations in Miniaturized Rectangular Dielectric Resonator Antennas: Experimental Validation

by

Makwana Gautam Durlabhji

(201021005)

A Thesis Submitted in Partial Fulfilment of the Requirements for the Degree

of

Doctor of Philosophy

in

Information and Communication Technology

to

Dhirubhai Ambani Institute of Information and Communication Technology,

Gandhinagar

August 2016

Declaration

This is to certify that

1. the thesis comprises my original work towards the degree of Doctor of Philosophy in Information and Communication Technology at DA-IICT and has not been submitted elsewhere for a degree,

2. due acknowledgment has been made in the text to all other material used.

Signature of Student

Certificate

This is to certify that the thesis work entitled "Bandwidth Considerations in Miniaturized Rectangular Dielectric Resonator Antennas: Experimental Validation" has been carried out by Makwana Gautam Durlabhji (201021005) for the degree of Doctor of Philosophy in Information and Communication Technology at this Institute under our supervision.

Prof. Deepak Ghodgaonkar

(Thesis Supervisor)

Abstract

In this thesis, an issue of bandwidth is considered in a rectangular dielectric resonator antenna (RDRA). Two techniques (merging of modes and stacking) of bandwidth improvement are introduced with miniaturized resonator. Single narrowband in RDRA is also introduced and investigated. Dual narrowband is proposed in a L-shaped DRA. It is compact structure as compared to a conventional DRA structure.

Theoretical analysis of a rectangular DRA is discussed. Resonant modes in the RDRA are presented with field distribution. Dielectric waveguide model (DWM)-mixed magnetic model (MMW) is discussed to predict resonant frequency, impedance bandwidth, and radiation Q-factor of the RDRA for $TE^z_{11\delta}$ mode. Variation of resonant frequency with length, height and depth are studied as a function of relative permittivity of material. Effect of aspect ratios (length/height and depth/height) on resonant frequency is discussed. Expression of impedance bandwidth and radiation Q-factor are discussed as a function of physical parameters of the RDRA. Predicated maximum and minimum impedance bandwidth are discussed for different values of the aspect ratios.

Literature survey on dielectric resonator antenna is carried out for bandwidth improvement as well as single- and dual narrowband. For bandwidth improvement, survey of various methods such as merging of modes, stacking/embedding DRA elements, modified shapes of the DRA, and hybrid DRAs is presented. In the merging of modes of DRA, simple rectangular and cylindrical DRA designs are described. In the stacking/embedding method, two disk DRAs, triangle DRAs and embedded ring-disks DRA designs are presented with their structure and reported performance. Modified shaped of DRAs namely, notched RDRA, truncated tetrahedron DRA, semi trapezoid DRA, flipped staired pyramid DRA, and L-shaped DRA are discussed for bandwidth improvement. Hybrid DRAs, the DRA is attached with other kind of antenna, are discussed for ultra wideband operation. Two different methods of a narrowband DRA designs are reported in literature. Using metallization on surface of the DRA, low-profile single narrowband designs are presented. A narrowband compact DRA designs using high permittivity are discussed. Literatere survey on dual narrowband DRA designs are also discussed.

Two nearby modes of a basic RDRA are merged to obtain wide frequency operation (5.65 GHz to 6.48 GHz) and miniaturization is obtained by using high permittivity material. A simple microstrip line excitation is used at the edge of the RDRA instead of a conventional way of excitation. Due to this novel way of excitation nearby multiple modes are excited to achieve wide bandwidth. The performance of the antenna has been confirmed by measurements of various characteristics and radiation patterns. For compactness, the proposed RDRA is compared and discussed with reported miniaturized DRA designs around 5-6 GHz band.

A design of stacked RDRA is proposed at 5.2 GHz with 13.56 % of bandwidth. A 50 Ω microstrip line is used in the proposed antenna as a feeding mechanism. The proposed stacked RDRA consists of two rectangular slabs of two microwave dielectric materials with dielectric constant of 10 and 32, stacked vertically to obtain improvement in bandwidth as compared to the conventional RDRA. Physical parameters of stacked RDRA have been optimized by extensive simulations using Ansoft HFSS. The parameters of antenna are $17 \times 7 \times 4.56$ mm^3 with a grounded substrate's size: 80×50 mm^2. The prototype is fabricated. Measured and simulated results are both in good agreement. The proposed antenna is suitable for wireless local area networks (WLAN) application in 5 GHz frequency band. This stacked RDRA exceeds the bandwidth requirements for IEEE 802.11a WLAN applications within a 2:1 standing wave ratio (SWR).

In this thesis, a narrowband and compact RDRA is proposed by placing single metal strip on top surface. A new radiating $TE^x_{\delta 10}$ mode is found. To validate the $TE^x_{\delta 10}$ mode and a conventional lowest order $TE^x_{\delta 11}$ mode, simple RDRA with and without a metal strip is designed, fabricated, and measured. The RDRA is mounted on a grounded substrate and fed by a simple microstrip line. Based on parametric study and electric field distributions, dimension along the y-axis is principally used to determine the resonant frequency of the proposed mode. The proposed mode has an impedance bandwidth of 35 MHz at 2.24 GHz and gain of 2.35 dBi. The radiating $TE^x_{\delta 10}$mode has broadside radiation patterns. As compared to the conventional $TE^x_{\delta 11}$ mode, $TE^x_{\delta 10}$ mode give reduction in resonant frequency (58 %) and impedance bandwidth (79 %).

A L-shaped DRA with metallic patch is proposed for dual narrow band operation. A microstrip line is used as a feeding mechanism. The patch is also L-shaped and is placed on inner side or outer side or top side or combination of sides of the antenna. Parametric study is performed on different arm length of patch placed on outer side and inner side of the L-shaped DRA. This study confirms the dual narrow band operation around 2.4 GHz and 5.2 GHz. The proposed antenna is compact, circular polarized, high radiation efficiency and dual narrowband operation.

Acknowledgment

Above all, I pray the Almighty for his kind love to me, which shall bring me through victoriously! Show me the path I have to work on, Lord. Show me the door that I have opened to the enemy. I resist him in the name of Lord, and I command him to leave with all of his oppression and attacks. God, you are the Lord of my life, and I submit to you and will never deny you no matter what happens. Praise God!

This would mean nothing if I don't thank my mother Late Mrs. Vinodiniben D. Makwana who I do know that all your blessing shower on me from the heaven. You will be happy that your cub is completing Ph.D. In my misty remember, I see you teaching me to fight till end for all things that are for truth or progress. This has inspired and this Ph.D. work is result of that. You have taught me to never concede defeat and to always be fair in all that I did. I cherish every second that you spent with me. I just feel sad that you are not around to see me.

Although I never would have been able to complete my Ph.D. without the support of many brilliant people. I would therefore like to offer my sincere thanks to them.

I from the bottom of my heart express my sincere thank to Prof Deepak Ghodgaonkar for his guidance, understanding, patience, and most importantly his mentorship during my Ph.D. at Dhirubhai Ambani Institute of Information and Communication Technology (DA-IICT). His mentorship was paramount in providing a well- rounded experience consistent to my long-term career goals. He encouraged me to grow not only as a Ph.D. scholar, but also as a successful instructor and an independent thinker. His achievements, his work ethics, and his keen eye for every important detail have been an inspiration throughout all the years I worked with him. For everything you have done for me, Prof. Ghodgaonkar, I thank you.

I thank Prof. Sanjeev Gupta for providing me the opportunity to complete my Ph.D. thesis. His support and guidance made my thesis work possible. He has being actively interested to advise at each step in this work. I am very grateful for his patience, moti-

vation, enthusiasm, and immense knowledge taken together, make him a great co-mentor.

I wish to acknowledge all the Professors of DA-IICT who have inspired me directly or indirectly. I am thankful to Prof. Manjunath V. Joshi - the chairman of my synopsis committee, Prof. Sanjeev Gupta, and Prof. Shrinivas Rao Zinka, Prof Anil Roy for their constructive criticisms, comments and suggestions in the improvement of the thesis during my synopsis and RPS. Also, I express my sincere gratitude to Prof. P. Vijaykumar, Prof. Anjan Ghosh, Prof. L. Pilutta for their motivation and support during my comprehensive examination.

I also would like thankful to The Director, The Registrar, The Dean-AP, The Convener-PG, and all other staffs who directly or indirectly helped me throughout my tenure at DA-IICT. I am indebted to administrative and technical staff members of DA-IICT who have been kind enough to advise and help me in their respective roles. My sincere gratitude extends to the staff of resource center of DA-IICT.

I express my sincere sense of gratitude to Prof. K. J. Vinoy (Microwave laboratory, Indian Institute of Science, Bangalore) for all his technical support, valuable inputs and remarks during fabrications and measurements of my Ph.D. work. I am indebted to his help, kind care and understanding during my difficult times I had, in the journey of my work.

I also thank to the anonymous reviewers of our publications and the examiners of my thesis for their constructive comments and suggestions which have greatly improved the level of publications and the thesis, respectively.

I was lucky to make many new friends at DA-IICT, who helped me in many ways during my study. It is not possible to name every colleague and friend separately, so I thank one and all for everything they did good for me.

I express my love and gratitude to my father whose inherited understanding and help led me to where I am. My mother whose compassion and determination helped me to become what I am. Though knowing very little what I am striving for, my 86 years old grandma

always selflessly prayed god to help achieve my goals. I love her for her simplicity and express my respect to her.

And finally, special thanks to my enjoyable children Bansari and Liva, for their sacrifice, endless patience and understanding. They, all kept a magnificent balance between my career, study and family life.

List of Symbols

ϵ_r	Dielectric constant/relative permittivity
λ	Dielectric wavelength
λ_0	Free-space wavelength
Z_L	Impedance of a low permittivity region
Z_0	Impedance of a high permittivity region
Q_u	Unloaded quality (Q)-factor
$\tan\delta$	Dielectric loss tangent/Loss factor
$\bar{E}$	Electric-field intensity
$\bar{n}$	Normal vector
$\bar{H}$	Magnetic-field intensity
f_{r1}	Resonant frequency of 1^{st} order approximation
k_x	Wavenumber along x-axis
k_y	Wavenumber along y-axis
k_z	Wavenumber along z-axis
k_0	Wavenumber in free-space
ϵ_0	Permittivity of free-space
μ_0	Permeability of free-space
H_x	Magnetic field component along x-axis
H_y	Magnetic field component along y-axis
H_z	Magnetic field component along z-axis
E_x	Electric field component along x-axis
E_y	Electric field component along y-axis
E_z	Electric field component along z-axis
δ	Fraction of a half cycle the field variation
f_r	Resonant frequency of the DRA
Q_{rad}	Radiation quality (Q)-facator
S	Standing wave ratio
W_e	Stored energy
P_{rad}	Radiated power

P_m	Magnetic dipole moment
F_L	Lower frequency of bandwidth
F_U	Upper frequency of bandwidth
f_c	Center frequency of bandwidth
Γ	Reflection coefficient
S_{11}	Return loss characteristic
S_{21}	Transmission gain or loss
α	Figure of merit
P_r	Received power of the receiver antenna
P_t	Trasmitted power of the trasmitter antenna
G_r	Gain of the receiver antenna in Watt
G_t	Gain of the trasmitter antenna in Watt
$(G_t)_{dB}$	Gain of the trasmitter antenna in dB
$(G_r)_{dB}$	Gain of the receiver antenna in dB
$(G_{UT})_{dB}$	Gain of the antenna under test in dB
R	Separation between two antenna in meter
$(G_{Horn})_{dB}$	Gain of the horn antenna in dB
$(PL)_{dB}$	Path loss in dB
Θ_1	Half power beam width of E-plane radiation patter in degree
Θ_2	Half power beam width of H-plane radiation patter in degree
η	Radiation efficiency
P	Total power lost
P_{dis}	Dissipated power
Q_{dis}	Dissipated Q-factor
D	Maximum dimension of an antenna
λ_g	Guide wavelength
c	Speed of light
ϵ_{eff}	Effective permittivity
ϵ_s	Dielectric cons
f_{os}	Simulated resonant frequency
f_{oc}	Calculated resonant frequency
f_1	Resonant frequency of TE^y_{111} mode

f_2	Resonant frequency of TE^y_{211} mode
D_0	Directivity

List of Abbreviations

DRA	Dielectric resonator antenna
MPA	Microstrip patch antenna
MIC	Microwave integrated circuit
GSM	Global system for mobile
PCS	Personal computer system
DR	Dielectric resonator
IMT	International mobile telecommunication
UWB	Ultra wideband
RFID	Radio frequency identification
RDRA	Rectangular dielectric resonator antenna
CDRA	Cylindrical dielectric resonator antenna
HDRA	Hemispherical dielectric resonator antenna
MMW	Magnetic mix waveguide model
DWM	Dielectric waveguide model
MoM	Method of moments
FDTD	Finite defference time domain
TE	Transverse electric
TM	Transverse magnetic
BW	Bandwidth
SWR	Standing wave ratio
FCC	Federal communication commission
CPW	Coplanar waveguide
HFSS	High frequency structure simulator
RF	Radio frequency
PEC	Perfect electric conductor
PMC	Perfect magnetic conductor
FEM	Finite element method
PNA	Performance network analyzer
HPBW	Half power beamwidth

DRoP	Dielectric resonator on patch
DRR	Dielectric ring resonator
WLAN	Wireless local area network
PDA	Personal digital assistant
RHCP	Right handed circular polarization
LHCP	Left handed circular polarization
EM	Electromagnetic
EMC	Electromagnetic compability
EMI	Electromagnetic interference
ALPS	Adaptive Lanczos-Pade sweep
PCB	Printed circuit board
IC	Integrated circuit
VNA	Vector network analyzer
PTFE	Poly tetra fluoro ethylene
EDA	Electronic design automation
MATLAB	Matrix laboratory
SPICE	Simulation program for integrated circuit emphasis
UWB	Ultra wideband
SMA	Subminiature version A
MIMO	Multi input multi output
GPS	Global position system
Wi-fi	Wireless fidelity
UHF	Ultra high frequency
ISM	Industrial, scientific & medical radioband
FNBW	First null beamwidth

Contents

List of Figures

List of Tables

Chapter 1

Introduction

Keeping with the market demand, requirements for an antenna design are changing continuously. Today's consumer market demands electronic systems of high efficiency, wide bandwidth and reduced equipment size. Meeting these demands in the RF and wireless domain is a major challenge since it involves design of the antenna to be embedded into wireless products. Most of antennas that are in current use in microwave band and millimeter region cannot be simply scaled up in frequency. Conduction loss in any metal portion of a radiating element does not remain constant after scaling, and as a result, this loss may become too high for system requiring efficient operation [1].

In this thesis, bandwidth is defined as range of frequency at which the impedance of antenna is matched with the feed line. It is called as an impedance bandwidth. The bandwidth is in term of return loss or VSWR (S). % of impedance bandwidth is percentage of the frequency difference (upper frequency, F_U - lower frequency, F_L) over the center frequency of the impedance bandwidth. Where, f_U and f_L are frequency having S = 2 or S_{11} = -10 dB. Center frequency is $(f_U + f_L)/2$.

Over the last decades, two classes of antennas, microstrip patch antennas (MPAs) and dielectric resonator antennas (DRAs), have been under investigation for modern wireless applications. The MPA is made of metallic conductor placed on a grounded substrate. It is a 2-D planar structure. The DRA is made of microwave material placed on a grounded substrate. It is a 3-D structure. As compared to the MPA, the DRA has a much wider impedance bandwidth ($\approx$ 10 % for dielectric constant $\epsilon_r \approx 10$). This is because the

microstrip antenna radiates only through two narrow radiation slots, whereas the DRA radiates from all the faces of the DRA except, the ground part. Avoidance of surface waves is another attractive advantage of the DRA over the MPA. Due to absent of conducting metallic part, the DRA has high radiation efficiency than that of the very popular microstrip antenna. In [2], the radiation efficiency of a cylindrical DRA and circular disk microstrip patch antenna (MPA) is reported at Ka band (at 35 GHz). Both the antenna elements were designed with similar feeding networks (microstrip line) on a RogerTM dielectric substrate with a thickness of 0.254 mm, a dielectric constant of 2.2 and a loss tangent of 0.001. Reported measured % impedance bandwidth (S_{11} < - 10 dB) is 15.6 % and 2.6 % for DRA and MPA, respectively. An intrinsic efficiency of the both antennas is extracted by separating its radiation loss from the losses of the feeding microstrip line, the connector and the test system, which are measured to be 0.1 dB, 0.5 dB and 1.1 respectively. After the above correction, the measured radiation efficiency of the DRA is up to around 95 % at 35.5 GHz, while 78 % at 35.2 GHz for the MPA. In [3], the radiation efficiency is reported around 100 % and 95 % at 4.1 GHz for cylindrical DRA (CDRA) and circular microstrip antenna (CMA), respectively. The both antennas have % bandwidth (VSWR < 2.5) of 2.9 %. Also the radiation efficiency is reported around 100 % and 97 % at 7.0 GHz for CDRA and CMA, respectively. The CDRA has % bandwidth of 5 %, while the CMA has % bandwidth of 4.7 %.The DRA has wider beamwidth as compared to the MPA. [2, 4]

On the other hand, many characteristics of both the antennas are common because they both behave like resonant cavities. For example, the dielectric wavelength (λ) is smaller than the free-space wavelength (λ_0) by a factor of $1/\sqrt{\epsilon_r}$, both of them can be made smaller in size by increasing ϵ_r. Additionally, all excitation methods such as coaxial probes, microstrip lines, coplanar waveguides and apertures that are applicable to the MPA can also be used for the DRA [1, 4].

1.1 Basic Characteristics of the DRA

A dielectric resonator antenna (DRA) structure mainly consists of ground plane, substrate, and dielectric resonator made from a low-loss microwave dielectric material. Basi-

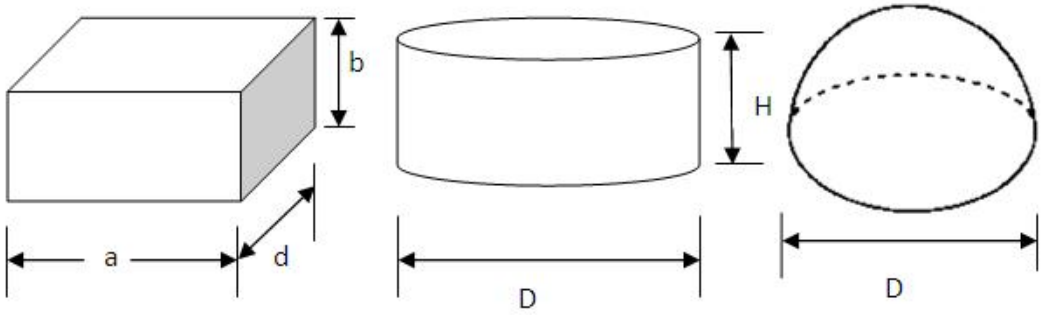

Figure 1.1: Basic shapes of DRAs

cally, hemispherical, cylindrical and rectangular shapes/geometries (shown in Figure 1.1) are available. Alongwith mechanical simplicity, mathematical formulations are easier for them. Resonant frequency of the DRA is fundamentally a function of shape/geometry, dimensions, and relative permittivity. To compare the geometries of the DRA, dimensional degrees of freedom are considered. Tunable dimensions i.e. degrees of freedom for hemispherical, cylindrical, and rectangular shapes are one, two and three, respectively. For example, with a certain material, once the resonant frequency of a hemispherical DRA is found by the radius, everything is fixed, including an impedance bandwidth, radiation efficiency, and other performance parameters. One-dimensional degree of freedom makes the hemispherical DRA easy to design but at the same time it is difficult to optimize for specific performances. It is also difficult to fabricate the shape. As a consequence, the hemispherical DRAs are not popular in practice. In the cylindrical DRA (CDRA), a certain resonant frequency has a number of radius-height (aspect ratio) pairs. It is possible to have a tall or wider cylindrical DRA for a specific resonance frequency with different Q-factor, the impedance bandwidth operation, excited modes, radiation patterns, volume, gain, and directivity. Two-dimensional degrees of freedom in the cylindrical shape provide ability to optimize for particular specifications. The cylindrical and hemispherical DRA can support degenerative modes because of existence of certain symmetry. The degenerative mode is two modes exhibit same resonant frequency, hence interact with each other, which result into a lack of mode purity. This will increase spurious radiations that degrade linear polarization. For dual and circular polarization designs, these degenerative modes are constructive. Moreover, manufacturers of raw dielectric materials are manufactured in form of long rods, so cylindrical DRA can

be easily prepared and fabricated. Because of this, the cylindrical DRA is more popular than the hemispherical/spherical DRA. In rectangular DRA, a resonant frequency is determined by its geometry i.e. length, width and height. The resonant frequency can have a number of length-height and width-height pairs. It may have either a tall or wider or longer rectangular DRA for a particular resonance frequency. These antennas have different performance in respect to Q-factor, the impedance bandwidth, resonant modes, radiation pattern, volume, gain and directivity. Three-dimensional degrees of freedom in rectangular DRAs give more design of flexibility. Degenerative modes in RDRA can be avoided by properly choosing the aspect ratios (length/height and width/height). It is easy to fabricate from raw dielectric material. Due to these, The rectangular DRA is more popular and better choice other than cylindrical and hemispherical shapes [5, 6].

The impedance bandwidth is a function of the material's relative permittivity and aspect-ratios. For lower relative permittivity, the bandwidth is high and also size is large. Narrow bandwidth can be obtained with high dielectric constant and compact in size. It shows tradeoff between the impedance bandwidth and volume. There is no straight forward relationship between the bandwidth and aspect ratios. By choosing the proper aspect ratios, the Q-factor can be controlled and hence the impedance bandwidth. [7, 8]

Relative permittivity of the order of 8 to 100 gives additional degree of freedom. By this, researchers can have control over physical size and bandwidth. The materials used for the DRA are poly tetra fluoro ethylene (PTFE), barium titanate, magnesium titanate, zirconium titanate, lithium ferrite, and solid state solutions of combination of magnesium, calcium, silicon and titanium oxides [5, 9].

There is no metallic part in dielectric resonators. So, high radiation efficiency (≥ 95 %) is a major merit of DRAs. Especially, at high frequency millimeter wave applications, DRA is an attractive candidate as compared to the popular MPA. As compared to the MPA, no surface waves are exhibited in DRA and hence, spurious radiations are less. DRAs have a high dielectric strength and therefore a higher power handling capacity. DRA can operate in a wide temperature range due to the temperature-stable ceramics (order of tolerance: $\pm$ 0.5; $\pm$ 1.0; $\pm$ 2.0 $ppm/^{\circ}$ C). Several feeding mechanisms (including aperture

slots, coaxial probes, microstrip transmission line, dielectric image guide, and coplanar waveguide lines) are suitable for efficient coupling of DRA. The DRA can be excited in various modes, many of which have radiated pattern similar to short electric or magnetic dipoles, resulting with broadside or directional patterns for different structures [5,9].

In general, the DRA is operated in its fundamental boreside or endfire mode. The broadside DRA radiates like a magnetic dipole with its maximum radiation fields being normal to the ground plane. The endfire DRA radiates like an electric monopole. This mode can be excited by axially feeding the DRA with a coaxial probe. Theoretically, its radiated E-field is maximum along the ground plane direction, but practically it has a titling angle due to a finite ground plane effect. However, only fundamental broadside modes are considered in most of research [10].

These versatile characteristics, make the DRAs to be used in numerous applications in wireless systems because of freedom of the design parameters. Many techniques are available for enhancing antenna performances with regard to radiation patterns, impedance bandwidth, gain, directivity, and compactness. Some of techniques are discussed in chapter 2.

1.2 Challenges

For a given resonant frequency, the dimensions of isolated dielectric resonator antenna (DRA) and material's dielectric constant ϵ_r are closely related. Employing a high relative permittivity material, the dimension can be reduced to the order of $\lambda_0/\sqrt{\epsilon_r}$. The drawback however is increase of Q-factor and as a consequence reduction in bandwidth. For examples, in global system of mobile communication (GSM) and personal communication system (PCS) system, the antenna should be compact and with higher bandwidth. For example at 900 MHz, the cylindrical DRA with dielectric constant, ϵ_r, of 12 will have dimension of 68 mm radius, 34 mm height with 13.8 % bandwidth. An isolated rectangular DRA will have dimension of $72 \times 72 \times 54$ mm^3 for the same frequency and dielectric constant with 8.4 % of bandwidth. At 1800 MHz, the dimensions are almost reduced to half and volume is reduced by a factor of eight with the same % of bandwidth.

However, at these frequencies, the dimensions of DRAs are generally too large to be used in the systems. To achieve the same bandwidth in rectangular DRA, i.e. 8.4 % at 900 MHz, dimension will be $25 \times 100 \times 12$ mm^3 for the dielectric constant of 48. A reduction of 10 % in volume can be achieved by increasing the dielectric constant by four times [6,9].

A simple technique to further reduce the volume is to put DRA on a large ground plane so that it acts as image plane. This will reduce the dimension to half that is normal to the ground plane, thus further reducing the volume by a factor of two. At 900 MHz, the dimensions of the rectangular DRA become $72 \times 72 \times 27$ mm^3. This scheme can only be applied when the ground plane does not violate boundary conditions of modes. Even with this technique, the dimensions are too large to be used in the systems. There is need to improve the design methodology for miniaturized and wideband DRAs.

The resonant frequency of the DRA is predominantly a function of size, shapes, material permittivity, modes, and feeding mechanisms. The impedance bandwidth is a function of aspect ratio and the material permittivity. To obtain specific requirements such as the impedance bandwidth and resonant frequency, there should be more number of degrees of freedom. For researchers, it is a challenge to obtain closed form formula for design of the DRAs. [5, 9]

In reported designs of the various DRAs in literature, most of the proposed schemes are based on experimental studies. These studies are based on trials and errors. There is lack of closed form formulas for designs of the DRAs due to complicated structures and more degrees of freedom.

During fabrication of the DRA structures, there is probability of air-gaps between the dielectric bodies and metal bodies. These kinds of fabrication-imperfections will cause deviation in performance of the antennas. The deviation becomes more severe when miniaturized DRA operate at very high frequency or using high dielectric constant materials. Some methods are already suggested in literature to nullify these effects. But it is not possible to apply these methods to all kind of designs. [11]

Another main challenge is to develop DRAs on silicon based IC surface in the form of microwave integrated circuits (MICs). Without success of this, researchers cannot use DRA for wireless applications [12].

1.3 Historical Developments of DRAs

Ritchmyer in 1939 [13] used the term "dielectric resonator (DR)" for the first time and showed that a block of dielectric material having very high dielectric constant resonates in free space and exhibits radiation damping. He claimed that the dielectric object behaves as a resonating cavity. However, his theoretical investigations failed to generate significant interest in researches and remain unattended experimentally over 25 years due to lack of revolution in dielectric materials. In the early of 1960s, Okaya and Barash [14] reported the DR in the form of crystal developed from low-loss ceramics. At that time, the DRs were often enclosed in metal cavities to prevent radiation and to maintain a high Q-factor, critical for filter or oscillator designs. A breakthrough in the dielectric material occurred during in 1975s, when Van Bladel [15] reported detailed theory on evaluation of modes in DRs.

In 1983s, the first use of DR as a radiator was reported by Long et al,. DR is excite in certain modes with no shielding and work as an efficient radiators instead of an energy storage device. This concept led to the exploration of DRs as antennas known as dielectric resonator antenna (DRA). Long et al examined the characteristics of DRAs of hemispherical, cylindrical and rectangular shapes [7, 8]. Their work demonstrated that the DRAs could be an attractive alternative of low-gain antennas. A linear array of DRAs fed by a dielectric image guide [16] and a planar array of circular-polarized DRAs [17] were examined during this decade. In early 1990s, the research was focused on analyzing the various radiating modes of various basic shapes of DRAs with a various feeding schemes, and applying analytical and numerical techniques were applied to determine the input impedance, Q-factor, coupling, and radiation patterns. These investigations were summarized in a much-cited paper published in 1994 by Mongia and Bhartia [6]. In this paper, they proposed standardized nomenclature of the modes, with a set of equations for predicting the resonant frequency and Q-factor of rectangular DRAs with various feeding

schemes.

By the late 1990s, linear and planar arrays of DRAs were reported from two-element arrays to 300 elements phased arrays [18–21]. Also during this period, low-profile [22] and compact designs [23], mutual coupling analysis of array elements [24], circular polarized DRAs [25], multi-band and wideband designs [26, 27], tunable DRAs [28], and beginning of hybrid designs [29] were reported.

By the early to late 2000s and 2010s, research continued in the field of miniaturization techniques, low-profile designs, dual and circular polarized designs, bandwidth improvement techniques, and multi-band designs. New developments of enhanced gain techniques, finite-ground-effects, tunable DRAs, ultra-wideband designs, and dual-function DRA designs were introduced. Much of work include experimental study of new shapes of DRAs such as conical, tetrahedral, hexagonal, pyramidal, elliptical, stair-stepped shapes with various feeding methods. Also there was focus on designs of DRAs for specific applications into mobile handsets for personal computer system (PCS), international mobile telecommunication (IMT)-2000, wireless local area network (WLAN), and ultra wideband (UWB) applications. DRAs were also reported in radar applications, breast-cancer imaging, and radio frequency identification (RFID) systems. Techniques for improving DRA array manufacturing, integrations in systems, and packaging techniques were studied. Up to 2010s, the focus was on improvement of one of the performance parameters such as bandwidth, miniaturization, radiation patterns, gain, multi-bands, input impedance, and efficient couplings. It was accomplished with combinations of shapes, size, dielectric material, feeding mechanisms, and structure around the DRAs [11, 19].

Nowadays, main focus of research on DRAs is improvements in two or more of the performance parameters in a design structures, and theoretical analysis of various DRAs. To date, published frequency: lowest - 55 MHz [30] and highest - 94 GHz [31] for which DRAs have been design and fabricated. The smallest physical DRA with radius of 0.33 mm; height of 0.30 mm [32] whereas, the largest physical DRA with radius of 275 mm; height of 200 mm [30] were reported. The lowest profile of rectangular DRA with height of $0.026\lambda_0$ was demonstrated [33].

These developments of dielectric resonator antennas show that there are many untouched area such as aspect of theoretical as well as improvement in performance parameters.

1.4 Motivation

The modern trends in communication and wireless systems are to integrate different modules into a system. There is a need for miniaturization of every component to the possible extent of the system. In the system, an antenna is an important component for communication. Physical size of the antenna is depending on the operating frequency. At lower frequencies, due to the physical size of antenna, integration of the antenna into a package is not easy. As antenna gets electrically small, it will be constrained by narrow bandwidth, lower radiation efficiency, and low gain [34]. Main focus of this thesis is to propose miniaturized, wideband, and highly efficient antennas.

Long et al., demonstrated in 1983 that dielectric resonators made of low permittivity materials ($8 \leq \epsilon_{\mathrm{r}} \leq 20$) placed in open environment exhibit small radiation Q-factor if excited in their lower order modes [7,8]. The high radiation losses of these resonators make them useful particularly as radiating elements, especially in high-frequency applications where ohmic losses are a serious problem for the conventional microstrip antennas. Apart from their low dissipation loss and the subsequent high radiation efficiency, dielectric resonators offer many other attractive features, such as good mechanical and temperature stability, compatibility with microwave integrated circuits (MICs), small size and weight due to the scaling of the DR dimensions with the relative permittivity. Also, the DRs have versatility in terms of their shape, feeding mechanism, efficient control on excited modes, polarization, and radiation patterns.

DRAs have been investigated since 1983 [13], it has received more attention only in the last 15 years. This is mainly due to three reasons. (1) The fabrication cost was too high as compared to the metallic antennas, (2) the unavailability of dielectric materials having a relative permittivity, ϵ_r, from 10 to 100 with low dielectric losses, and (3) lack of theoretical analysis of various shapes, with variety of feeding mechanisms [5, 9–11].

Nowadays, wide range of inexpensive and low-loss dielectric materials is available because of progress in material science. This prompted the antennas researchers to show interest in the DRAs. In spite of these, ongoing research in DRAs is still largely unexplored, and immature.

1.5 Contributions of the Thesis

Objectives of the thesis "Bandwidth Considerations in Miniaturized Rectangular Dielectric Resonator Antenna: Experimental Validation" is to deal with two different aspects of bandwidth: wideband and narrowband. Two DRAs are proposed for bandwidth improvement (wideband) and two DRAs are introduced for narrowband frequency operation. All four DRAs result in miniaturized antennas.

- The first DRA is to excite two nearby modes of a simple rectangular DRA with a simple and novel way of excitation using microstrip line. It is claimed that the proposed scheme has a wider bandwidth (5.65 GHz to 6.48 GHz) and miniaturized as compared to the reported designs of conventional RDRA.

- The second DRA of bandwidth improvement is studied using stacking of two different dielectric materials in a rectangular shape. A design of the stacked RDRA is proposed at 5.2 GHz with 13.6 % impedance bandwidth. Results show that the proposed design has improvement in bandwidth as compared to a usual RDRA at 5.2 GHz.

- A narrowband operation can be achieved by using dielectric material of high permittivity. Here, the narrowband is proposed by placing a metallic conducting patch on the surface of the rectangular DRA. By using the metallic patch, a new radiating $TE^{x}_{\delta 10}$ mode is observed in RDRA. The proposed antenna is resonated at 2.24 GHz with 35 MHz (1.2 %) impedance bandwidth. The antenna is a miniaturized as compared to the conventional RDRA at the same resonant frequency.

- Dual narrowband is investigated in a L-shaped DRA. The proposed antenna uses a metallic patch on the surface of the L-shaped DRA. It is optimized at 2.4 GHz and 5.2 GHz with 1 % impedance bandwidth for both bands. It is compared with reported dual band DRA designs and claimed to be miniaturized.

In this study, Ansoft High Frequency Structure Simulator (HFSS) tool, as described in Appendix A, is used to perform parametric study. Return loss characteristics, resonant frequency, 10- dB impedance bandwidth, radiation patterns, gain, and directivity are initially observed based on the simulation study. Based on the study, physical parameters of the proposed RDRA are optimized. Due to unavailable sample for the proposed dual narrowband L-shaped DRA, the antenna is not validated experimentally. Other three proposed DRAs are validated experimentally and compared with simulated results.

1.6 Organization of the Thesis

Six chapters of the thesis are organized as below:

Chapter 2 presents basic theory of a rectangular DRA. The operation and properties of the RDRA are presented. Its resonating modes, models to determine of its resonance frequencies and radiated Q-factor are examined. Parametric studies on length, depth, height, and dielectric constant are presented. For the given RDRA, allowable minimum and maximum limit of impedance bandwidth are discussed. Literature survey of existing DRA designs for bandwidth improvement as well as single- and dual narrowband is presented and discussed. Important characteristics of the reported DRA designs such as range of frequency, bandwidth, dielectric constant, volume, type of DRA shapes and feeding techniques, and size are compared. Also design procedure is discussed.

In chapter 3, a technique is introduced for bandwidth improvement. Using simple and novel way of excitation by a microstrip line, nearby multiple modes are excited for wideband operation in a RDRA. The parametric study is presented on different dimensions of the RDRA. For validation, field distributions are presented. Theoretical analysis of excitation of dual modes is introduced. Experimental results are compared and discussed with simulated results. Reported DRA designs are compared with the proposed work for miniaturized and wideband rectangular DRA.

Chapter 4 demonstrates another technique of bandwidth improvement. A stacked rectangular DRA made from two different dielectric materials is proposed. Parametric study

is performed and optimized parameters at 5.2 GHz are obtained. The prototype is fabricated and results are compared with simulated one.

In Chapter 5, a new radiating $TE^{x}_{\delta 10}$ mode with a narrow band is investigated in a rectangular DRA. Parametric study on dimensions of the antenna is presented and discussed. Field distributions and theoretical analysis are presented. The experimental results of the new mode and a conventional mode are presented and compared with simulated results.

Chapter 6 introduces a new technique for dual narrowband operation. A L-shaped DRA is operated at 2.4 GHz and 5.2 GHz. Simulated parametric studies are presented and discussed. Comparison is presented with existing multiband DRA designs.

Finally, Chapter 7 includes conclusions of the thesis. It also provides directions of possible future work in this research area.

References

[1] R. Garg, P. Bhartia, I. Bahl, A. Ittipiboon, "Microstrip Antenna Design Handbook", *Artech House*, 2001.

[2] Q. Lai, G. Almpanis, C. Fumeaux, "Comparison of the radiation efficiency for the dielectric resonator antenna and the microstrip antenna at Ka band", *IEEE Transactions on Antennas and Propagation*, Vol. 56, No. 11, pp. 3589-3592 Nov. 2008.

[3] G. Drossos, Z. Wu, and L.E. Davis, "A comparative study of circular microstrip and cylindrical dielectric resonator antennas", *Proceeding of* 10^{th} *IEEE International Conference on Antenna and Propagation*, No. 436, April, 1997.

[4] Y.M.M. Antar, "Antennas for wireless communication: recent advances using dielectric resonators", *IET Circuits Devices System*, Vol. 2, No. 1, pp. 133-138, 2008.

[5] K. M. Luk and K.W. Leung, "Dielectric resonator antenna", *Research Studies Press,Baldock, England*, 2003.

[6] R. K. Mongia, A. Ittipiboon, "Theoretical and experimental investigation on rectangular dielectric resonator antennas",*IEEE Transactions on Antennas and Propagation*, Vol. 45, No. 9, pp. 1348-1356,1997.

[7] S.A. Long, M.W. McAllister, and L.C. Shen, "Rectangular dielectric resonator antenna," *IEEE Electronics Letters*, Vol.19, pp. 218-219,1983.

[8] S.A. Long, M.W. McAllister, and L.C. Shen. "The resonant cylindrical dielectric cavity antenna", *IEEE Transactions on Antennas and Propagation*,Vol. 31, No. 3, pp. 406-412, March 1983.

[9] Petosa A., "Dielectric Resonator Antenna Handbook", *Artech House*, 2007.

[10] K.W. Leung, E. H. Lim, and X.S. Fang "Dielectric resonator antennas: from the basic to the aesthetic"', *Proceeding of the IEE*, Vol. 100, No. 7, pp. 2181-2193, July 2012.

[11] A Petosa, A. Ittipiboon, "Dielectric resonator antennas: A historical review and the current state of the art", *IEEE Antennas and Propagation Magazine*, Vol. 52, No. 5, pp. 91-116, Oct. 2010.

[12] J.Oh, T. Baek, D. Shin, J Rhe and S. Nam,"60-GHz CPW fed dielectric-resonator-above-patch (DRAP) Antenna for broadband WLAN applications using micromachining technology", *Microwave and Optical Technology Letters*, Vol. 49, No. 8. pp. 1859-1861, August, 2007.

[13] R.D. Richtmyer, "'Dielectric resonators"', *Journal of Applied Physics*, Vol. 11, pp. 391-398, June 1939.

[14] A. Okaya, L.F. Barash,"The dielectric microwave resonator", *Proceeding of the IRE*, Vol. 50, pp. 2081-2092, Oct. 1962.

[15] J. Van Bladel, "On the resonances of a dielectric resonator of very high permittivity"', *IEEE Transactions on Microwave Theory and Techniques*, Vol. 23, No. 2, pp. 199-208, 1975.

[16] M.T. Birand, R.V. Gelsthrope, "Experimental milimetric array using dielectric radiators fed by means of dielectric waveguide", *IEEE Electronics Letters* , Vol. 17, No. 18, pp. 633-635, Sept. 1985.

[17] M. Haneishi, H. Takazawa, "Broadband circularly polarized planar array composed of a pair of dielectric resonator antennas", *IEEE Electronics Letters*, Vol. 21. No. 10,pp. 437-438, May 1985.

[18] G.D. Loos,Y.M.M. Antar,"A new aperture-coupled rectangular dielectric resonator antenna array", *Microwave and Optical Technology Letter*, Vol. 7, No.14, pp. 642-644, Oct. 1994.

[19] A. Petosa, R.K.Mongia, A. Ittipiboon, and J.S. Wight, "Design of microstrip-fed series array of dielectric resonator antennas", *IEEE Electronics Letters*, Vol. 31, No. 16, pp. 1306-1307, August 1995.

[20] A. Petosa, R. Larose, A. Ittipiboon, M. Cuhaci, "Active phased array of dielectric resonator Antennas", *Proceeding of IEEE International Symposium on Antennas and Propagation*, June 1997, Montreal, Canada, pp. 690-693.

[21] M. Haneshi, B. Wu, "Array antenna composed of circularly polarized dielectric resonator antennas", *Proceeding of IEEE Antenna and Propagation Symposium Digest*, Orlando, FL, 1999, pp. 252-255.

[22] K.W. Leung, K. M. Luk, E.K.N. Yung, and S. Lai, "Characteristics of a low-profile circular DR antenna with very high permittivity", *IEEE Electronics Letters*, Vol. 31, No. 6, pp. 417-418, Nov. 1995.

[23] R. K. Mongia, "Small electric monopole mode dielectric resonator antenna", *IEEE Electronics Letters*, Vol.32, No. 11, pp.947-949, May 1996.

[24] Y. X. Guo, K. M. Luk, and K.W. Leung, "Mutual coupling between millimeter-wave dielectric antennas", *IEEE Microwave Theory and Techniques*, Vol. 47, No. 11, pp. 2164-2166, Nov. 1999.

[25] R.K.Mongia, A. Ittipiboon, M.Cuhaci, and D. Roscoc, "Circularly polarized dielectric resonator antenna", *IEEE Electronics Letters*, Vol. 30, No. 17, pp. 1361-1362, Aug. 1994.

[26] S. M. Shun, K. K. Luk, "Stacked annual ring dielectric resonator antenna excited by axi-symmetric coaxial probe", *IEEE Transactions on Antennas and Propagation*, Vol. 43, No. 8, pp. 889-892, Aug. 1995.

[27] Z. Fan and Y.M.M. Antar, "Slot-coupled DR antenna for dual-frequency operation"', *IEEE Transactions on Antennas and Propagation*, Vol. 45, No. 2, pp. 306-308, Feb. 1997.

[28] Z. Li, C.Wu, J. Litva, "Adjustable frequency dielectric resonator antenna", *IEEE Electronics Letters*, Vol. 32, No. 7, pp. 606-607, Feb. 1996.

[29] E. K. N. Yung, W. S. S. Lee, and K. M. Luk, "Microstrip antenna top-loaded by a dielectric resonator", *Microwave and Optical Technology Letters*, Vol. 7, No. 2, pp. 55-57, Feb. 1994.

[30] S.P. Kingsley and S. G. O'Keefe,"Beam steering and monopulse processing of probe-fed dielectric resonator antennas", *Proceeding of IEEE Radar Sonar and Navigation*, No. 3, pp. 121-125, 1999.

[31] J. Svedin, L.G. Huss, D. Karlen, P. Enoksson, and C. Rusu, "A micro machined 94 GHz dielectric resonator antenna for focal plane array applications", *Proceeding of IEEE International Microwave Symposium*, Honolulu, Hawaii, USA, pp. 1375-1378, June 2007.

[32] P.V. Bijumon, A. P. Freundorfer, M. Sayer, and Y. M. M. Antar, "On-chip silicon integrated cylindrical dielectric resonator antennas for millimeter wave applications", *Proceeding of International Symposium on Signals, Systems and Electronics ISSSE-2007*, Montreal, pp. 489-492, 2007.

[33] R.K.Mongia, "Reduced size metalized dielectric resonator antennas", *Proceeding of IEEE International Symposium on Antennas and Propagation*, Montreal, Canada, pp. 2202-2205, June 1997.

[34] C.A. Balanis, "Antenna Theory: Analysis and Design", Second edition, *John Wiley and Son, Inc., New York*, 1982.

Chapter 2

Theory and Literature Survey of Rectangular Dielectric Resonator Antenna

A dielectric resonator antenna (DRA) in rectangular cross-section (which will be called simply a rectangular dielectric resonator antenna - RDRA) is characterized by height b, depth d, length a, and dielectric constant ϵ_r. The rectangular shape offers a two degree of freedom (one more than the cylindrical and two more than the hemispherical DRA), making it the most versatile of the basic shapes. There is a greater amount of flexibility in designing of the RDRA to achieve desired profile and bandwidth characteristics for a given resonant frequency and dielectric constant, since two of the three physical dimensions can be chosen independently. Thus, either a tall and slender or a thin and wide RDRA can be selected, depending on a specific requirement of an application. A choice of aspect ratio has an impact on the radiation Q-factor, which allows greater design flexibility [1]. The choice of three dimensions of RDRA can be made to ensure that the resonant frequencies of the modes are separated apart from each other. Thus, the rectangular DRA need not suffer from the mode degeneracy problem exhibited by other shapes [2] . Comparision of resonance frequency and impedance bandwidth between rectangular, cylindrical and hemispherical DRAs at the same volume for different dielectric constants is discussed in [3]. The resonant frequency of the RDRA and hemisphrical DRA (HDRA) are the highest and lowest among the three cases, respectively, whereas that of the CDRA

lie between the two. The impedance bandwidth of the RDRA and HDRA are the widest and narrowest among the three cases, respectivley.

In this chapter, theoretical analysis of the rectangular dielectric resonator antenna is described. In this thesis, mixed magnetic wall (MMW) model-dielectric waveguide model (DWM), Fang & Leung Model are discussed. Based on DWM-MMW model, theoretical study of resonant frequency, Q-factor, and impedance bandwidth on various parameters of the RDRA such as length, depth, height, and dielectric constant is described. In section 2.2, the literature survey of wideband DRA is carried out with all possible techniques for bandwidth improvement. In section 2.3, single- and dual- narrowband DRA designs are discussed with their characteristics.

2.1 Theoretical Analysis of a Rectangular DRA

Dielectric resonators (DRs) made of low loss dielectric material, with relative permittivity in the range of 10 to 100 and loss tangent ($\tan\delta$) around 10^{-4}, have been widely used in shielded microwave circuits, such as in oscillators and filters. In such applications, DRs exhibit a very high unloaded Q-factor given as $Q_u = 1/\tan\delta$. However, if a DR is placed in an open environment, there is loss due to radiation and reduction in Q-factor. This fact makes dielectric resonator useful as an antenna element. One of the features of a dielectric resonator antenna (DRA) is that it is available in number of simple shapes. The most common shapes are circular and rectangular. The rectangular shape is the most versatile since it has two degrees of freedom as described in chapter 1. An analytical closed-form solution for all shapes is not available. Various numerical techniques such as method of moments (MoM) and finite difference time domain (FDTD) method can be used for analysis of DRAs. But these techniques are time consuming, memory intensive, and not amenable to design or optimization [4,5]. For design of the DRAs, several models, namely, MMW-DWM, Marcatili model [6], Know & Toulio's model [7] have been developed to estimate resonant frequency (f_r) and Q-factor [8, 9].

2.1.1 Resonant Modes for a RDRA

All resonators have a series of resonant modes or field structures, which are determined by their electrical characteristics and boundary conditions. The modes of a spherical DRA are of transverse electric (TE) or transverse magnetic (TM) modes [9], whereas the modes of cylindrical DRA are of TE, TM, or hybrid type [10]. Figure 2.1 shows an isolated RDRA and characterized by length a, depth d, height b and dielectric constant ϵ_r. Unlike spherical or cylindrical DRAs', no rigorous classification of modes of the RDRA exists.

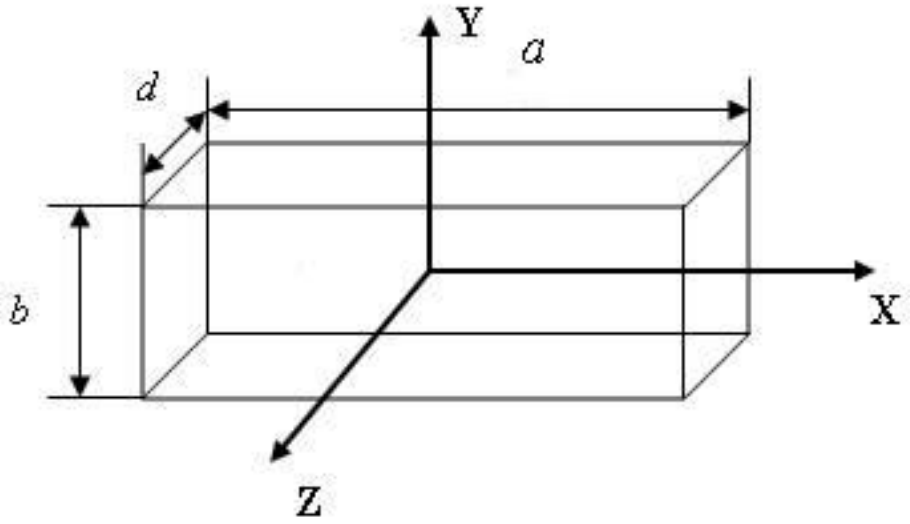

Figure 2.1: Isolated rectangular dielectric resonator antenna

Van Bladel has given a general classification of the resonant modes of an arbitrarily shaped dielectric resonator made of a high permittivity material [11,12]. According to Van Bladel, modes of a DR can be a confined or nonconfined type. For both confined and nonconfined modes, the following condition should be satisfied at all the interfaces/surfaces of the resonator.

$$\bar{E} \bullet \hat{n} = 0 \tag{2.1}$$

Where, $\bar{E}$ denotes the electric-field intensity and $\hat{n}$ denotes the normal vector to the surface of the resonator. This condition states that there is no electric field intensity

normal to the boundary. For a magnetic wall, following condition should be satisfied.

$$\hat{n} \times \bar{H} = 0 \tag{2.2}$$

where, $\bar{H}$ denotes the magnetic field intensity. Equation (2.2) is not necessarily satisfied at all the surfaces of the DR by all the modes. The modes of a DR which satisfy both conditions (2.1 and 2.2) are known as confined modes (e.g TM mode of a cylindrical DR), while those which satisfy equation (2.1) only are known as nonconfined modes. A lowest order nonconfined and confined mode is radiated like magnetic and electric dipole, respectively. It has also shown that confined modes can be supported by dielectric bodies of revolution such as sphere and cylinder (exhibiting axial-symmetric properties) [11]. Since a rectangular DR is not a body of revolution, it supports only nonconfined modes. These modes or field structures are classified as E and H modes (as per the Van Bladel's nomenclature for modes). The E modes, are confined modes, do not have large magnetic fields and the lowest order mode resemble an electric dipole. The H modes, corresponding to the nonconfined mode, have a large magnetic field perpendicular to the interface, with the lowest order mode resembling a magnetic dipole structure shown in Figure 2.2.

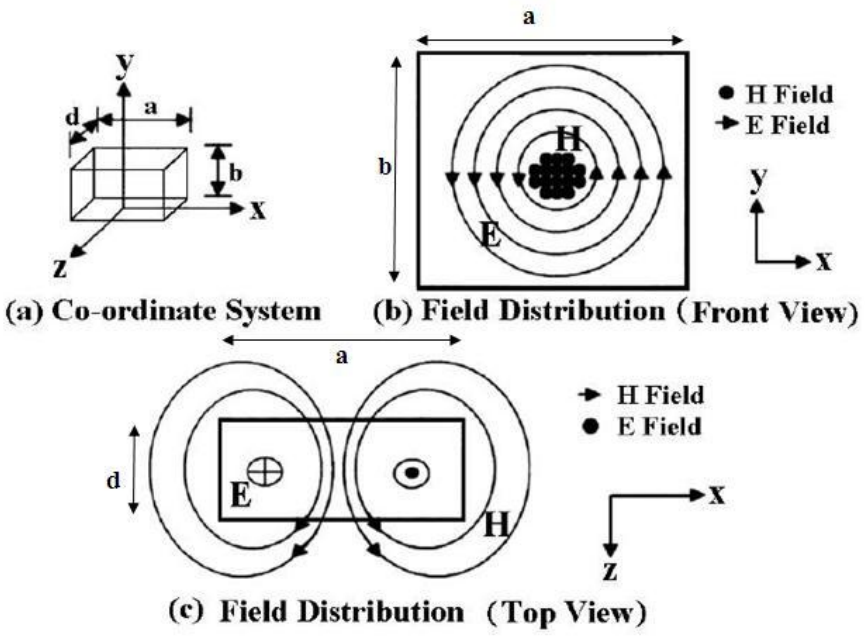

Figure 2.2: The internal E and H fields distribution of H modes

Okaya and Barash provided an approximate but simple analysis of a rectangular DR [13]. They suggested that modes of the rectangular DR can be divided into two types: TE and TM. They first classified the H mode to the transverse magnetic (TM) mode and the E mode to the transverse electric (TE) mode. However, later work by Yee [14] used the opposite notation. This convention (i.e. H mode to TE and E mode to TM) continues to be used nowadays, with two or three subscripts to identify the specific mode order. The subscripts denote the field variations in the appropriate orthogonal component, depending on the coordinate system employed. Extensive experiments showed that not all the modes in the rectangular DRAs predicted by Okaya and Barash's analysis are observed [15]. When the dielectric waveguide model (DWM) is used to find the lowest order TM modes in the rectangular DRA [15], it is found that they do not satisfy (2.1). The existence of TM modes in the RDRAs, therefore, appears to be doubtful. On the other hand, the existence of lower order TE modes is confirmed [16], and also satisfied the condition of nonconfined modes. Therefore, in this chapter, only TE modes in the rectangular DRAs will be discussed. The rectangular DRA can support TE^x, TE^y and TE^z modes which are typically radiate like short magnetic dipoles in the x-, y-, and z-directions, respectively. In TE^z mode, the RDRA is considered as a waveguide which is truncated along the z-direction at $\pm d/2$ with magnetic walls [2]. Wave is propagated along the z-direction. The standing waves inside the RDRA are formed in x- and y- directions, while the fields outside the RDRA are exponentially decayed along the z-directions. The lowest order modes are $TE^x_{\delta 11}$, $TE^y_{1\delta 1}$ and $TE^z_{11\delta}$ for a > b > d, where the subscripts represent the field variation in the x-, y-, and z-directions, respectively, as defined in Figure 2.1. If it is assumed that smallest dimension of the RDRA is in the z-direction (i.e. a, b > d), then a dominant lowest order mode will be $TE^z_{11\delta}$ mode. Where, δ is fraction of half cycle field variation. The subscript, 1, indicates a half cycle variation of the field variation.

2.1.2 Dielectric Waveguide Model-Mixed Magnetic Wall Model

An analytic model of the rectangular DRA can design the antenna without costly and tedious experimental iterations and simulations. It may allow the researcher to discover physical interpretation of the RDRA's operation. With the analysis models, designers should be able to predict the antenna performance parameters such as the resonant fre-

quency, bandwidth, input impedance, radiation patterns and radiation efficiency. The rectangular DRA generally has a three-dimensional radiating dielectric structure on a finite ground plane and categorized as a three-dimensional planar and/or nonplanar structure for analysis purpose. There are various analysis methods available for the RDRAs.

The RDRA has six end surfaces (high relative permittivity to air interfaces). Based on boundary conditions on the these surfaces, there are two approximation methods, namely, first order and second order approximation, are used to predict the resonant frequncy of the RDRA [13]. The first-order approximation is the method where all available six surfaces of the RDRA have perfect magnetic conductor (PMC) [1] boundary conditions. By applying the condition (2.1) on the six surfaces, the resonant frequency can be determined. The resonant frequency is denoted by f_{r1}. Where, k_x, k_y, and k_z are wave numbers in x-, y-, and z-axis, respectively. k_0 is the free-space wave number. The resonant frequency f_{r1} for 1^{st} order approximation can be found from following equations.

$$f_{r1} = \frac{1}{2\pi\sqrt{\mu_0\epsilon_0\epsilon_r}}\sqrt{k_x^2 + k_y^2 + k_z^2} \tag{2.3}$$

Seperation equation is

$$k_x^2 + k_y^2 + k_z^2 = \epsilon_r k_0^2 \tag{2.4}$$

where,

$$k_x = \frac{m\pi}{a}, m = 1, 2, 3, ... \qquad k_y = \frac{n\pi}{b}, n = 1, 2, 3, ... \qquad k_z = \frac{p\pi}{d}, p = 1, 2, 3, ... \tag{2.5}$$

The second order approximation in which four side walls are to be considered as PMC and the other two opposite end walls are to be considered as imperfect magnetic conductor boundaries. The continuity of the magnetic field intensity is used to perform the matching of tangential components across the imperfect interfaces. While, the condition (2.1) is

[1]Perfect Magnetic Conductor (PMC):The intrinsic impedance of the material is inversely proportional to square root of dielectric constant. In region of high permittivity, the impedance is very low. In transmission line theory, the reflection coefficient is given by $\left[\frac{Z_L - Z_0}{Z_L + Z_0}\right]$. For a wave travelling from high permittivity (DRA) to low permittivity region (air), Z_0 (impedance of high permittivity region) is much smaller than Z_L (impedance of low permittivity region). Thus, the reflection coefficient approaches 1. This is close to open circuit, thus the surfaces (interface of high permittivity to air) is to be a perfect magnetic conductor (PMC) [17].

applied on four perfect interfaces. This approximation is now commonly referred to as the mixed magnetic wall (MMW) model. The MMW is based on Okaya and Barash [13] work in 1968. This is the first model to deal with the dielectric waveguide.

Resonant Frequency of the RDRA

An approximate theory is given for predicting resonant frequencies of the RDRA made of a section of an infinite rectangular dielectric waveguide. In a typical design, one first computes guide wavelength, λ_g, of an infinitely long dielectric waveguide by using an approximate analysis such as the one developed by Marcatili [6] and then the resonant frequency is computed by assuming the end surfaces of the resonator are magnetic walls [18]. Guillon and Garault [19] were the first to calculate the resonant frequency of the analogous $TE_{11\delta}$ mode. The dielectric waveguide model (DWM) was used by Itoh and Rudokas [20] on the circular cross section DR. An isolated RDRA in free space (length (a), depth (d), and height (b)) shown in Figure 2.3 (b) or RDRA (length (a), height (h=b/2), and depth (d)) with a finite ground plane shown in Figure 2.4 is considered for modeling. Initially, it can be assumed that the RDRA is a truncated section of an infinite dielectric waveguide (as shown in Figure 2.3 (a)) having transverse dimensions same as those of the RDRA. It is assumed that wave is propagating along the z-direction in the waveguide. The RDRA is considered as waveguide which is truncated along the z direction at $\pm d/2$.

It is assumed that the smallest dimension of the RDRA is in the z direction, then the dominant lowest order mode will be $TE^z_{11\delta}$ mode (a, b > d). Using the DWM, leads to following fields within the DRA [1, 21].

$$H_z = \frac{(k_x^2 + k_y^2)}{j\omega\mu_0} \cos(k_x x) \cos(k_y y) \cos(k_z z) \tag{2.6}$$

$$E_z = 0 \tag{2.7}$$

$$E_y = -k_x sin(k_x x) \cos(k_y y) \cos(k_z z) \tag{2.8}$$

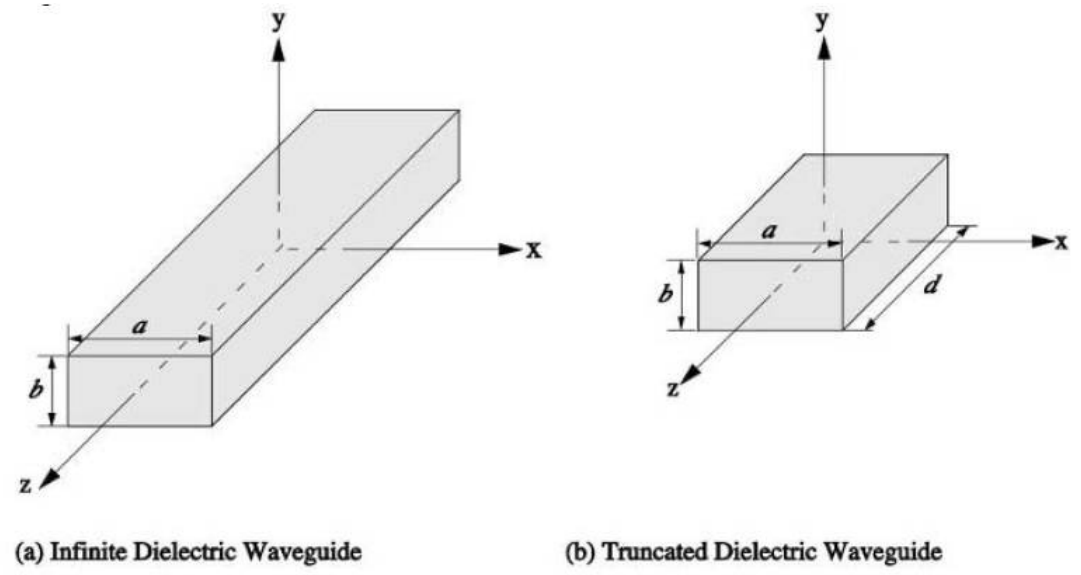

Figure 2.3: Geometry of analytical model for the RDRA (a) Infinite dielectric waveguide, (b) Truncated dielectric waveguide

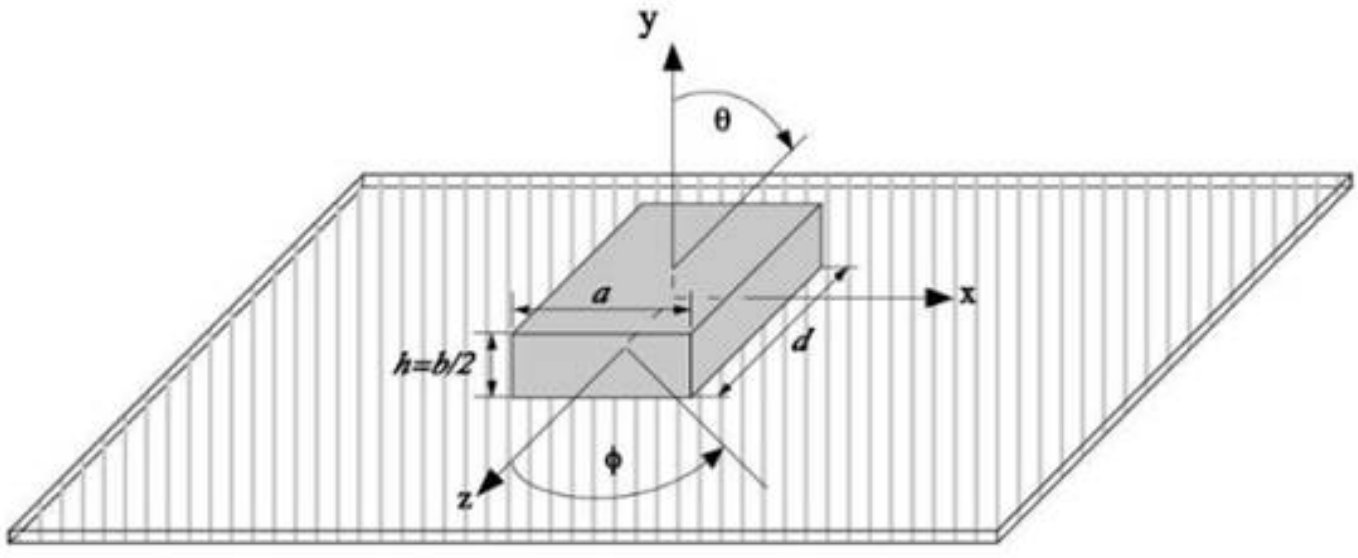

Figure 2.4: RDRA on ground plane [2]

$$E_x = k_y \cos(k_x x) sin(k_y y) sin(k_z z) \tag{2.9}$$

$$H_y = \frac{k_x k_y}{j\omega\mu_0} \cos(k_x x) sin(k_y y) sin(k_z z) \tag{2.10}$$

$$H_x = \frac{k_x k_y}{j\omega\mu_0} sin(k_x x) \cos(k_y y) sin(k_z z) \tag{2.11}$$

Enforcing the magnetic wall boundary condition (2.1) at the surfaces of the RDRA, i.e., at $|x| = \mathrm{a}/2$ and $|y| = \mathrm{b}/2$, that is the 2^{nd} order approximation method (MMW), following equations are obtained for the wavenumbers k_x and k_y:

$$k_x = \frac{m\pi}{a}, m = 1, 2, 3, ... \qquad k_y = \frac{n\pi}{b}, n = 1, 2, 3, ... \tag{2.12}$$

Further, by applying the continuity of the magnetic field intensity is used to perform the matching of tangential component across the imperfect interfaces at $|z| = \mathrm{d}/2$, the following transcendental equation is obtained for the wavenumber k_z:

$$k_z \tan(k_z \frac{d}{2}) = \sqrt{(\epsilon_r - 1)k_0^2 - k_z^2}, \tag{2.13}$$

The wavenumber k_x, k_y, and k_z also satisfy following separation equatin

$$k_x^2 + k_y^2 + k_z^2 = \epsilon_r k_0^2 \tag{2.14}$$

For the $TE^z_{11\delta}$ mode, the value of δ can be defined as fraction of a half cycle of the field variation in the z-direction ($0 < \delta < 1$) which is given by

$$\delta = \frac{k_z}{\frac{\pi}{d}} \tag{2.15}$$

For given dielectric constant and physical dimensions (a, b and d) of the RDRA, the resonant frequency can be found by substituting (2.12) and (2.14) in (2.13). The transcendental equation (2.13) is solved for k_z. The resonant frequency can then be obtained by solving for k_0 in (2.14). The resonant frequency of $TE^z_{11\delta}$ can be expressed from (2.14) as:

$$f_r = \frac{c}{2\pi\sqrt{\epsilon_r}} \sqrt{k_x^2 + k_y^2 + k_z^2} \tag{2.16}$$

The equations for the resonant frequencies of $TE^x_{\delta 11}$ and $TE^y_{1\delta 1}$ modes are similiar.

Comparison of theoretical resonant frequencies of 1^{st} and 2^{nd} order approximations with experimental resonant frequency for different samples of RDRA is given in Table 2.1. Experimental resonant frequencies, f_r(Exp), of $TE^z_{11\delta}$ mode of a probe coupled various samples of RDRAs [21] are used for the comparision. It is assumed that all subscripts

(m,n, and p) are equal to 1 for the lowest-order TE^z_{111} mode in the first order approximation. For the second order approximation, subscripts (m, and n) are equal to 1 for the lowest order $TE^z_{11\delta}$ mode. Calculated resonant frequencies of the both approximations, and percentage (%) of errors which are calculated with reference to experimental result for resonant frequencies of 1^{st} and 2^{nd} order approximations are listed in Table 2.1. It is observed that as compared to the experimental resonant frequency of various samples of RDRA, % of error is of the order of 11% to 45 % for the 1^{st} order approximation. Error in 2^{nd} order approximation as compared to the experimental resonant frequency is in the range of 1 to 10 %. It is noticed that resonant frequency of the 2^{nd} order approximation model provides accurate prediction for the lower order mode in the RDRA.

Table 2.1: Comparison of theoretical resonant frequency of 1^{st} and 2^{nd} order approximation with experimental result [21]

ϵ_r	a (mm)	$\frac{b}{2}$ (mm)	d (mm)	f_r (GHz) Exp [21]	f_{r1} (GHz) Theory	% of Error 1^{st} order	f_r (GHz) Theory	% of Error 2^{nd} order
20.0	10.16	7.11	10.16	4.71	5.23	11.04	4.63	1.7
20.0	10.16	10.16	7.11	4.55	6.63	45.71	4.60	1.0
37.84	7.62	15.24	7.62	4.08	4.80	17.64	3.88	4.9
79.46	7.70	7.70	7.70	3.17	3.78	19.24	2.84	10.4

For the lowest order $TE^z_{11\delta}$ mode, m and n are equal to 1, a sketch of the field configuration of RDRA is shown in Figure 2.5. The DRA has dimension of $w \times h \times d$. Where, h is equal to b/2. The H_z component of magnetic field is dominant along the center of the DRA, while the E fields (predominantly E_x and E_y) circulate around the H_z component. These fields are similar to those produced by a short magnetic dipole. Higher-order modes of the RDRA can also be possible for certain aspect ratios. Figure 2.6 shows sketches of the E-fields of $TE^z_{21\delta}$, $TE^z_{31\delta}$, and $TE^z_{31\delta}$. The $TE^z_{31\delta}$ and $TE^z_{13\delta}$ modes will produce radiation patterns similar to the $TE^z_{11\delta}$, having a peak in the broadside direction (along the y-axis), while the $TE^z_{21\delta}$ mode will have a null at broadside. (Note that the $TE^z_{21\delta}$ mode cannot exist for the case of the RDRA mounted on the ground plane, due to the boundary condition that forces the tangential E-field to zero at y is equal to 0, since the $TE^z_{21\delta}$ mode would require the E-field to be maximum at that location [1].

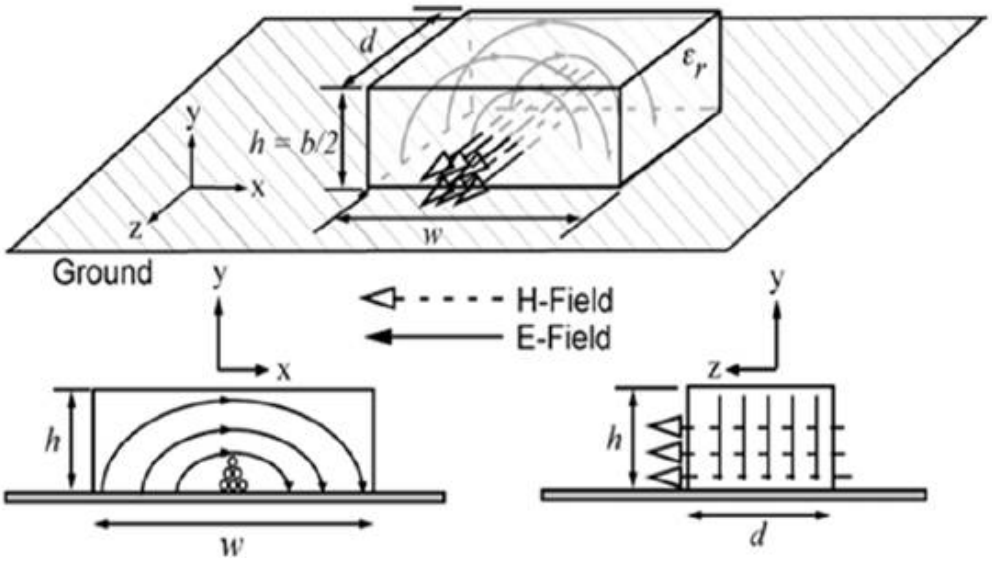

Figure 2.5: Sketch of the fields for the $TE^z_{11\delta}$ mode of the RDRA [1]

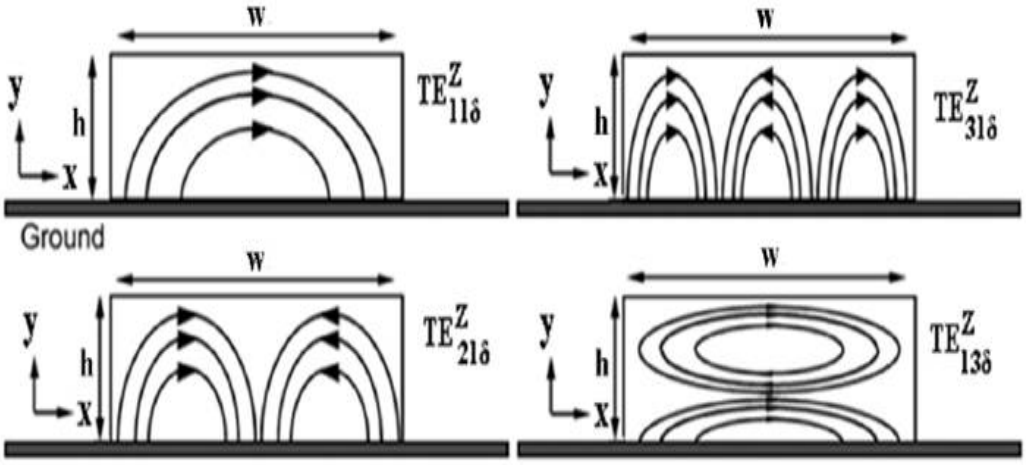

Figure 2.6: E-field of selected higher modes within the RDRA [1]

In order to study variation of the resonant frequency with height b, length a, and depth d, aspect ratios (length/height and depth/height), using equations (2.12) to (2.14), the theoretical analysis is performed. Variation of the resonance frequency in GHz as a function of dielectric constant for different values of height, b, are shown in Figure 2.7. The other dimensions of the RDRA, operated in $TE^z_{11\delta}$ mode are depth of 10 mm and length of 30 mm. From the Figure 2.7, it is seen that for low profile RDRA, the resonance frequency varies from 18 GHz to 4 GHz when dielectric constant varies from 6 to 100. For high profile rectangular DRA, the resonance frequency varies from 8 GHz to 2 GHz. This shows that for a given physical parameters of the RDRA, the low-profile RDRA is resonated at higher frequency as compared to the high profile.

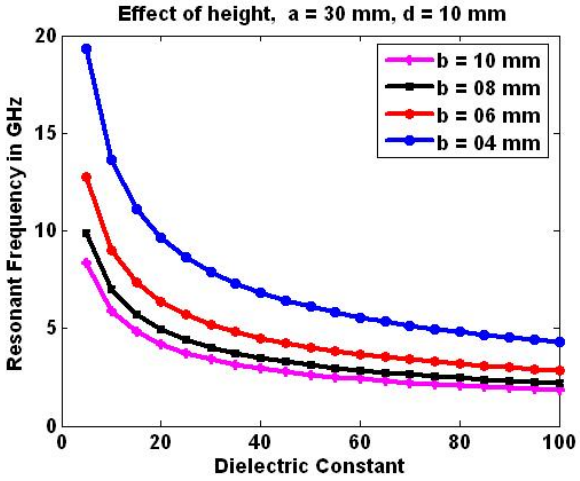

Figure 2.7: Plot of resonant frequency with dielectric constant for different values of height of the RDRA

For different values of depth, d, variation of the resonance frequency as a function of dielectric constant are shown in Figure 2.8. The other dimensions of the RDRA are height of 12 mm and length of 25 mm. From Figure 2.8, it is observed that for wider and thinner RDRA, the resonant frequency is estimated around 7 GHz to 1.5 GHz for different values of the dielectric constant (6 to 100). There is a very small difference in the resonant frequency for different values of depth irrespective of material used in the RDRA.

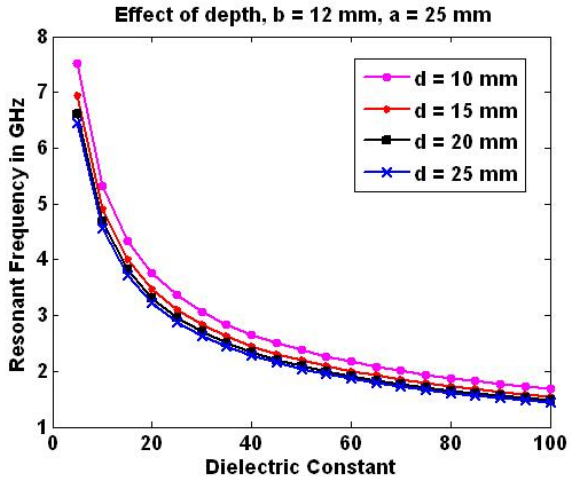

Figure 2.8: Plot of resonant frequency with dielectric constant for different values of depth of the RDRA

Figure 2.9 shows variation of the resonance frequency with dielectric constant (ϵ_r varies

from 6 to 100) for different values of length, a. The other dimensions are height of 10 mm, depth of 10 mm. It is seen , from the Figure 2.9, that there are more variation in the resonance frequency for longer and shorter rectangular DRA.

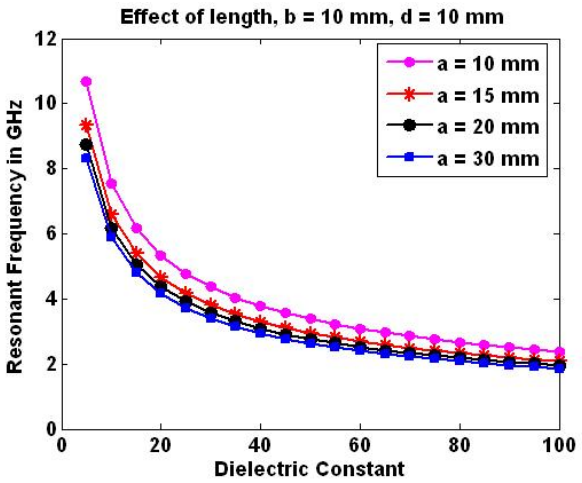

Figure 2.9: Plot of resonant frequency with dielectric constant for different values of length of the RDRA

Predicted resonance frequency as a function of the aspect ratio, depth/height, (d/b) for different aspect ratio, length/height, a/b of 0.5, 1, 2, 3, and 5 are shown in Figure 2.10. The rectangular DRA made of material with dielectric constant of 15 is used in this numerical study. From the Figure 2.10, it is observed that the resonant frequency can be predicted between 16 GHz to 12 GHz for a/b of 0.5 if the d/b vary from 0.1 to 3. For a/b of 3, the resonance frequency can be expected between 11 GHz to 5 GHz for same variation of d/b. For higher value of a/b, there is a small variation in the resonant frequency. It is also seen that there is small variation of the resonance frequency for the aspect ratio (d/b), more than 1.5 for all values of a/b. Figure 2.11 shows variation in resonant frequency as a function of the aspect ratio depth/height, (d/b), for different values of dielectric constant. It is assumed that aspect ratio, length/height is equal to 1. It is observed that the predicted resonant frequency decreases as the dielectric constant increases for all value of d/b.

From all these theoretical studies, it is observed that resonant frequency is a function of the physical parameters namely, the length, the depth, the height, the dielectric constant and the two aspect ratios. To predict resonant frequency for the RDRA, it is necessary

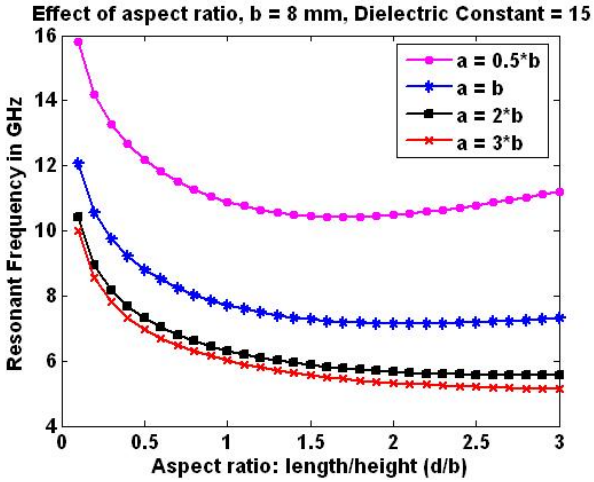

Figure 2.10: Plot of resonant frequency with aspect ratios (d/b) for different values of aspect ratio (a/b) of the RDRA

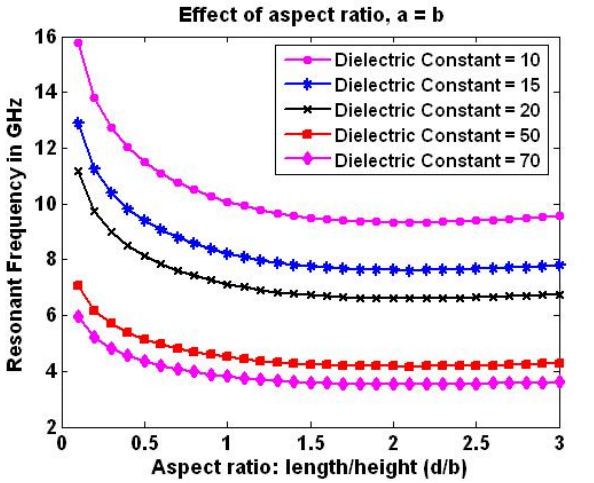

Figure 2.11: Plot of resonant frequency with aspect ratios (d/b) for different values of dielectric constant

to optimize all the physical parameters.

Fang and Leung [22] have given following new equations for resonant frequency (f_r) of TE^y_{111} mode of a strip-fed RDRA resting on a ground plane. However, the excitation source is neglected and only the source-free RDRA is considered. The RDRA has length a, depth d, and height b, with a > b.

$$f_r = \frac{c}{2\pi a\sqrt{\epsilon_r}}\left(\frac{s_1}{s_2 + e^{s_3 p}} + s_4\right) \tag{2.17}$$

where,

$$s_1 = -5.29q^4 + 15.97q^3 - 17.71q^2 + 8.812q - 3.198 \tag{2.18}$$

$$s_2 = 0.2706q^4 - 0.7232q^3 + 0.7857q^2 - 0.4558q - 1.023 \tag{2.19}$$

$$s_3 = -8.03q^4 + 23.06q^3 - 24.53q^2 + 11.75q - 3.588 \tag{2.20}$$

$$s_4 = 43.18q^4 - 124.7q^3 + 134.5q^2 - 65.85q + 15.37 \tag{2.21}$$

where, p = $\frac{b}{a}$ and q = p = $\frac{d}{a}$ are aspect ratios. Figure 2.14 shows f_r as a function of ϵ_r for different ratio of d/a. For comparision, the DWM result is also shown in the Figure 2.12. It can be seen that an excellent agreeement is observed between the two results. When compared with the DWM model, the error is less than 3 % over the range of 0.4 $\leq$ p $\leq$ 1, 0.2 $\leq$ q $\leq$ 1, and 6 $\leq \epsilon_r \leq$ 100.

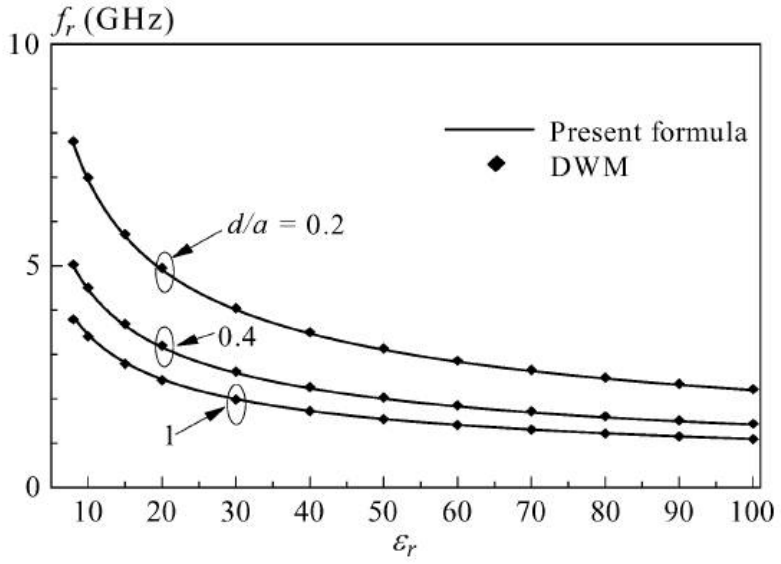

Figure 2.12: Resonance frequency of the RDRA as a function of dielctric constant (ϵ_r) for different values of $\frac{d}{a}$ = 0.2, 0.4, and 1: a = 20 mm, b = 12 mm, comparision of curve fitting method with DWM [22]

If the design frequency f_r is specified, then the length, a, of a RDRA can be determined from (2.36) as follows when the parameters of ϵ_r, p, and q are given:

$$a = \frac{c}{2\pi f_r \sqrt{\epsilon_r}} \left(\frac{s_1}{s_2 + e^{s_3 p}} + s_4 \right) \tag{2.22}$$

Once the length ,a, is calculated, the other two dimensions b, d can be obtained from the

ratios of p and q, respectively. If the ratios of p, and q are not specified, they can then be arbitrarily chosen within their valid ranges of $0.4 \leq p \leq 1$, $0.2 \leq q \leq 1$.

Impedance Bandwidth and Radiation Q-factor:

Bandwidth of the antenna can be considered to be range of frequencies, on either side of a center frequency (usually resonance frequency), where the antenna characteristics (such as input impedance, pattern, beamwidth, polarization, gain, beam direction, radiation efficiency) are within an acceptable value of those at the center frequency. Impedance variation with frequency of the antenna element results in a limitation of the frequency range over which the antenna can be matched to its feed line [23]. Impedance bandwidth for antenna is usually specified in terms of a return loss (typically less than -10 dB) or maximum standing wave ratio (S) which is typically less than 2.0. Impedance bandwidth is a frequency range from one S level to another which can be accomplished by using the following relation between bandwidth (BW) and radiation Q-factor (Q_{rad}) [1].

$$BW = \frac{S-1}{Q_{rad}\sqrt{S}} \tag{2.23}$$

Equation (2.23) relates the calculated radiation Q (Q_{rad}) to the observed impedance bandwidth (BW) for a specific maximum acceptable standing wave ratio (S). Numbers of assumptions are made for deriving the equation (2.23). First, it is assumed that the equivalent circuit of the antenna can be represented by a RLC shunt resonator across a lossless transmission line. In practice, the self reactance of the feed will affect both resonant frequency and bandwidth of the RDRA [23] as different feed schemes are used for the same RDRA. Second, impedance bandwidth will refer to the S of 2:1 for the matched antenna, which result in following equation.

$$BW = \frac{1}{\sqrt{2}Q_{rad}} \tag{2.24}$$

The unloaded Q-factor of a shielded DR is typically defined as $1/\tan(\delta)$. For low loss dielectric material, the dielectric loss is a very small fraction of the radiation loss for unshielded DR and thus, the radiation Q-factor of the antenna is given by the following

standard relation:

$$Q_{rad} = \frac{2\omega_0 W_e}{P_{rad}} \tag{2.25}$$

where, W_e and P_{rad} are stored energy and radiated power, respectively. The radiated power is given by [2] for the $TE^z_{11\delta}$ mode of the RDRA

$$P_{rad} = 10k_0^4|P_m|^2 \tag{2.26}$$

The magnetic dipole moment (P_m) of the RDRA is

$$P_m = -\frac{j\omega 8\epsilon_0(\epsilon_r - 1)}{k_x k_y k_z} sin(\frac{k_z d}{2})\hat{a}_z \tag{2.27}$$

Stored energy is given by following equation.

$$W_e = \frac{\epsilon_0 \epsilon_r abd}{32}(1 + \frac{sin(k_z d)}{k_z d})(k_x^2 + k_y^2) \tag{2.28}$$

After substituing equation of P_{rad} and W_e in equation (2.19), following equation is obtained for Q_{rad}

$$Q_{rad} = \sqrt{\frac{1}{\epsilon_0\mu_0}} \frac{\epsilon_r abdk_x^2 k_y^2 k_z^2 (k_y^2 + k_z^2)}{1024k_0^4\omega_0(\epsilon_r - 1)^2} \frac{[1 + \frac{sin(k_x a)}{(k_x a)}]}{sin^2(\frac{k_x a}{2})} \tag{2.29}$$

Them, impedance bandwidth can be calculated by (2.24).

For antennas, the impedance bandwidth is also expressed as % of the frequency difference (upper frequency (f_U) minus lower frequency (f_L)) over the center frequency of the bandwidth. Where, f_U and f_L are frequencies having S equal to 2. The center frequency is $(f_L + f_U)/2$. The higher the percentage, wider the bandwidth. For an example, a 5 % impedance bandwidth indicates that the frequency difference of acceptable operation is 5 % of the center frequency of the impedance bandwidth. In this thesis, % of impedance bandwidth less than 4 % is called narrowband antenna and % of impedance bandwidth between 10 % to 50 % is called wideband antenna. Ultra wideband (UWB) is between 3.1 GHz and 10.6 GHz.

In Figure 2.13, predicted Q_{rad} and % of impedance bandwidth (S is equal to 2) are plotted as a function of dielectric constant (ϵ_r varies from 10 to 100) for a rectangular DRA

(length of 30 mm, depth of 10 mm, and height of 6 mm). Q_{rad} and % of impedance bandwidth are shown in right-side and left-side of Figure 2.13, respectively. For the given rectangular DRA, it is observed that Q_{rad} is increased as the dielectric constant increases. While, the % of impedance bandwidth is decreased when the dielectric constant increases. Q_{rad} and impedance bandwidth are controlled by proper choice of dielectric constnat of material used in the rectangular DRA.

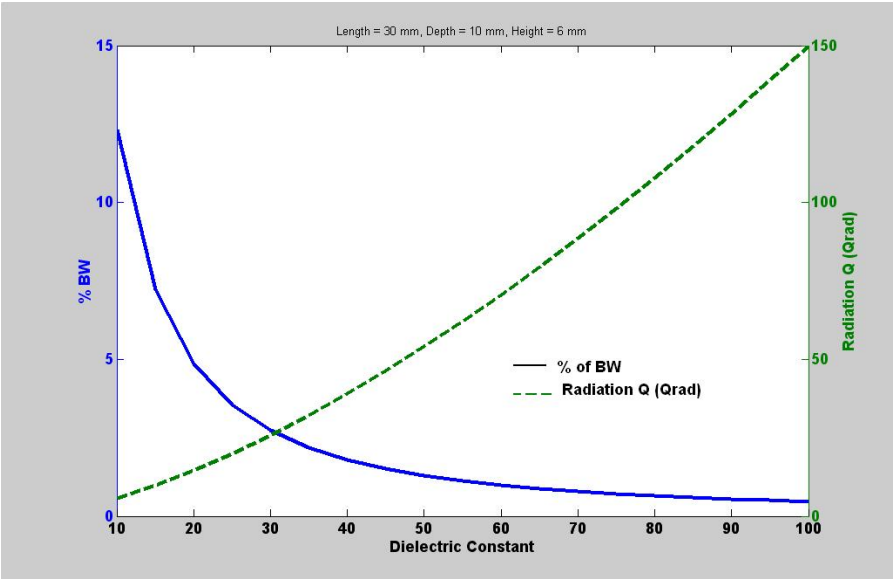

Figure 2.13: Variation of radiation Q-factor and % bandwidth as a function of ϵ_r for the RDRA

Table 2.2: Theoretical resonant frequencies, radiation Q-factor, and impedance bandwidth of $TE^z_{11\delta}$ mode

Dielectric Constant	a (mm)	$\frac{b}{2}$ (mm)	d (mm)	F_r (GHz) Theofy	Q_{rad} Theory	% of BW
10.8	15.24	7.62	3.10	6.95	5.8	12.19
20.0	10.16	7.11	10.16	4.63	18.9	3.74
20.0	10.16	10.16	7.11	4.60	15.9	4.45
37.84	9.31	4.60	9.31	4.16	48.1	1.47
37.84	7.62	15.24	7.62	3.88	23.5	3.01
37.84	9.31	9.31	4.60	4.00	34.8	2.02
79.46	12.70	2.54	2.54	4.92	86.8	0.81
79.46	12.70	6.35	6.35	2.40	139.6	0.51
79.46	7.70	7.70	7.70	2.84	117.6	0.60

Theoretical resonant frequency (2.12-2.14), radiation Q-factor (2.29) and % of impedance

bandwidth are calculated for different values of dielectric constants for $TE^z_{11\delta}$ mode and are listed in Table 2.2. From the Table 2.2, it is observed that for simple rectangular DRA, the % of impedance bandwidth is around 12 % for ϵ_r of 10.8. It is around 3 to 4 % for ϵ_r of 20.0 and 1 to 3 % for ϵ_r of 37.84, while for ϵ_r of 79.46 it is less than 1 %. Thus, to achieve bandwidth improvement with simple RDRA is a challenging objective for high permittivity materials. To achieve a narrow bandwidth with the simple RDRA, it is required to have a material of high relative permittivity. To achieve the narrow bandwidth by the RDRA with the material of low relative permittivity is also challenging. The main objective of our study is to propose methods of wide bandwidth as well as narrow bandwidth with a simple miniaturized rectangular DRA with a material of medium value of relative permittivity.

Also, the Q_{rad} depends on physical dimension a, b, and d of the RDRA as per the equation (2.29). Theoretical analysis has been carried out on the aspect ratios (a/b and d/b) for Q_{rad} and percentage of BW at resonant frequency of 5.2 GHz for $TE^z_{11\delta}$ mode in RDRA. The range of aspect ratios $0.1 \leq \frac{a}{b}$ and $\frac{d}{b} \leq 2$ are considered. The dimensions a, d, b,

Table 2.3: Study on aspect ratios for $TE^z_{11\delta}$ mode, $\epsilon_r = 10$

a/b	d/b	a (mm)	d (mm)	$b/2$ (mm)	Q_{rad}	% of BW
0.1	0.1	12.90	12.90	129	0.77	91.85
0.1	2	9.14	182.80	91.40	0.11	660.50
0.5	0.1	46.53	9.31	93.05	0.41	174.40
0.5	2	9.60	38.40	19.2	2.06	34.41
1	0.1	91.72	9.17	91.7	0.21	333.80
1	2	10.79	21.58	10.95	5.19	13.64
1.5	0.1	137.20	9.15	91.45	0.14	496.50
1.5	2	12.42	16.57	8.30	7.07	9.995
2	0.1	182.80	9.14	91.35	0.11	660.50
2	2	14.36	14.36	7.15	7.75	9.126

Q_{rad}, and % of bandwidth are tabulated for ϵ_r equal to 10, 32, and 79 in Table 2.3, 2.4, and 2.5, respectively. From the Table 2.3, a maximum % of bandwidth is 660.5 % for ϵ_r of 10, with $\frac{a}{b}$ equal to 0.1, $\frac{d}{b}$ equal to 2 (a = 9.14 mm, d = 182.80 mm, b = 182.76 mm) and $\frac{a}{b}$ equal to 2, $\frac{d}{b}$ equal to 0.1 (a = 182.80 mm, d = 9.14 mm, b = 182.76 mm) with volume of 205128 mm^3. From the Table 2.4, the maximum % of bandwidth is 133.5 %

Table 2.4: Study on aspect ratios for $TE^{z}_{11\delta}$ mode, $\epsilon_r = 32$

a/b	d/b	a (mm)	d (mm)	b/2 (mm)	Q_{rad}	% of BW
0.1	0.1	7.21	7.21	72.10	3.82	18.54
0.1	2	5.11	102.20	51.10	0.53	133.50
0.5	0.1	26.01	5.20	52.05	2.01	35.24
0.5	2	5.37	21.47	10.75	10.17	6.95
1	0.1	51.27	5.13	51.25	1.05	67.38
1	2	6.04	12.07	6.05	25.56	2.77
1.5	0.1	76.70	5.11	51.10	0.70	100.30
1.5	2	6.96	9.28	4.65	34.72	2.04
2	0.1	102.20	5.11	51.1	0.53	133.50
2	1.5	9.28	6.96	4.65	34.72	2.04

Table 2.5: Study on aspect ratios for $TE^{z}_{11\delta}$, $\epsilon_r = 79$

a/b	d/b	a (mm)	d (mm)	b/2 (mm)	Q_{rad}	% of BW
0.1	0.1	4.59	4.59	45.90	14.25	4.96
0.1	2	3.25	65.02	32.5	1.99	35.59
0.5	0.1	16.56	3.31	33.1	7.52	9.41
0.5	2	3.42	13.67	6.85	37.99	1.86
1	0.1	32.63	3.26	32.65	3.93	18.01
1	2	3.84	7.69	3.85	95.41	0.74
1.5	0.1	48.81	3.25	32.55	2.63	26.90
1.5	2	4.43	5.91	2.95	129.4	0.55
2	0.1	65.02	3.25	32.50	1.99	35.59
2	2	51.24	5.12	2.55	141.10	0.50

for ϵ_r of 32, with $\frac{a}{b}$ equal to 0.1, $\frac{d}{b}$ equal to 2 (a = 5.11 mm, d = 102.20 mm, b = 102.10 mm) and $\frac{a}{b}$ equal to 2, $\frac{d}{b}$ equal to 0.1 (a = 102.20 mm, d = 5.10 mm, b = 102.10 mm) with volume of 53320 mm^3. From the Table 2.5, the maximum % of bandwidth is 35.59 % for ϵ_r of 79, with $\frac{a}{b}$ equal to 0.1, $\frac{d}{b}$ equal to 2 (a = 3.25 mm, d = 65.00 mm, b = 65.00 mm) and $\frac{a}{b}$ equal to 2, $\frac{d}{b}$ equal to 0.1 (a = 65.00 mm, d = 3.30 mm, b = 65.00 mm) with volume of 13942 mm^3. From these analysis, it is observed that the maximum bandwidth is obtained with a wider (small value of $\frac{a}{b}$, large value of $\frac{d}{b}$) or longer (large value of $\frac{a}{b}$, small value of $\frac{d}{b}$) RDRA. It is also noticed that by increasing the dielectric constant ϵ_r of material by 3.2 times, there is decrease in % of bandwidth by a factor of 5 and decrease in volume by a factor of 5.72. By increasing the dielectric constant ϵ_r of material by a

factor of 7.9, there is decrease in % of bandwidth by a factor of 18.5 and decrease in volume by a factor of 22.2. This study on aspect ratio shows that by proper choosing the dimensions of the RDRA, it is possible to achieve the maximum impedance bandwidth. These numerical studies indicate that maximum impedance bandwidth is possible with larger value of a/b and smaller value of d/b and vice versa.

For the Table 2.3, minimum % of bandwidth is 9.13 % for ϵ_r of 10 with $\frac{a}{b}$ equal to 2, $\frac{d}{b}$ equal to 2 (a = 14.40 mm, d = 14.40 mm, b = 14.40 mm) with a volume of 2985 mm^3. From the Table 2.4, minimum % of bandwidth is 2.04 % for ϵ_r of 32, with $\frac{a}{b}$ equal to 2, $\frac{d}{b}$ equal to 1.5 (a = 9.30 mm, 7.00 mm, 9.30 mm) with a volume of 605 mm^3. From the Table 2.5, minimum % of bandwidth is 0.5 % for ϵ_r of 79, with $\frac{a}{b}$ equal to 2, $\frac{d}{b}$ equal to 2 (a = 5.10 mm, 5.10 mm, 5.10 mm) with a volume of 132 mm^3. It is observed that minimum bandwidth is obtained with a square DRA.

The theoretical percentage of bandwidth and Q_{rad} can differ from measured value. These are partially attributed to the loading caused by the feeding techniques. When probe coupled RDRAs were measured [21], the percentage difference was limited to 1 to 12 % for the resonant frequency and 2 to 108 % for the Q_{rad}. Since the intent of the DWM-MMW model is to obtain approximate value for the resonant frequency, impedance badnwidth and Q_{rad} of the RDRA. It is usually sufficient to use the model for initial dimensions of the RDRA. If more accuracy is required, a full-wave analysis will have to be undertaken, which take into account such factors as the feeding mechanisms, ground plane size, and imperfect magnetic interfaces [24].

2.1.3 Feeding Techniques for Rectangular Dielectic Resonator Antenna

Previous section described the RDRA and presented design equations for predicting resonant frequency, impedance bandwidth and radiation Q-factor for the $TE^z_{11\delta}$ mode. The models for deriving these equations assumed the RDRA was in isolation or mounted on an infinite perfect conducting ground plane and did not account for feeding techniques used to excite the RDRA. The selection of the feed and that of its location both have

played important roles in determining which mode is excited. This will determine input impedance and radiation characteristics of the RDRA. The feeding technique can also have a significant impact on the resonant frequency, impedance bandwidth and radiation Q-factor, which previous equations failed to predict. This section presents a brief review of various feeding techniques for the RDRA.

Aperture/Slot Coupling:

In aperture coupling method, a microstrip feed line is printed on bottom of a feed substrate and a slot is made over a ground plane on the top of the feed substrate as shown in Figure 2.14. A RDRA is placed on top of the slot usually at a center. This coupling mechanism has an advantage that the feed network is located beneath the ground plane, thus minimizing spurious radiation. The microstrip feed line should be positioned at right angles to the center of the slot for efficient coupling. Positioning the feed line away from the slot will reduce the coupling efficiency. The coupling level can be adjusted by moving the RDRA laterally across the slot [25]. Improvement in impedance bandwidth can be obtained by lateral displacement of the RDRA over the slot. Shape of the cou-

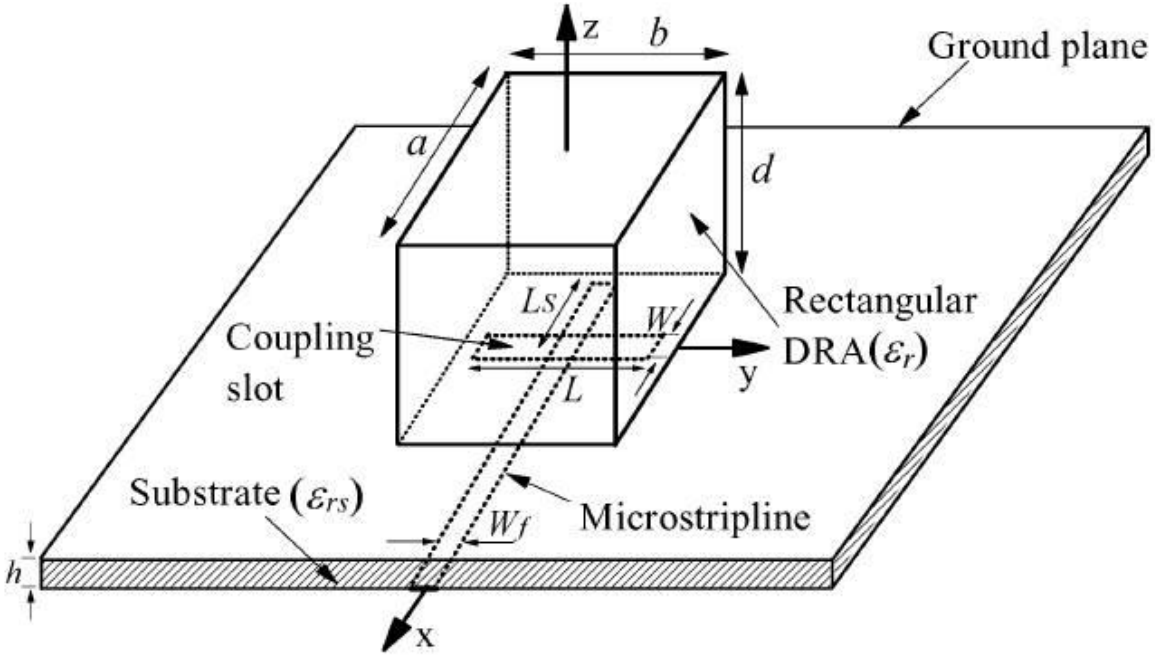

Figure 2.14: Aperture/slot coupled rectangular DRA

pling aperture has a significant impact on the strength of coupling between the feed line

and RDRA. Rectangular coupling slots are commonly used as they give better coupling than ring aperture. Annular slot [26], cross-slot [27] are some of the other types used for efficient coupling. These slots provide improvement in impedance bandwidth. Modified shape of slot produces circular polarization and dual polarization apart from linear polarization. The improvement in bandwidth is due to flexibility offered by the slot length and coupling aperture size. The aperture coupling method can be extended for feeding a DRA array similar to the microstrip line feed method. The ground plane serves as an effective shield between the radiating aperture and the feed network. Disadvantage of aperture coupling is that it radiates a small amount of power in the backside direction. But in practice a metal cavity is located some distance below the feed layer to eliminate this radiation.

Direct Microstrip Feed Line:

A common method for coupling to a RDRA is a microstrip feed line which is shown in Figure 2.15. The microstrip feed line is printed on a substrate. The RDRA is attached/placed on top of the microstrip line. Microstrip coupling excites magnetic fields in the RDRA. The coupling is affected by a characteristic impedance of the feed line, width of the feed line, location of the RDRA with respect to the feed line and length of the line underneath the RDRA [28]. A more dominant parameter affecting the degree

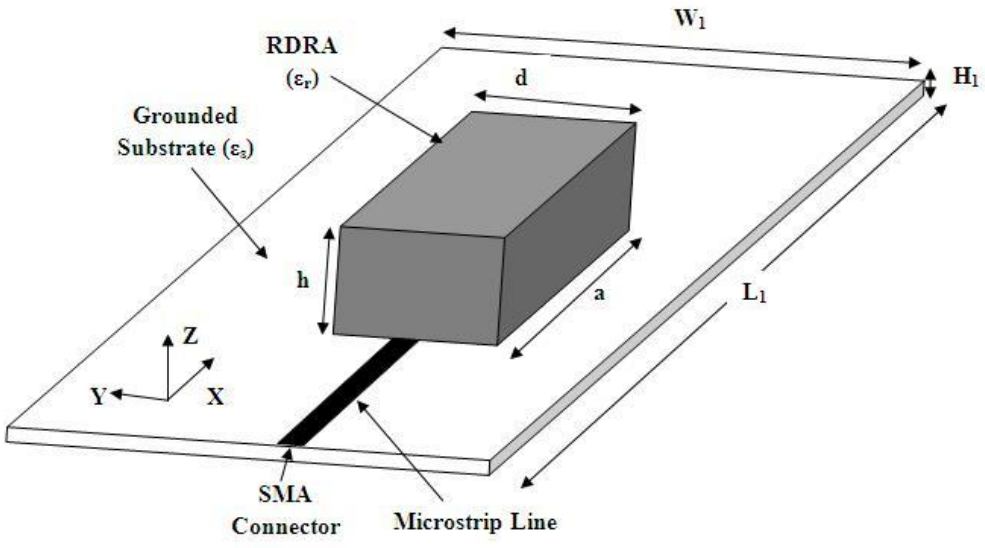

Figure 2.15: Direct microstrip line feeding to a RDRA

of coupling is the dielectric constant of the RDRA. For higher value ($\epsilon_r > 20$), strong coupling is achieved; however, the maximum amount of coupling is significantly reduced if the dielectric constant of the DRA is lowered [1, 21]. The microstrip line can be used as a series feed for DRA arrays. Direct coupling from the microstrip lines to the DRA elements for feeding DRA arrays make it easy to integrate with microwave printed circuits [29]. However, disadvantage of this method is that polarization of the RDRA is determined by orientation of the microstrip line. Also, in an open environment, there is radiation from the microstrip line. Hence the radiation pattern of the RDRA may be distorted.

Coaxial Probe Feed :

Another common method for coupling to DRAs is with a coaxial probe, as shown in Figure 2.16. The coaxial probe consists of a center pin of a coaxial line that extends through the ground plane. The probe can either be located adjacent to the DRA or can be embedded within DRA. Amount of coupling can be optimized by adjusting the probe height and the DRA location. Also, depending on the location of the probe, various modes can be excited. One advantage of the coaxial probe excitation is that a direct coupling into a 50 Ω system without need for a matching network. The probe length is generally chosen to be less than the height of the DRA, to avoid probe radiation [1, 21]. Rigorous analyses for probe-fed hemispherical and cylindrical DRAs have been carried out, showing the effects of both the probe position and length on the input impedance and resonant frequency of the DRA [30,31]; however, there are no simple equations to design the required probe height for a given set of DRA dimensions and dielectric constant. The center pin of probe can also be soldered to a flat metal strip that is placed adjacent to the DRA [32], whose length and width can be adjusted to improve the impedance bandwidth. Instead of a coaxial line, the flat metal strip can also be connected to the microstrip line [33]

Coplanar Waveguide Feeding:

A coplanar waveguide (CPW) feed is an efficient, low cost feed system for microwave

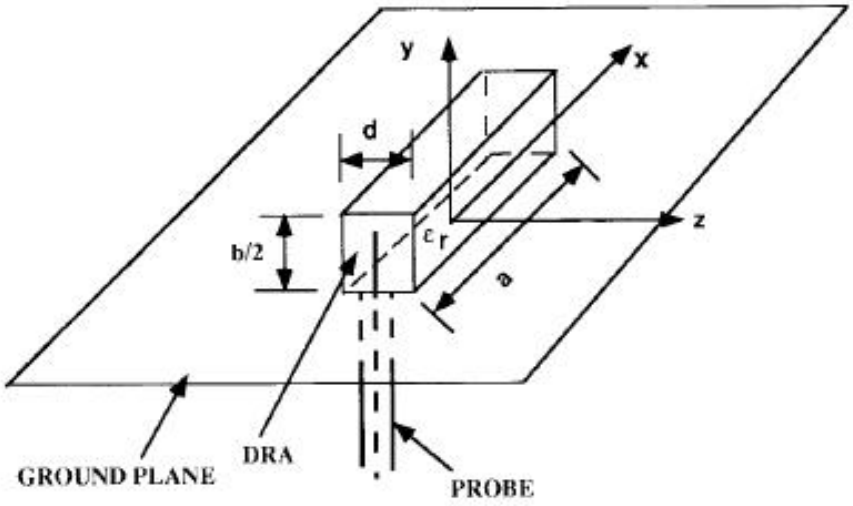

Figure 2.16: Coaxial probe fed RDRA

printed antennas. Coupling from the coplanar line to a DRA is accomplished via a slot in a ground plane to which the coplanar line is connected either inductively or capacitively. Coupling level can be adjusted by moving the DRA laterally across the slot as

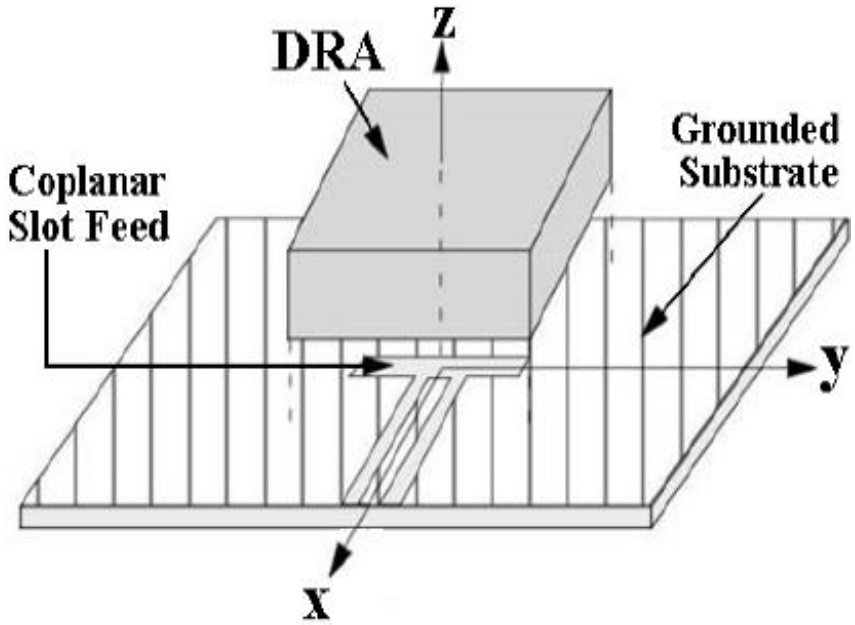

Figure 2.17: Coplanar waveguide feeding to a rectangular DRA

shown in Figure 2.17. As the DRA is moved with respect to the feed line, both reactance and resistance of the antenna are changed. The coplanar waveguide technique provides a convenient uniplanar feed structure, allowing for an easy integration of active devices,

thus leading to a simple manufacturing process [1].

Dielectric Image Guide Line:

A dielectric resonator antennas can be coupled to a dielectric image guide line as shown in Figure 2.18. The dielectric image guide offer advantages over a microstrip line at millimeter-wave frequencies, since it does not suffer from conductor losses. As with the microstrip line, an amount of coupling to the DRA is generally quite small, especially for DRAs with lower dielectric constant, although it may be possible to increase the coupling by operating the guide closer to a cut-off frequency. The dielectric image guide is thus best utilized as a series feed to a linear array of DRAs [34, 35].

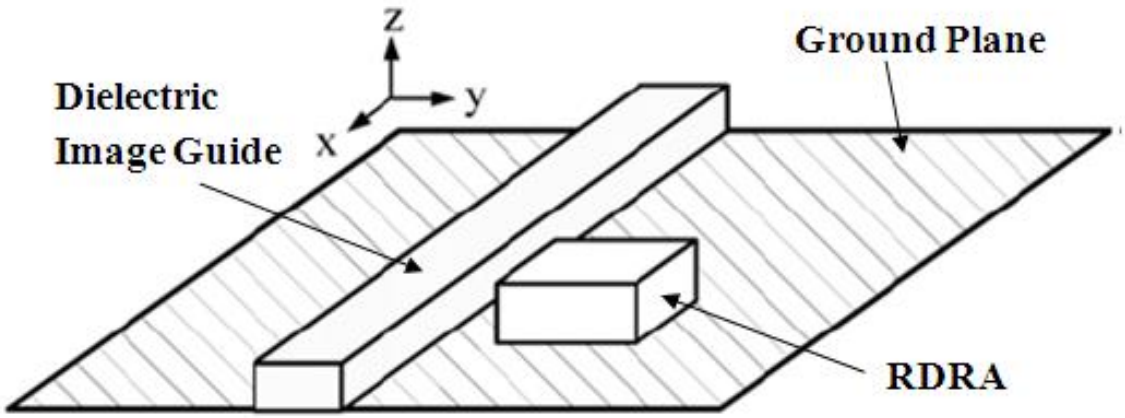

Figure 2.18: Dielectric image guide feeding to a rectangular DRA

2.2 Literature Survey on Wideband RDRA

In this section, literature survey on various bandwidth enhancement techniques is presented. With the development of modern communication applications, there is an increasing demand for antenna element that provides wide bandwidth as well as miniaturized structure without sacrificing performances. Bandwidth enhancement of the antenna is required to increase fast information transfer without any complexity. As discussed in the previous section, dielectric resonator antennas are versatile elements that can be adapted

to numerous designs by properly choosing the design parameters, namely, the relative permittivity of the material and the dimensions. The impedance bandwidth is inversely proportional to the Q_{rad} (2.24), while the Q_{rad} of the RDRA is proportional to the permittivity of the material (2.29). High dielectric constant of the material increases the Q_{rad}, which results in narrow bandwidth. On the other hand low dielectric constant of the material decreases the Q_{rad} which yields wide bandwidth. Whereas, the dimensions of the RDRA are inversely proportional to square root of the relative permittivity of the material (2.16). The RDRA made from the material of high relative permittivity is compact in nature, while the RDRA with the material of low relative permittivity has a large structure. This indicates that there is a tradeoff between bandwidth and miniaturized RDRA structure. As discussed in the previous sections (Table 2.2), the simple RDRA with relative permittivity of 10 gives 12 % of bandwidth, while the relative permittivity of 79 gives 0.6 % of bandwidth which operate at different resonant frequencies.

Following methods of bandwidth improvement are discussed.

- Merging the Modes of Simple DRAs
- Stacked/Embedded DRAs
- Modified Shaped of DRAs
- Hybrid DRAs

2.2.1 Merging of Modes of Simple DRAs

In this section, before examining this method of bandwidth improvement, the reported bandwidth of dielectric resonator antennas of simple shapes (circular and rectangular) are discussed. With a RDRA having a dielectric constant, ϵ_r, of 10.8 and dimension $15 \times 7.5 \times 3\ mm^3$, was found to have experimentally impedance bandwidth of 12 % for probe fed [36] and aperture fed [37] mechanisms when the RDRA is operated in the lowest order mode. As per the DWM-MMW theory, predicated impedance bandwidth of about 20-25% for simple rectangular and cylindrical DRAs for the lowest order mode is possible without considering loading effects from a feed, but experimentally it is reported only around 12 %. To achieve an enhancement in impedance bandwidth, two or more

nearby modes are excited in simple rectangular and cylindrical DRAs which are reported in literature.

Table 2.6: Bandwidth achieved by merging of modes of simple DRAs

DRA Shapes	f_c (GHz)	ϵ_r	Excitation	Volume (mm^3)	% of BW	Ref.
Rectangular	2.6	12	Slot	11905	25 %	[38]
Rectangular	3.8	10.2	Annular	4244	23 %	[39]
Rectangular	5.5	10.2	CPW	2420	29 %	[40]
Rectangular	4.5	9.8	Probe	9480	42 %	[41]
Cylindrical	2.7	48	Microstrip	3118	26 %	[42]
Cylindrical	3.5	12	Probe	6517	27 %	[43]
Cylindrical	3	20.8	Microstrip	3301	35 %	[44]
Cylindrical	6.5	10	Aperture	1344	38 %	[45]

Table 2.6 summarizes few of published designs on bandwidth improvement by merging of modes. The Table 2.6 lists the center frequency f_c, ϵ_r, excitation schemes, volume in mm^3, and % of impedance bandwidth of the reported designs of simple DRAs. In the literature, RDRAs are achieved bandwidths of 25 % to 42 % by operating in two or more modes using microstrip line, annular slot, coplanar waveguide (CPW) and probe fed mechanisms [38–41]. While, 26% to 38 % impedance bandwidth is achieved in cylindrical DRAs (CDRAs) by operating two or more modes using microstrip, probe and aperture coupling feeding methods [42–45]. Figure 2.19 shows some of examples of reported dual modes RDRA designs.

In [38], wide bandwidth is achieved by merging resonances due to a slot and a RDRA as shown in Figure 2.19 (a). In this structure, the slot works as a feeding mechanism to the RDRA as well as an antenna element. Both the resonances are having same antenna polarization and radiation patterns. In [39], bandwidth improvement is achieved by a simple RDRA with a feed structure, shown in Figure 2.19 (b). The feed structure comprises of a complementary pair of a magnetic loop and a magnetic dipole. A probe is used to excite a coplanar waveguide feed which is connected to the annular ring and horizontal slot. Broad impedance is observed due to presence of dual resonance. In [40], multiple resonance technique based on a hybrid DRA structure is reported for wideband

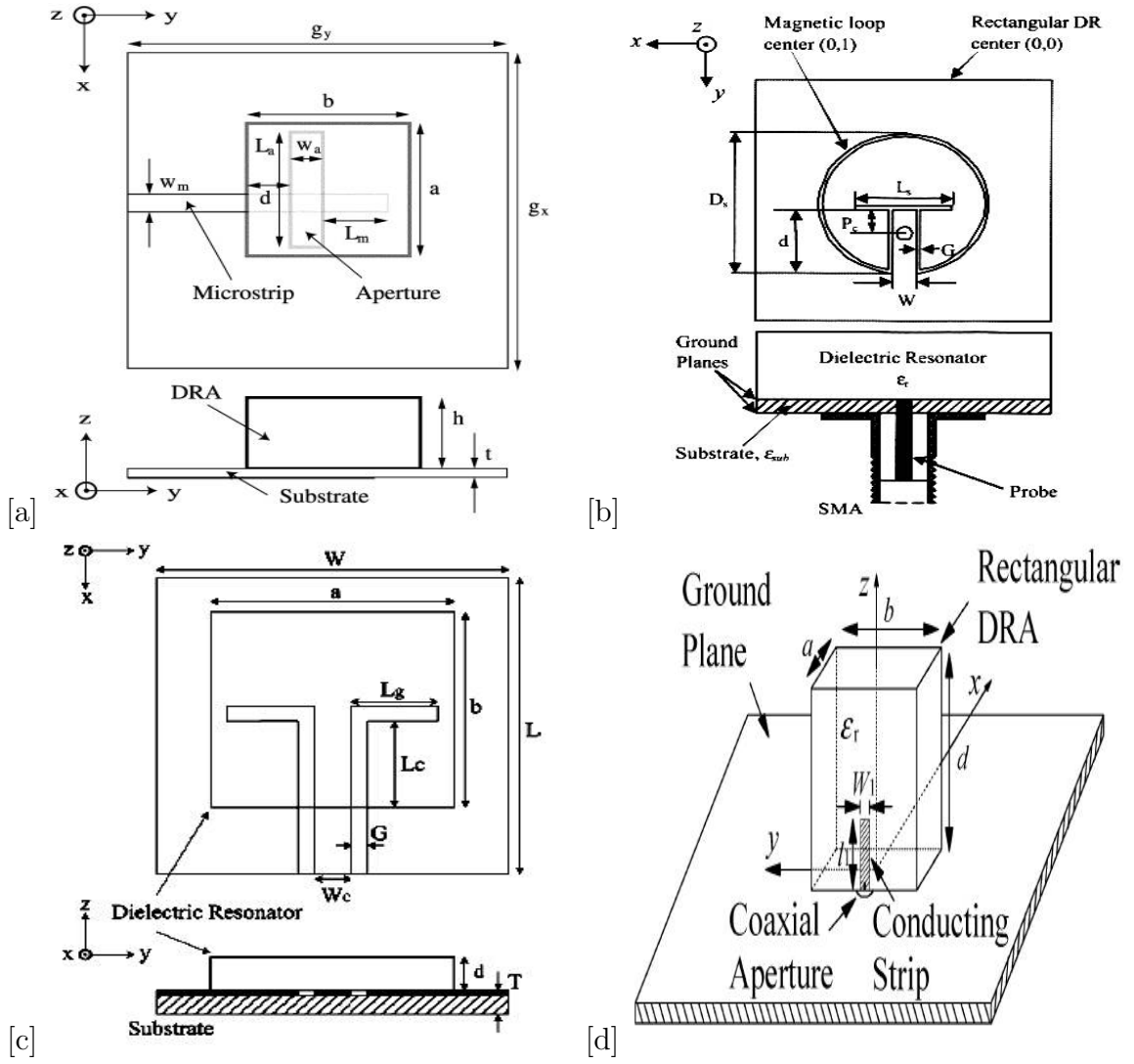

Figure 2.19: Examples of dual modes in the rectangular DRA: (a)f_c = 2.6 GHz, 25 % of BW [38] , (b) f_c = 3.8 GHz, 23 % of BW [39], (c) f_c = 5.5 GHz, 29 % of BW [40], (d) f_c = 4.5 GHz, 42 % of BW [41].

operation. A dominant mode of a RDRA has been merged with a resonance of a coplanar waveguide inductive slot which also works as an excitation of the RDRA as shown in Figure 2.19 (c). In [38–40], one mode is due to the RDRA, while the other is due to the feeding scheme. The resonance of the other mode is dependent on the dimensions of slot and coplanar waveguide. This adds extra degree of freedom for bandwidth improvement which leads to extra complexity in designs. In [41], bandwidth enhancement is achieved by exciting two nearby modes in a RDRA itself. Dual resonance is achieved by a feeding strip (fed by a probe) which is placed in the middle of the RDRA side wall as shown in Figure 2.19 (d). Two nearby modes, TE^y_{111} and TE^y_{113}, of the RDRA are excited due to proper length of the strip and dimensions of the RDRA.

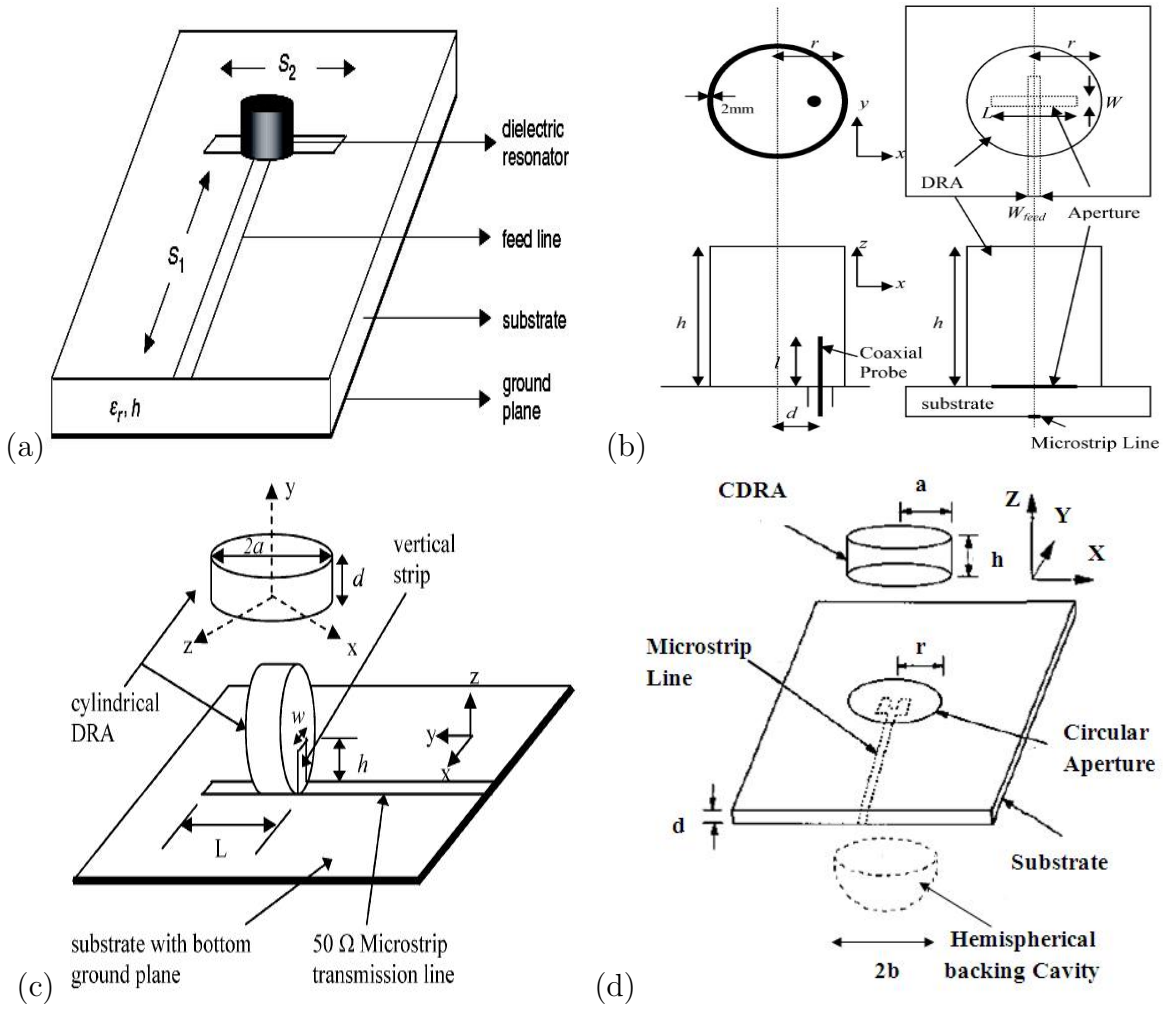

Figure 2.20: Examples of dual modes in the cylindrical DRA: (a) $f_c = 2.7$ GHz, 26 % of BW [42], (b) $f_c = 3.5$ GHz, 27 % of BW [43] , (c) $f_c = 3.0$ GHz, 35 % of BW [44] (d) $f_c = 6.5$ GHz, 38 % of BW [45].

In Figure 2.20, designs of bandwidth improvement using the cylindrical DRA (CDRA) are shown. In [42], bandwidth improvement is achieved by exciting a single mode in a cylindrical DRA (CDRA). As shown in Figure 2.20 (a), instead of a simple microstrip line, a modified T-shaped microstrip line is used for excitation. An arm length S_2 is optimized for 26 % impedance bandwidth, but when S_2 equal to 0, the feed geometry becomes the simple microstrip line, then impedance bandwidth is reduced to 12 %. In [43], bandwidth improvement is achieved by exciting two modes, a $HEM_{11\Delta}$ $(1 < \Delta < 2)$ mode at a frequency close to a $HEM_{11\delta}$ $(0 < \delta < 1)$ in a cylindrical DRA. A coaxial probe is drilled inside the CDRA as shown in Figure 2.20 (b) instead of outside the CDRA. Dual resonance is obtained by adjusting a radius to height ratios equal to 0.329. In [44], a

cylindrical DRA is oriented as shown in Figure 2.20 (c) instead of a conventional orientation. A microstrip line with a vertical strip attached to the CDRA surface is used for an excitation. Wide impedance is exhibited due to optimum dimensions and position of the vertical strip on the horizontal microstrip line. In [45], wideband operation is obtained by a CDRA using an aperture coupled with a microstrip fork-like tuning stub as shown in Figure 2.20 (d). A backing cavity is placed beneath the stub to block undesirable backside radiations. In all the reported CDRA designs, second resonance is due to the modified normal feeding scheme [42, 45], the CDRA itself [43] and the additional vertical strip [44] which leads to one more degree of freedom and add more complexity in design. Radiation patterns of these designs are quite similar, and therefore do not significantly degrade performance over the reported impedance bandwidth.

2.2.2 Stacked/Embedded DRAs

In this section, a method of bandwidth improvement, stacking/embedding of two different elements, is described. In the scheme, one resonance is due to one element and second resonance is due to second element. Both the resonances are combined and bandwidth improvement is obtained as compared to a single element. Table 2.7 lists some of reported designs of bandwidth enhancement using two or more DRA geometries vertically stacked and horizontal embedded. Table 2.7 lists the center frequency f_c, ϵ_r, excitation schemes, volume in mm^3, and % of impedance bandwidth of the reported designs of the method. Figure 2.21 shows some of exampes of reported designs of the stacked/embedded DRAs.

Table 2.7: Bandwidth achieved by Stacked/Embedded DRAs

Description	f_c (GHz)	ϵ_r	Excitation	Volume (mm^3)	% of BW	Ref.
2 stacked disk DRAs	8.9	4.5,10.5	Probe	772	25 %	[46]
2 stacked disk DRAs	5.2	9.5,82	Aperture	3626	25 %	[47]
Embedded Ring and Disk DRA	6.5	30.5,36.7	Probe	2714	38 %	[48]
2 stacked Triangle DRA	2.35	9.2	Probe	27654	64 %	[49]

In [46], wide impedance is achieved by stacking two cylindrical DRAs of different materials

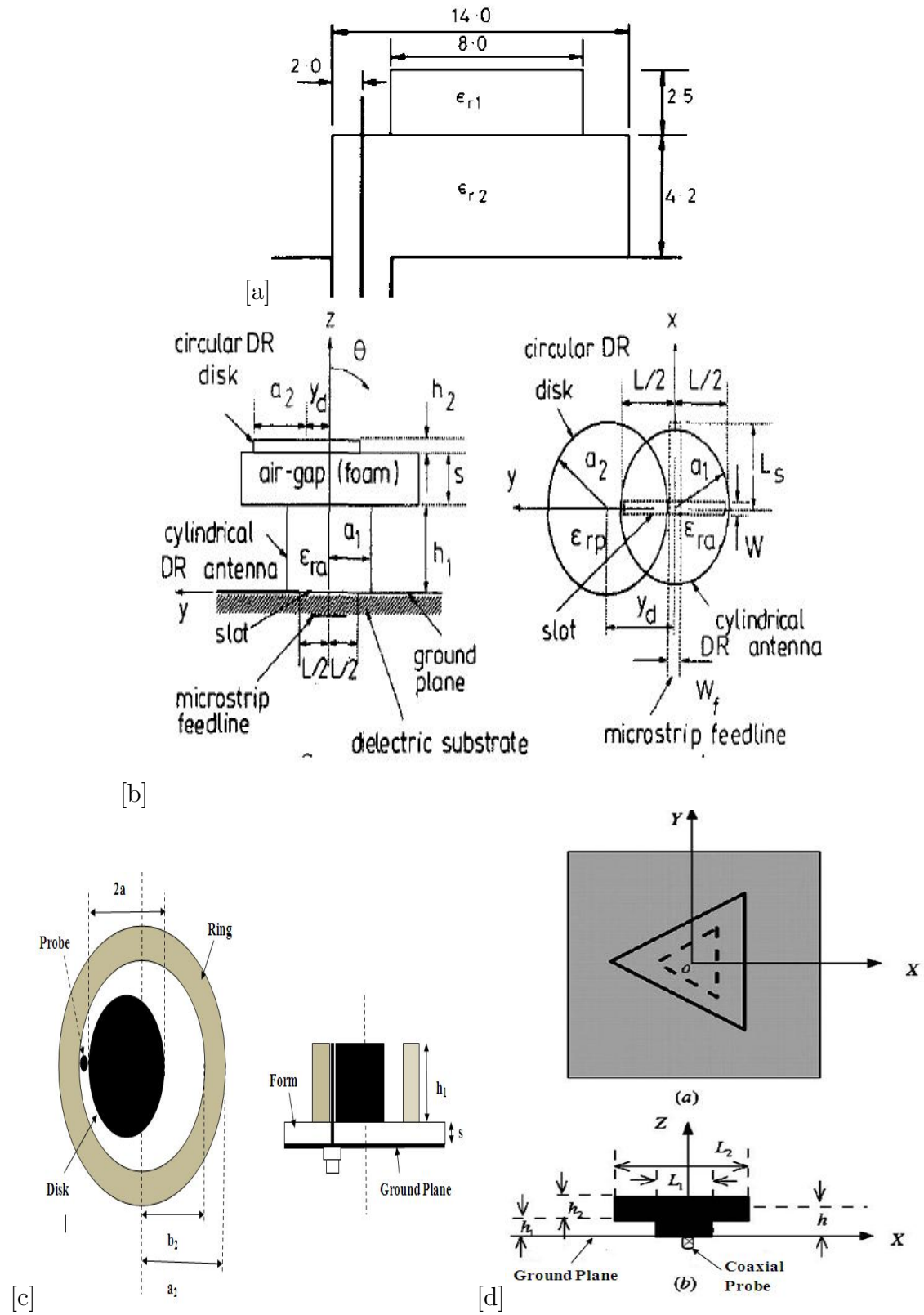

Figure 2.21: Examples of Stacked/Embedded DRAs: (a) $f_c = 8.9$ GHz, 25 % of BW [46], (b) $f_c = 5.2$ GHz, 25 % of BW [47] , (c) $f_c = 6.05$ GHz, 38 % of BW [48] (d) $f_c = 2.35$ GHz, 64 % of BW [49].

as shown in Figure 2.21 (a). A lower resonator is made of a material with ϵ_r of 4.5, diameter of 14 mm and height of 4.2 mm. An upper resonator is made of a material with ϵ_r of 10.5, diameter of 8 mm and height of 2.5 mm. A coaxial probe is passed through the lower resonator (resonated at 10 GHz) and ends 1.2 mm above its top to couple with the upper resonator (resonated at 12 GHz). The antenna is reported 25 % bandwidth. In [47], a cylindrical DRA (driven element) having ϵ_r of 9.5 is loaded by a low-profile circular dielectric resonator (DR) disk (parasitic element) having dielectric constant of 82. An air-gap and offset between the driven and parasitic elements are shown in Figure 2.21 (b). This design has demonstrated 25 % impedance bandwidth due to the loading of the low-profile disk on the very high permittivity resonator. It is required to optimize the air gap and offset to achieve wide bandwidth. In [48], a low-profile cylindrical DRA of relative permittivity of 36.7 is embedded into a cylindrical ring of the same height but with different relative permittivity of 30.7. The structure is excited by a coaxial probe with an air-gap between a ground plane and DRs as shown in Figure 2.21 (c). This structure has demonstrated 38 % bandwidth improvements and has compact geometry (aspect ratio of 6). In [49], a triangular shaped DRA with two equilateral-triangle cross sections are placed on a finite ground plane. The two equilateral triangles are made from same dielectric material having different heights and side lengths. The side length of the top triangle is chosen to be larger than the side length of the bottom triangle as shown in Figure 2.21 (d), An air-gap between the top equilateral triangle and the ground plane is formed in order to decrease of radiated Q-factor and consequently gives increase in bandwidth. The structure has exhibited 64 % of impedance bandwidth. Improved bandwidths using multiple DRAs in various stacked and coplanar embedded configurations are experimentally demonstrated with impedance bandwidth ranging from 24 % to 64 %. There are no closed form relations yet derived for bandwidth improvement by this method [46–49].

2.2.3 Modified Shaped of DRAs

In this section, instead of simple available geometries of the DRA, modified shapes of the DRAs are discussed for bandwidth improvement. As described in section 2.1.2, low Q_{rad} has exhibited higher impedance bandwidth. The low Q_{rad} can be achieved by adjusting

the aspect ratios of the basic shapes which requires thorough insight of the theoretical analysis. Another way to lower the Q_{rad} is based on a study reported by Verplanken and Van Bladel for dielectric ring resonator (DRR) [50]. They show that the Q_{rad} of a dielectric ring resonators can be reduced by increasing a ratio of inner to outer radii, thus lowering an amount of stored energy. The same principle, by removing some portion of the basic shapes of DRAs, can be applied for bandwidth improvement lead to modifying the shapes. Then, an effective dielectric constant is reduced as compared to a solid DRA. This results decrease in the Q_{rad} and increase in bandwidth.

Table 2.8: Bandwidth achieved by Modified shapes DRAs

Description	f_c (GHz)	ϵ_r	Excitation	% of BW	Ref.
Notched RDRA	11.9	10.8	Aperture	28 %	[51]
Truncated Tetrahedron DRA	2.5	12	Probe	40 %	[52]
Semi Trapezoid DRA	7.75	9.8	Probe	62 %	[53]
Flipped Staired Pyramid DRA	10.85	12	Aperture	62 %	[54]
L-Shaped DRA	6.02	9.8	Patch	71 %	[55]

Figure 2.22 shows some of reported designs on modified shaped DRAs and Table 2.8 summarizes the center frequency f_c, ϵ_r, excitation schemes, and % of impedance bandwidth of reported modified shapes of DRAs. In [51], a slot fed RDRA with a centre portion removed is shown in Figure 2.22 (a). This structure and its image form a rectangular dielectric ring. The antenna has 28 % impedance bandwidth. In [52], a novel shaped DRA is investigated for wideband operation. As shown in Figure 2.22 (b), a truncated tetrahedron with a narrow base attached to a ground plane is used to achieve 40 % of impedance bandwidth. The performance is achieved by proper choice of height, side lengths of an equitrianglular base and top surface of the tetrahedron DRA. As shown in Figure 2.22 (c), the semi-trapezoid DRA is investigated for 60 % impedance bandwidth. The structure resonates multiple modes such as TE^{y}_{111}, TE^{y}_{113} and TE^{x}_{121} and TE^{y}_{1mn} with (m, n > 1), due to the shape and position of a coaxial probe which lead to matching input impedance of these modes to characteristic impedance of the probe [53]. In [54], 71.4 % impedance bandwidth is achieved by a simple inverted L-shaped DRA. This structure is excited by a conformal inverted-trapezoidal patch which is connected to a microstrip line

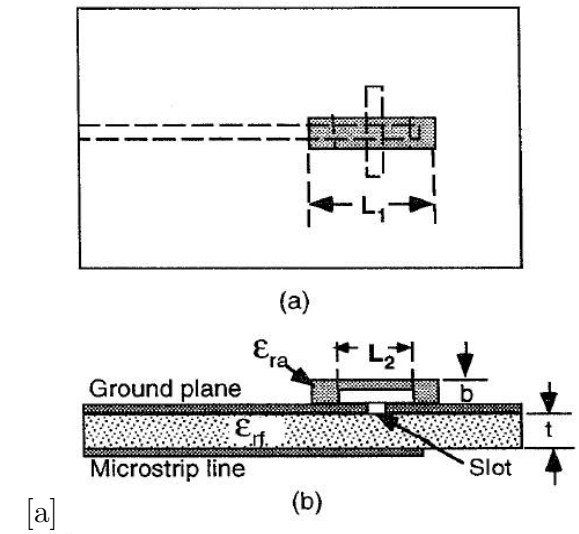

[a]

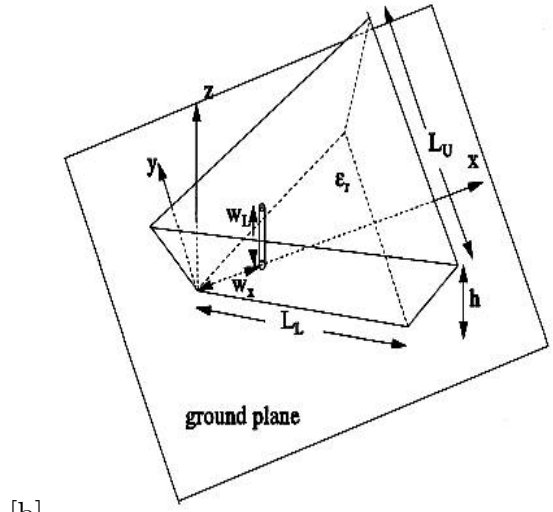

[b]

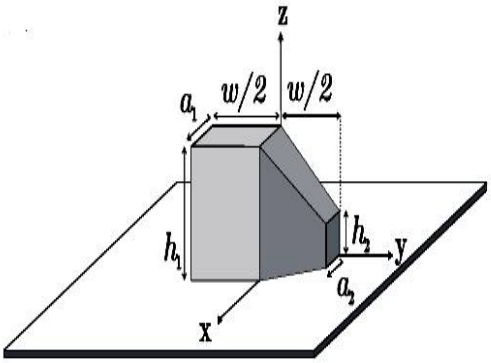

[c]

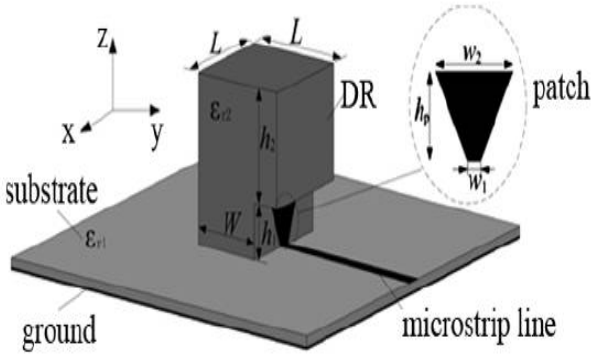

[d]

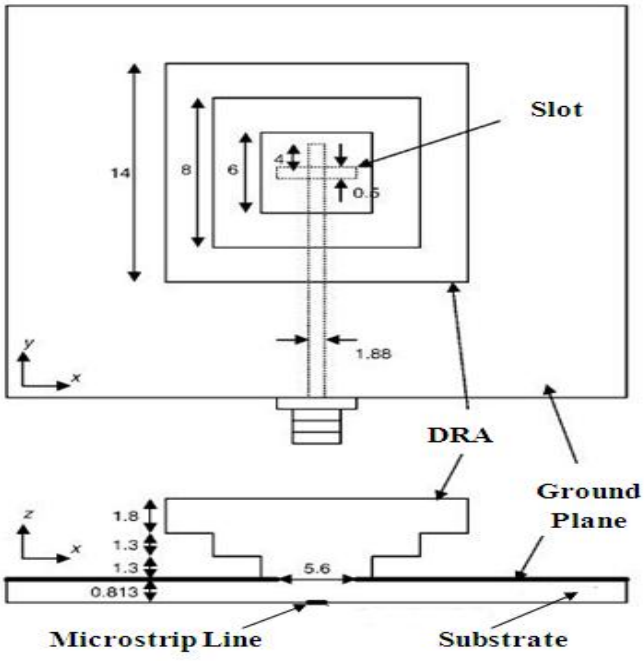

[e]

Figure 2.22: Examples of Modified shapes of DRAs: (a) $f_c = 11.9$ GHz, 28 % of BW [51], (b) $f_c = 2.5$ GHz, 40 % of BW [52] , (c) $f_c = 7.75$ GHz, 62 % of BW [53] (d) $f_c = 6.02$ GHz, 71 % of BW [54], (e)$f_c = 10.85$ GHz, 62 % of BW [55]

as shown in Figure 2.18 (d). In [55], a resonator is constructed on a two-step flipped stair geometry as shown in Figure 2.22 (e), is claimed to have 62 % impedance bandwidth. Thickness of each step, from top to bottom, is 1.8 mm, 1.3 mm and 1.3 mm and side wall of each step, from bottom to top, is 6 mm, 8 mm and 14 mm. A small base of the resonator is placed at the center of a narrow rectangular shaped aperture. In all the modified shaped DRA designs, improvement in impedance bandwidth is achieved at the cost of difficulty in fabrication and optimization of physical parameters.

2.2.4 Hybrid DRAs

In previous sections, it is described that 25 % to 71 % impedance bandwidth was achieved by merging modes of DRAs, stacking/embedding of two different DRAs and modifying the basic shapes of DRA. In these methods, low dielectric constant, ϵ_r of 10, is used in most of the reported designs. In the literature, materials with dielectric constant less than 10 were not used for the DRA. Till now, none of these methods gave around 100 % impedance bandwidth. For ultra wideband bandwidth (about 100 %), a hybrid kind of a structure is required. In the hybrid antenna, the DRA is attached with other kind of antenna such as microstrip patch antenna, monopole, slot radiator, coplanar waveguide inductive slot etc. Each antenna in the hybrid structure is designed to radiate in its separate band. If the separate bands are close enough, then, the hybrid resonator can offer ultra wideband operation. In the hybrid structure, ultra wideband bandwidth can be possible by using the bandwidth improvement techniques of the DRA as well as the other antennas. Figure 2.23 show some of reported design of the hybrid DRAs. Table 2.9 tabulates the center frequency f_c, ϵ_r, excitation schemes, and % impedance bandwidth of the reported hybrid DRA designs.

Table 2.9: Bandwidth achieved by Hybrid DRAs

Description	f_c (GHz)	ϵ_r	Excitation	% of BW	Ref.
Annualar DRA and Monopole	11.75	10	Probe	89 %	[56]
Annualar DRA and Monopole	10.0	10	Probe	110 %	[57]
Conical DRA and Monopole	4.35	10	Probe	117 %	[58]

Figure 2.23 (a) shows hybrid structure having 89 % impedance bandwidth by combining properties of a quarter-wave monopole antenna with an annular DRA. In this arrangement, general design steps for achieving ultra wideband performance are; 1) a quarter-wave monopole is designed to resonate at a lower end of the frequency band, 2) a DRA is designed to have a resonance near an upper end of the required spectrum, 3) the resonance frequency of the dominant mode of DRA should be chosen approximately 2.2 times the resonance frequency of the $\frac{\lambda}{4}$ monopole, 4) height of the DRA, required to position the second resonance in the center of the required spectrum, is a function of the relative permittivity of the material and an outer radius of the DRA (for a DRA of ϵ_r of 10, ratio h/a equal to 1 is used as starting point), and 5) a small air gap (about $\frac{\lambda_L}{100}$, λ_L: the lower operating frequency) should require between the monopole and an inner radius of the annular DRA. Using these guidelines, the ultra wideband hybrid resonator is optimized for the required spectrum [56].

In [57], A T-shaped monopole antenna loaded with an annular DRA (as shown in Figure 2.23 (b)) is reported to achieve 110 % ultra wideband. The reported bandwidth is achieved by adjusting a length of the monopole, load arm of the T-shaped monopole and dimension of the annular DRA. In [58], 117 % impedance bandwidth is achieved by a hybrid resonator which consists of a skirt monopole loaded with an inverted conical ring shape dielectric resonator. In this structure, the monopole antenna, operating at 2 GHz, is used as an excitation for the DR. The structure is shown in Figure 2.22 (c). In this structure, three different methods (modified shape, multiple resonance and hybrid structure) of impedance matching, low dielectric constant, and a ground plane shaping procedures have been applied to increase the antenna bandwidth. By shaping the DR and impedance matching methods, higher part of the frequency bandwidth can be controlled by exciting a higher order mode with the dominant resonant mode inside the DR. The lower part of impedance bandwidth can be adjusted using the ground plane shaping and matching method at the feed point of the monopole antenna. In these hybrid antennas, the UWB operation is achieved by using the annular DRA [56, 57] and the conical ring DRA [58] with the $\frac{\lambda}{4}$ monopole [56], the T-shaped monopole [57] and the skit monopole [58]. It is seen that there are many physical parameters of the both antennas (DRA and monopole) which are optimized for UWB operation. This method uses various

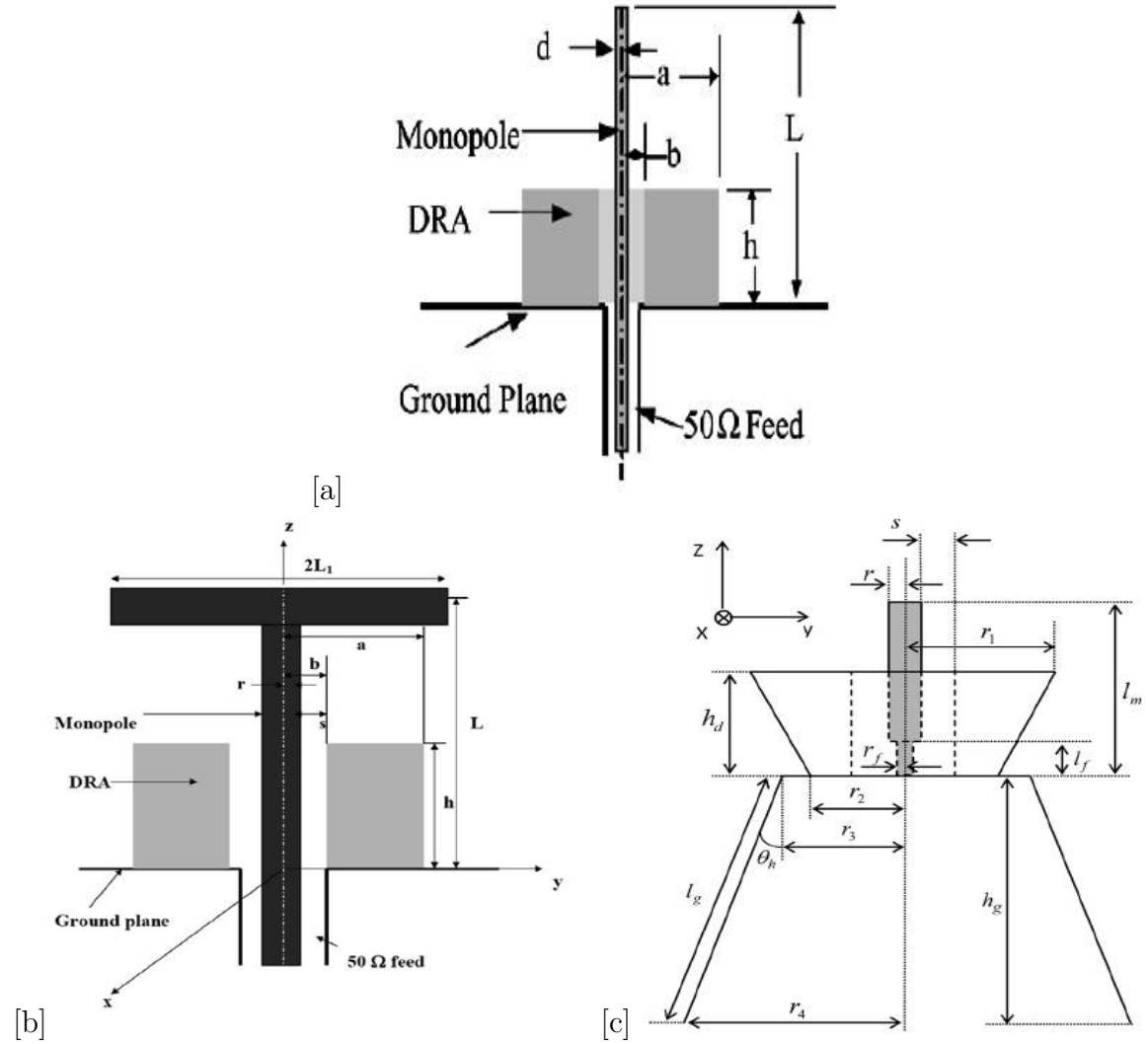

Figure 2.23: Examples of hybrid DRAs: (a) $f_c = 11.75$ GHz, 89 % of BW [56] , (b) $f_c = 10.0$ GHz, 110 % of BW [57] (c) $f_c = 4.35$ GHz, 117 % of BW [58]

techniques of bandwidth improvement.

2.3 Literature Survey on Narrowband DRA

Numerous wireless systems for consumer wireless devices require compact antenna to be integrated into small packages such as cell phones, laptop, palmtop, smart watch, and other portable devices. A key parameter for the wireless systems is a communication range which is a deciding factor in RF solution. Fundamentally, the range is dictated by a communication data rate. There are many options to increase range by reducing data rate. Two solutions are; scaling receiver bandwidth to the signal to reduce noise seen by the receiver (narrowband system) and adding coding gain on a higher rate signal to com-

bat a high receiver noise in a wideband receiver. Disadvantages of coding gain system are low spectrum efficiency, reduce communication reliability, number of devices in a given area and battery lifetime. Narrowband technique for long range and reasonably low date rate is widely accepted by an industry since it gives an optimum tradeoff between range and a transmission time [59]. In this section, various designs of narrowband DRAs are presented. As described in section 2 of this chapter, using high dielectric constants, the dimensions of the DRA are reduced. The low profile design in which the height of the DRA is in order of $\frac{\lambda_0}{20}$. Compact designs are those structure that have largest dimension of the DRA is in order of $\frac{\lambda_0}{10}$ [60].

2.3.1 Single Narrowband DRA

In this section, reported designs of low-profile and compact single narrowband DRAs are presented and shown in Figure 2.24. Table 2.10 summarizes the center frequency f_c, ϵ_r, largest and smallest dimensions (in terms of λ_0), excitation schemes, volume in (mm^3), and % of impedance bandwidth of the reported narrowband DRA designs. In [61], Mongia et al, a low-profile RDRA is fabricated from a material of high permittivity having dielectric constant of 100 as shown in Figure 2.24 (a). As radiated Q-factor is inversely proportional to ϵ_r, the Q - factor becomes high, leads to reduction in impedance bandwidth. The RDRA has 3.2 % impedance bandwidth. In this, a TE^z_{111} mode is excited as the length of the slot is along z-direction ('d' dimension). The resonance frequency of the mode can be determined using the relation (2.16). In the design, the dimensions of the RDRA were chosen such that d,a >> b, then equations (2.13) and (2.16) lead to following simple relation for height, b in terms of the resonance frequency f_r

$$b \approx \frac{c}{4f_r\sqrt{\epsilon_r}} \tag{2.30}$$

The resonance frequency of the low-profile RDRA can be determined by the height of the RDRA. In [62], a circular disk DR antenna shown in Figure 2.24 (b) made of a high permittivity material is reported with 3.8 % impedance bandwidth. The smallest dimension, height, is 0.028 λ_0. The antenna is resonated at dominant mode and the

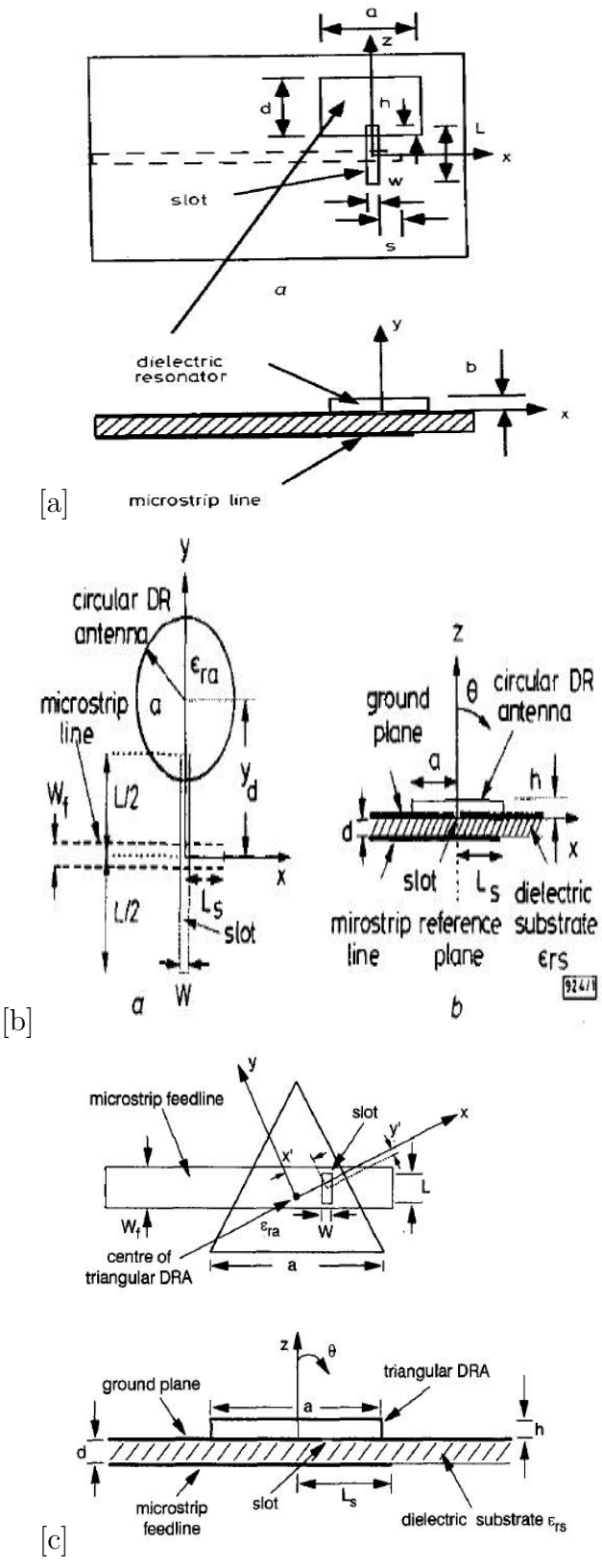

Figure 2.24: Examples of single narrowband low-profile DRAs: (a) $f_c = 7.72$ GHz, 3.2 % of BW [61], (b) $f_c = 4.25$ GHz, 3.8 % of BW [62] , (c) $f_c = 7.59$ GHz, 3.0 % of BW [63]

Table 2.10: Reported single narrowband low-profile DRAs

DRA Shapes	f_c (GHz)	ϵ_r	Largest Dimension	Lowest Dimension	Feeding Method	Volume (mm^3)	% of BW	Ref.
Rectangular	7.72	100	$0.327\lambda_0$	$0.026\lambda_0$	Slot	161	3.2 %	[61]
Cylindrical	4.25	82	$0.354\lambda_0$	$0.028\lambda_0$	Strip	981	3.8 %	[62]
Triangular	7.59	82	$0.506\lambda_0$	$0.028\lambda_0$	Slot	110	3.0 %	[63]

resonance frequency can be determined by a following equation.

$$f_{110}^{TM} \approx \frac{c}{4h\sqrt{\epsilon_r}} \tag{2.31}$$

In [63], an aperture coupled equilateral-triangular DR antenna of a material with very high permittivity is investigated as shown in Figure 2.24 (c). Impedance bandwidth of 3.0 % is reported and a fundamental TE_{10-1}^{TM} mode at 7.59 GHz is excited. The resonator has a >> h, the resonance frequency of the mode can be determined by following equation.

$$f_{10-1}^{TM} \approx \frac{c}{4h\sqrt{\epsilon_r}} \tag{2.32}$$

The equations (2.31), (2.32), and (2.33) show that the resonance is due to waves are bouncing between the top and the bottom faces of the DRAs, and hence the resonance frequency is insensitive to length and width of the RDRA [61], the radius of the circular disk DR [62] and side length of the equilateral-triangular DRA [63]. From these, it is observed that the low-profile DRA made of high permittivity material has no degree of freedom [61–63].

There are some other methods are reported in literature to achieve compact narrowband DRAs. Figure 2.25, 2.26, and 2.28 show few examples of the compact single narrowband DRA which are achieved by loading of metal plates. Table 2.11 lists the center frequency f_c, ϵ_r, largest and smallest dimensions (in terms of λ_0), excitation schemes, volume in (mm^3), and % of impedance bandwidth.

In [64], a RDRA loaded with a patch antenna (shown in Figure 2.25), in which a L-shaped

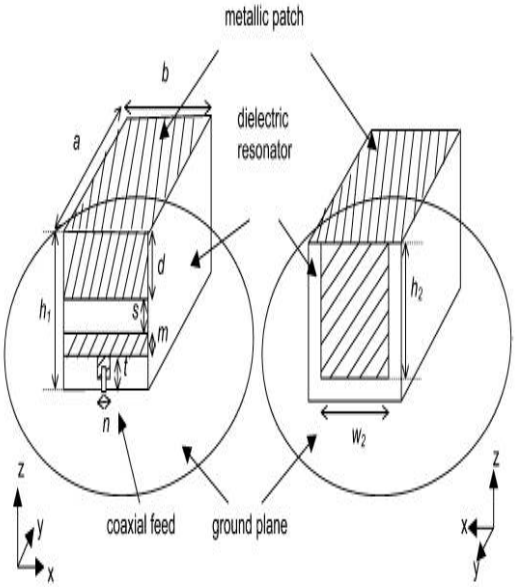

Figure 2.25: An example of compact single narrowband DRAs: f_c = 1.27 GHz, 2.2 % of BW [64]

Table 2.11: Reported single narrowband compact DRAs

DRA Shapes	f_c (GHz)	ϵ_r	Largest Dimension	Lowest Dimension	Feeding Method	Volume (mm^3)	% of BW	Ref.
Rectangular	1.27	10	$0.12\lambda_0$	$0.064\lambda_0$	Probe	9129	2.2 %	[64]
Rectangular	2.09	10	$0.11\lambda_0$	$0.10\lambda_0$	Aperture	3600	2.9 %	[65]
Hybrid DRA	3.5	90	$0.29\lambda_0$	$0.039\lambda_0$	T-shaped strip	585	2.4 %	[66]

folded patch and supported by the RDRA is reported with impedance bandwidth of 2.2 %. The L-shaped folded metallic patch is attached on the RDRA. The horizontal portion of the patch is covered an upper face of the RDRA and vertical portion of the patch (W_2 x h_2) is adhered to a back side of the RDRA. The vertical portion of L-shaped patch is not short-circuited to a ground plane. Another small vertical portion of the upper face of the patch with length of d is extended from an edge of the upper face to the front side of the RDRA. This portion of the folded patch and the T-shaped strip is attached to the front side of the RDRA and separated with a gap of s. A coaxial probe is connected to the vertical portion of the T-strip as shown in Figure 2.25. In this structure, for better impedance matching, various dimensions of patch and RDRA are optimized.

Recently, a new radiating $TE^x_{\delta 01}$ mode is reported in [65] with two metal strips placed on

side walls, perpendicular to the ground plane in a hybrid rectangular DRA mounted on a ground plane (shown in Figure 2.26(a)). A reference antenna 1, is a conventional RDRA, is shown in Figure 2.26 (b). A reference antenna 2, is the proposed antenna with height of 6.2 mm, is shown in Figure 2.26 (c). The structures are fed by a coupling slot. The comparison of E-field distribution for the $TE^x_{\delta 01}$ mode and a conventional $TE^x_{\delta 11}$ modes are shown in Figure 2.27. Due to the specific field distributions, the $TE^x_{\delta 01}$ mode can work at a much lower frequency than the conventional mode in the RDRA with the

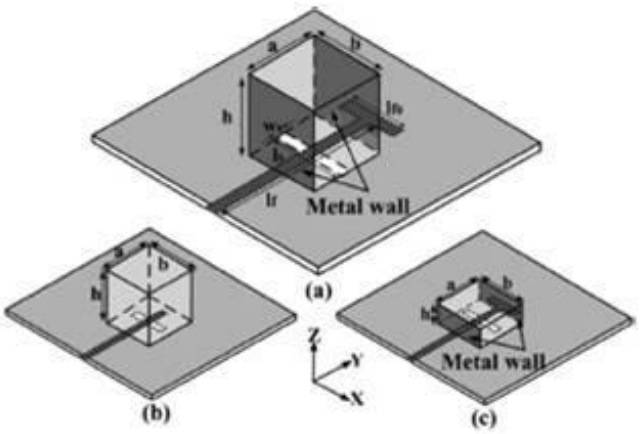

Figure 2.26: An example of compact single narrowband RDRA: (a) Geometries of the RDRA for (a) the proposed antenna: $TE^x_{\delta 01}$ mode, (b) Reference antenna 1 : the conventional $TE^x_{\delta 11}$ mode, (c) Reference antenna 2: the proposed $TE^x_{\delta 01}$ mode [65]

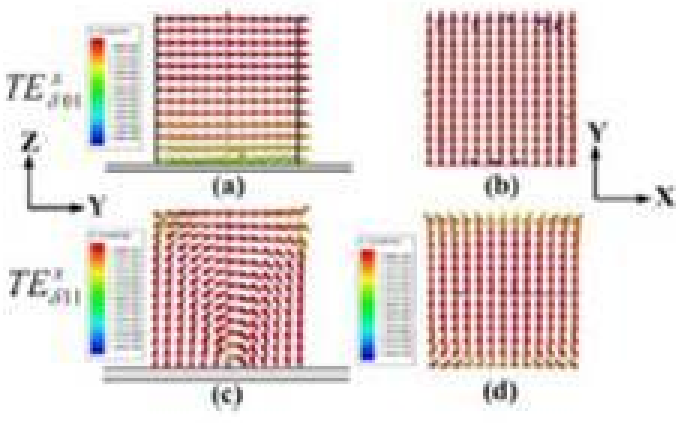

Figure 2.27: Simulated E-field distributions in the $TE^x_{\delta 01}$ mode (a) side view, (b) top view, and in the $TE^x_{\delta 11}$ mode (c) side view, (d) top view [65]

same dimensions. Comparing the proposed DRA to reference antenna 1, both antennas have the same size but resonance at different frequencies. This is due to the addition of

two vertical metal plates on the RDRA, the proposed antenna worked at 1.74 GHz, much lower than that of reference antenna 1 (f_c equal to 3.93 GHz). Comparing the reference antenna 1 to the reference antenna 2, it is seen that by decreasing the height of the metal-coated RDRA from 16 to 6.2 mm, both the antennas work almost at same frequency (f_c equal to 3.94/3.95 GHz). This shows that for a given frequency, the proposed structure is low-profile design. Due to the two metal plates, there is decrease in impedance bandwidth from 16 % to 2.9 %. The resonance frequency is independent of dimension along the y direction.

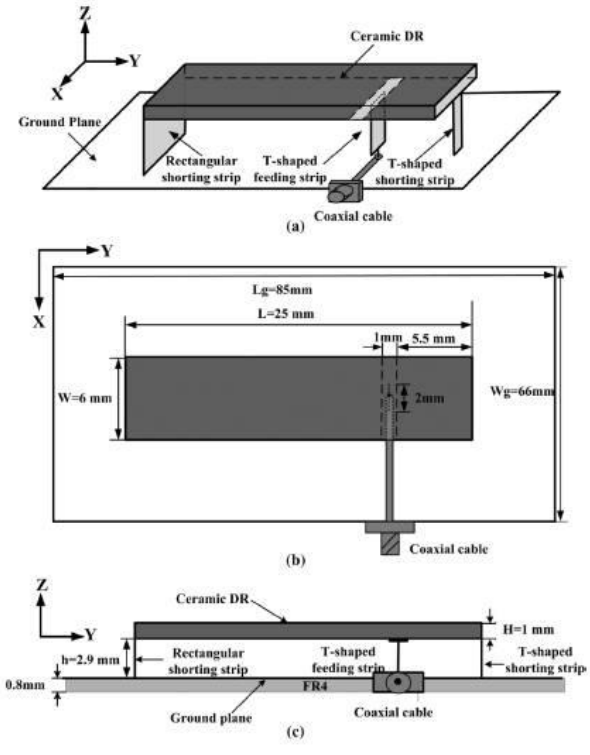

Figure 2.28: An example of compact single narrowband rectangular hybrid DRA: Geometries of the RDRA for (a) 3-D view, (b) Top view, (c) Side view [66]

Also, a $TE^x_{\delta 01}$ mode [66] is demonstrated in a hybrid rectangular dielectric-air-metal strips composite resonator antenna as shown in Figure 2.28. Figure 2.29 shows E-field distributions of the $TE^x_{\delta 01}$ mode. From the Figure 2.29, the E-fields of the $TE^x_{\delta 01}$ mode indicates that they vary from maximum to zero as the height decreases and vanish when they are closed to a ground plane. Since no horizontal electric fields exist over the ground plane, it is difficult to excite this type of mode in a RDRA directly mounted on the metallic ground plane by exciting methods namely slot, CPW, and microstrip coupling.

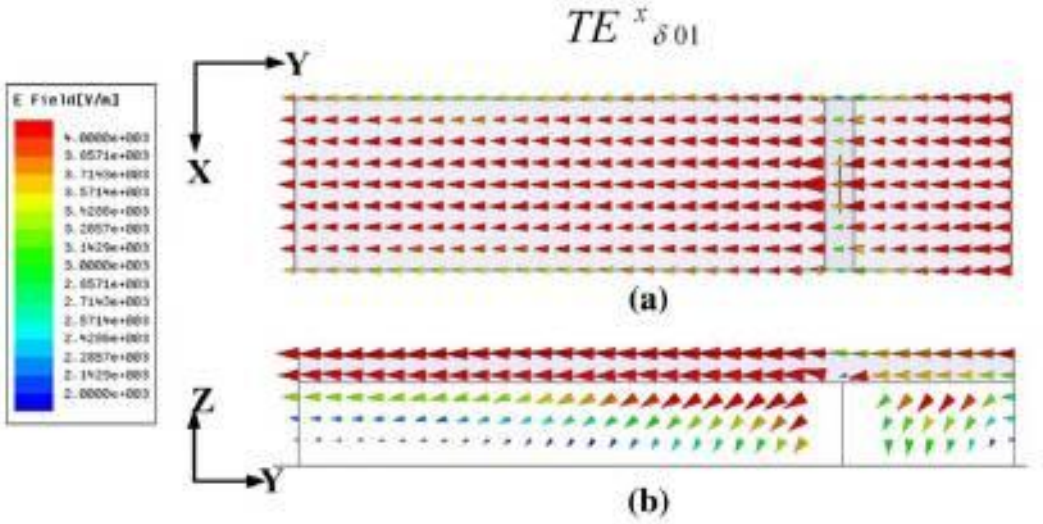

Figure 2.29: Simulated E-field distributions in the $TE^{x}_{\delta 01}$ mode in the rectanglar hybrid DRA: (a) Top view, (b) Side view [66]

As shown in Figure 2.28, an air-gap between the ceramic RDRA and the ground plane is introduced. This air gap with the ceramic RDRA forms the hybrid DR. The inserted air layer along the z-axis does not affect a homogeneity of the E-fields over the x-y plane. In this design, the RDRA made of a high permittivity material is used to maintain compactness. In order to satisfy the special boundary condition of the mode, two ends of the DRA are connected to the ground plane by metal strips, one with the rectangular shape, and other with a T-shape. A feeding mechanism is adopted another T-shaped metal strip attached to a bottom face of the RDRA and connected to an inner conductor of a coaxial probe as shown in Figure 2.28 (a). Better impedance match can be achieved by adjusting a distance between the feeding strip and the T-shaped shorting strips (5.5 mm). Simulated E-field distributions are shown in Figure 2.29. As shown in Figure 2.29 (a), E-fields distributed along the y-axis are nearly homogeneous, which is represented by the subscript 0. At the interfaces between ceramic material and air, E-fields along the x-axis show small variation. Therefore, δ ($\delta \rightarrow 0$) is used to represent almost uniform E-field distribution. As shown in Figure 2.29 (b), the horizontal E-fields vary from maximum to zero as the height decreases from the top face of the RDRA to the ground plane, which is represented by the subscript 1. The mode has the resonant frequency of 3.5 GHz with 2.43 % impedance bandwidth.

In [64–66], the compact and narrowband DRA designs are reported by using the met-

allization on the surfaces of the RDRA. This is second method to achieve the narrowband DRA design by metallization on the DRA. In [65, 66], metallization on appropriate surfaces of the RDRA, it is found that the new radiating $TE^{x}_{\delta 01}$ mode is investigated in the RDRA. As compared to a conventional mode ($TE^{x}_{\delta 11}$) of the RDRA, the new mode has lower resonant frequency and impedance bandwidth.

2.3.2 Literature Survey on Dual Narrowband DRAs

A dual band antenna provides an alternative to a wideband planar antenna for applications in which large bandwidth is needed for operating at two separate transmit-receive bands. When the two operating bands are far apart, a dual band antenna can be conceived to avoid use of separate antennas. Antennas that operate in dual- or multi-bands that can be integrated on a package for mass production are in high demand. Many of applications have additional requirement that the antennas to be small and conformal. DRAs are widely accepted for these requirements due to their important characteristics, as discussed before. In principle, dual band DRAs should operate with similar features, both in terms of radiation and impedance matching at two separate frequencies. Obtaining these features by using planar technologies is not a straightforward matter [67, 68], particularly when an intrinsic structural and technological simplicity of the DRA are to be preserved. In this section, reported designs of dual narrowband DRAs are presented

Table 2.12: Reported dual narrowband DRAs

DRA Shapes	f_c (GHz)	ϵ_r	Largest Dim.	Lowest Dim.	Feeding Method	Volume (mm^3)	% of BW	Ref.
Conical DRA	2.6 3.9	9.5	$0.195\lambda_0$	$0.195\lambda_0$	Slot	—-	—	[69]
Circular Disk DR	2.42 5.69	25	$0.281\lambda_0$	$0.063\lambda_0$	Slot	568	3.3 % 5.7 %	[70]
Rectangular	2.46 5.23	10	$0.262\lambda_0$	$0.131\lambda_0$	Slot	1058	4.48 % 6.17 %	[71]
Rectangular	3.47 5.3	10	$0.368\lambda_0$	$0.186\lambda_0$	Slot	4040	15.3 % 8.3 %	[72]

and shown in Figure 2.30. Table 2.12 summarizes the center frequency f_c, ϵ_r, largest and smallest dimensions (in terms of λ_0), excitation schemes, volume in (mm^3), and % of

impedance bandwidth of the reported dual narrowband DRA designs.

In [69],a hybrid resonator, consists of a conical dielectric resonator antenna and a pair of eccentric ring slot, is reported for dual narrowband operation. As shown in Figure 2.30 (a), the two eccentric ring slots are etched on a ground plane. The inner slot is directly driven by a coaxial probe and the inner slot excites the outer slot through electromagnetic coupling. The DRA is fed by the coupled dual ring slots. By optimizing radius, width, and position of each ring slot as well as the size of the conical DRA, the structure is operated in the desired dual narrow frequency range. An upper band is due to the DRA, while a lower band is due to the outer ring slot. In [70], a compact dual-band circular disk DRA using a parasitic C-slot fed by a microstrip line is reported as shown in Figure 2.30 (b). An offset distance between the center of the DRA and a ground plane, dimensions of the C- parasitic slot as well as DRA are optimized. The antenna is resonated at 2.4 GHz and 5.69 GHz with 3.3 % and 5.7 % impedance bandwidth, respectively. A lower band is due to the C-parasitic slot with dipole like patterns and an upper band is due to the DRA with broadband patterns. In [71], a RDRA is placed on top of a slotted cavity to form a hybrid dual-band antenna which is reported at 2.46 GHz and 5.23 GHz with 4.48 % and 6.17 % impedance bandwidth, respectively. As shown in Figure 2.30 (c), a zonal slot is cut onto a square cavity made of a copper plate. The zonal slot divides the cavity into a lower and an upper part. It is found that the lower part of cavity is required for dual-band operation to match the impedance of the two resonant modes. The upper part is supported by two pieces of foam, whereas the lower part is directly connected to a ground plane. On top of the cavity, the RDRA is coupled through the upper rectangular slot. A L-probe bisects the upper coupling slot. A lower band is due to the zonal slot and an upper band is due to the RDRA which is operated in a TE^{y}_{111} mode. Dual resonance in the structure after optimizing the dimensions of RDRA, metal cavity and slot are achieved. In [72], Fang and Leung have reported a rectangular DRA excited by coupling slot as shown in Figure 2.30 (d). In this structure, two modes (TE^{y}_{111}, TE^{y}_{113}) of the RDRA are excited. A coupling slot is used only for feeding the RDRA. The structure is resonated at 3.4 GHz and 5.18 GHz with 15.3 % and 8.3 % impedance bandwidth, respectively. This is simplest scheme to excite the dual band but it is not narrowband because low permittivity material is used. It is observed that one band is achieved by

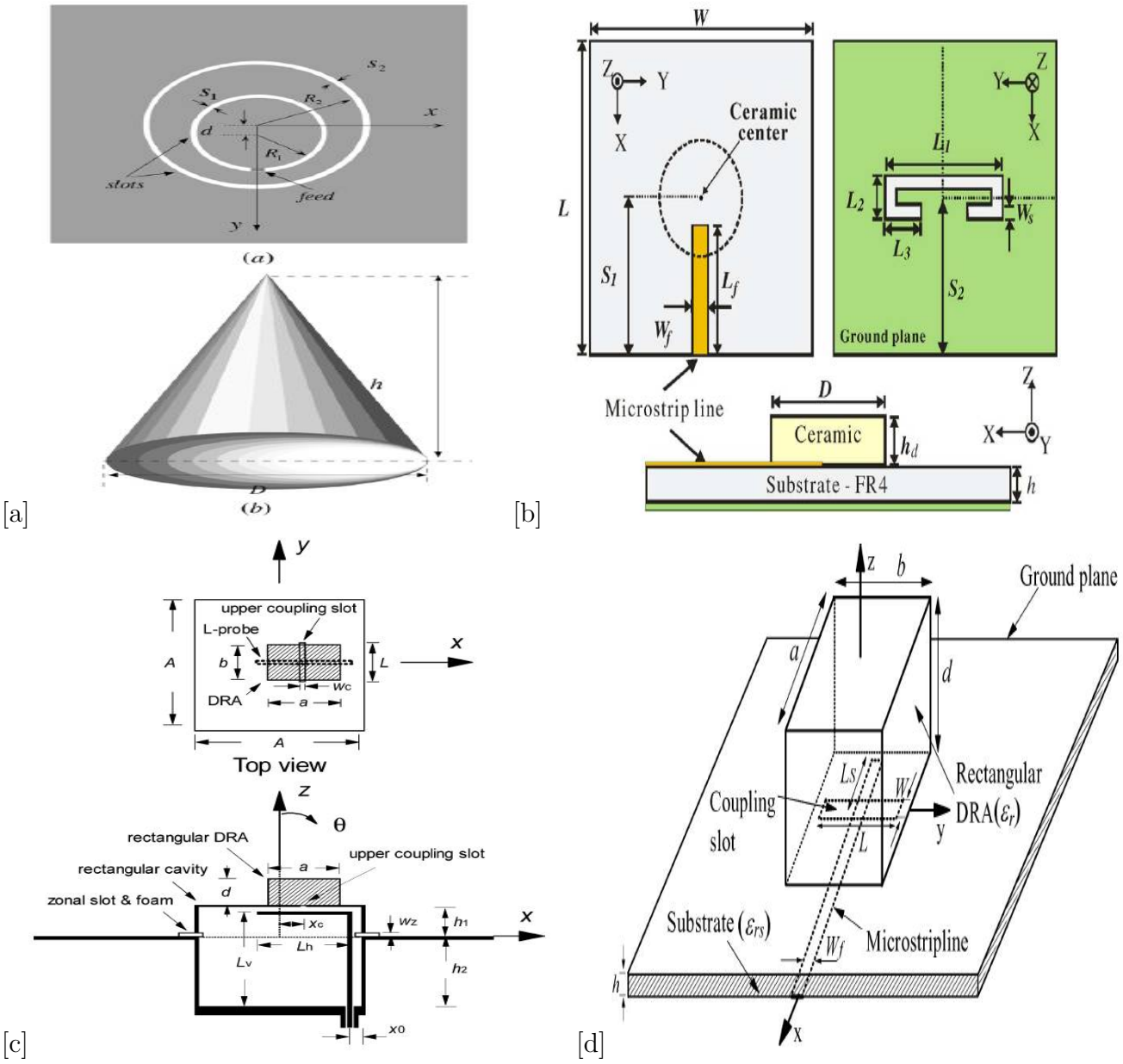

Figure 2.30: Examples of dual narrowband compact DRAs: (a) $f_c = 2.6$ GHz,3.9 GHz DD % of BW [69], (b) $f_c = 2.42$ GHz,5.69 GHz 3.3%,5.7 %of BW [70], (c) $f_c = 2.46$ GHz,5.23 GHz 4.8%,6.17 %of BW [71], (d) $f_c = 3.47$ GHz,5.3 GHz 15.3%,8.3 %of BW [72]

the DRA, whereas the second band is achieved by feeding methods such as eccentric ring [69], parasitic slot [70], and zonal slot [71]. This will add extra degree of freedom for dual narrowband DRA. Dual narrowband can be possible by exciting two RDRA modes by proper choosing the dimensions and high permittivity of the RDRA [72].

2.4 Conclusion

An isolated RDRA has three independent dimensions. The modes of the RDRA can be TE to any of three dimensions. If the dimensions of RDRA are such that a > b > d, the modes in the order of increasing resonant frequency are TE^{z}_{111}, TE^{y}_{111}, and TE^{x}_{111}. The analysis of all the modes is similar. Using dielectric waveguide model (DWM) and mixed magnetic wall model (MMW), it is noticed that resonant frequency is dependent on the physical parameters such as dielectric constant of material, length, depth and height. Analysis on resonance frequency as a function of dielectric constant for different values of height, width and length is carried out. Also analysis on resonance frequency for different aspect ratios (length/height and depth/height) is performed. From this, it is noticed that it is necessary to optimize all the physical parameters for prediction of resonance frequency. For the given RDRA, it is noticed that Q_{rad} is increased as dielectric constant increases. Impedance bandwidth is decreased when dielectric constant increases. For low dielectric constant material, impedance bandwidth is large as compared to high dielectric constant material. It is also observed that there is tradeoff between impedance bandwidth and size of the RDRA. For different values of aspect ratios (depth/height and length/height), analysis on impedance bandwidth and Q_{rad} is performed for different values of dielectric constant. From this, it is noticed that by proper choosing the aspect ratios, wider bandwidth can be achieved. Thus, wider bandwidth can be controlled by proper selection of dielectric constant and aspect ratios of the RDRA.

Literature survey is carried out on different techniques, such as merging of modes, stacked/embedded DRAs, modified shaped of DRA and hybrid DRAs, of bandwidth improvement. 23 % to 42 % of impedance bandiwdth can be achieved by merging of multiple modes in the DRA structure using feeding methods such as annular slot, CPW, modified microstrip line and conducting strip with coaxial probe. In this, proper choice of dimensions of feeding mechanism are required. 25 % to 64 % of impedance bandwidth is reported by stacking or embedding of different DRA elements which are made from different materials. By modifying basic shapes of the DRA, 28 % to 71 % of impedance bandwidth is achieved. A hybrid structure, consists of the DRA and other kind of antenna such as MPA, monopole, slot radiator, coplanar waveguide inductive slot, is re-

ported with 89 % to 117 % of impedance bandwidth. Also literature survery on single and dual narrowband is carried out. Single low profile narrow band can be achieved by using a material of high permittivity. Also it is obtained by metalization on surfaces of the DRA. Dual band designs are reported in literature. It is observed that the one narrowband is achieved by the DRA, while second narrowband is achieved by the feeding methods, namely, eccentric ring, parasitic slot and zonal slot. This add extra degree of freedom, i.e. optimize the parameters of the feeding methods, for dual narrowband DRA designs.

References

[1] Petosa A., Dielectric Resonator Antenna Handbook, *Artech* House, 2007.

[2] R. K. Mongia, P. Bhartia, "Dielectric resonator antennas- A review and general design relations for resonant frequency and bandwidth", *International Journal of Millimeter Wave Engineering*, Vol. 4, pp. 230-247, July, 1994.

[3] K.W. Leung, E. H. Lim, and X.S. Fang "Dielectric resonator antennas: from the basic to the aesthetic"', *Proceeding of the IEE*, Vol. 100, No. 7, pp. 2181-0000000, July 2012.

[4] B. Yao, Q. Zheng, J. Peng, R. Zhong, S. Li, and T. Xiang, "An efficient 2-D FDTD method for analysis of parallel-plate dielectric resonators", *IEEE Antennas and Wireless Propagation Letters*, Vol. 10, pp. 866-868, 2011.

[5] N. Kandeda, B. Houshmand, T. Itoh, "FDTD analysis of dielectric resonators with curved surfaces", *IEEE Transactions Microwave Theory Technology*, Vol. 45, No. 9, pp. 1645-1649, Sep. 1997.

[6] E.A.C. Marcatili, "Dielectric rectangular waveguide and directional coupler for integrated circuits" *Bell System Technical Journal*, pp. 2071-2103, March. 1969.

[7] R. M. Knox, P.P. Toulios, "Integrated circuits for the millimeter through the optical frequency range", *Proceeding of symposium Sub-Millimeter Waves*, New York, 1970.

[8] D. Kajfez, P. Guillon, "Dielectric resonators", Norwood, MA, *Artech House*, 1986.

[9] S.A. Long, M.W. McAllister, L.C. Shen, "The resonant cylindrical dielectric cavity antenna", *IEEE Transactions on Antenna and Propagation*, Vol. 31, pp. 406-412, May 1983.

[10] R. K. Mongia, A. Ittipiboon, M. Cuhaci, D. Roscoe, "Radiation Q-factor of rectangular dielectric resonator antenna, thoery and experiment", *Proceeding of IEEE International Conference of AP & S Symposium*, pp. 764-767, 1994.

[11] J. Van Bladel, "On the resonances of a dielectric resonator of very high permittivity", *IEEE Transactions on Microwave Theory Techniques*, Vol. 23, pp. 199-208, Feb. 1975.

[12] J. Van Bladel, "The excitation of a dielectric resonator of very high permittivity", *IEEE Transactions on Microwave Theory Techniques*, Vol. 23, pp. 208-215, Feb. 1975.

[13] Okaya A. K., Barash L.F., "The dielectric microwave resonator", *Proc. IRE*, Vol. 50, 2081-2092, 1962.

[14] H. Y. Yee, "Natural resonant frequencies of microwave dielectric resonators", *IEEE Transactions on Microwave Theory Techniques*, Vol. 13, pp. 256- , March, 1965.

[15] R. K. Mongia, "Theoretical and experimental resonant frequencies of rectangular dielectric resonators", *Proceeding of Instrumentation Electronics Engineering*, Vol. 139, pp. 98-104, Feb. 1992.

[16] A. Karp, H. J. Shaw, D. K. Winslow, "Circuit properties of microwave dielectric resonator", *IEEE Transactions on Microwave Theory Techniques*, Vol. 16, pp. 810-828, Oct. 1968.

[17] D.M. Pozar, "Microwave Engineering", *Addison-Sesley Publishing Co, New York*, 1990

[18] Jacobs H., Novic G.,LoCascio C.M., Chrepta M.M., "Measurement of guide wavelength in rectangular dielectric waveguide", *IEEE Transactions on Microwave Theory and Techniques*, Vol. 24, 815-820,1976.

[19] P. Guillon, Y. Garault, "Accurate resonant frequencies of dielectric resonators", *IEEE Transcation on Microwave Theory Techniques*, Vol. 25, pp. 916-922, Nov. 1977.

[20] T. Itoh, R.S. Rudokas, "New method for computing the resonant frequencies of dielectric resonators", *IEEE Transactions on Microwave Theory and Techniques*, Vol. 25, No. 1, pp. 52-54, January, 1997.

[21] Ittipiboon A., Mongia R. K., "'Theoretical And Experimental Investigation On Rectangular Dielectric Resonator Antennas"',*IEEE Transactions on Antennas and Propagation*, Vol.45, No.9, 1348–1356, 1997.

[22] X.S Fang, K.W. Leung, "Designs of single-, wide-band rectangular dielectric resonator antennas", *IEEE Transactions on Antennas and Propagation*, Vol. 59, No. 6, pp. 2409-2414, June, 2011.

[23] C.A. Balanis, *Antenna Theory: Analysis and Design*, Harper and Row, 1982.

[24] B. Yao, Q. Zheng, J. Peng, R. Zhong, S. Li, and T. Xiang, "An efficient 2-D FDTD method for analysis of parallel-plate dielectric resonators", *IEEE Antennas and Propagation Letters*, Vol. 11, pp. 866-868, 2011.

[25] A. Ittipiboon, R. K. Mongia, Y.M.M. Antar, P. Bhartia, and M. Cuhaci, "Aperture fed rectangular and triangular dielectric resonators for use as magnetic dipole antennas" *Electronics Letters*, Vol. 29, pp. 2001-2002, 1993.

[26] K.W. Leung, W.C. Wong, K.M.Luk, E.K.N. Yung, "Annular slot-coupled dielectric resonator Antenna", *IEEE Electronics Letters*, Vol. 34, No. 13, pp.1275-1277,June 1998.

[27] C.Y. Huang, J.Y. Wu, and K.L. Wong, "Cross-slot-coupled microstrip antenna and dielectric resonator antenna for circular polarization", *IEEE Transactions on Antennas and Propagation*, Vol. 47, No. 4, pp. 605-609, April 1999.

[28] R.A. Kranenburg, and S.A. Long, "Microstrip transmission line excitation of dielectric resonator antennas", *IEEE Electronics Letters*, Vol. 24, No. 18, pp. 1156-1157, Sept. 1998.

[29] R.K. Mongia, A. Ittipiboon, and M. Cuhaci, "Experimental investigations on microstrip-fed series dielectric resonator antenna arrays", *Symposium on Antenna*

Technology and Applied Electromagentics ANTEM 94, Ottawa, Canada, pp. 81-84, Aug. 1994.

[30] K.W. Leung, K.M. Luk, and K.Y.A. Lai, "Input impedance of a hemispherical dielectric resonator antenna", *IEEE Electronics Letters*, Vol. 27, No. 24, pp. 2259-2260, Nov. 1991.

[31] G.P. Junker, A.A. Kishk, A.W. Glison, "Input impedance of dielectric resonator antennas excited by a coaxial probe", *IEEE Transactions on Antenna and Propagation*, Vol. 42, No. 7, pp. 960-966, July 1994.

[32] Z. N. Chen, et al, "Effect of parasitic disk on a coaxial probe-fed dielectric resonator antenna", *Microwave and Optical Technology Letters*, Vol. 15, No. 3, pp. 166-168, June 1997.

[33] K.M. Luk, et al, "Technique for improving coupling between microstrip line and dielectric resonator antenna", *IEEE Electronics Letters*, Vol. 35, No. 5, pp. 357-358, March 1999.

[34] M.T. Birand, and R.V. Gelsthorpe, "Experimental millimetric array using dielectric radiators fed by means of dielectric waveguide", *IEEE Electronics Letters*, Vol. 17, No. 18, pp. 633-635, Sept. 1981.

[35] M. Wyville, A. Petosa, J.S. Wight, "DIG feed for DRA arrays", *IEEE Antennas and Propagation Symposium Digest AP-S*, Vol. 2b, pp. 176179, 2005.

[36] R. K. Mongia, A. Ittipiboon, "Theoretical and experimental investigation on rectangular dielectric resonator antennas", *IEEE Transactions on Antennas and Propagation*, Vol. 45, No. 9, pp. 1348-1356, Sept. 1997.

[37] A. Ittipiboon, et al, "Aperture fed rectangular and triangular dielectric resonators for use as magnetic dipole antennas", *IEEE Electronics Letter*, Vol. 29, No. 23, pp. 2001-2002, Nov. 1993.

[38] A. Buerkle, K. Sarabandi, H. Mosallaie, "Compact slot and dielectric resonator antenna with dual resonance, broadband characteristics", *IEEE Transactions on Antennas and Propagation*, Vol. 53, No. 3, pp. 1020-1027, March 2005.

[39] C.P.Chua, P.A. Pavovich, R. M. Dragos, M. S. Leung, "A compact and wideband rectangualr dielectric resonator antenna", *Proceeding of the* 7^{th} *Conference on Electronic Packing Technology*, Singapore, Vol. 1, pp. 313-316, Dec. 2005.

[40] Y. Gao, B. L. Ooi, W. B. Ewe, A. P. Popov, "A compact wideband hybrid dielectric resonator antenna", *IEEE Microwave and Wireless Components Letters*, Vol. 16, No. 4, pp. 227-229, April 2006.

[41] B. Li, K.W. Leung, "Strip-fed rectangular dielectric resonator antennas with/without a parasitic patch", *IEEE Transactions on Antennas and Propagation*, Vol. 53, No. 7, pp. 2200-2207, July 2005.

[42] P. V. Bijumon, S. K. Menon, M. N. Suma, M.T. Sebastian, P. Mohanan, "Broadband cylindrical dielectric resonator antenna excited by a modified microstrip line", *IEEE Electronics Letters*, Vol. 41, No. 7, pp. 385-387, March 2005.

[43] R. Chair, A. A Kishk, K. F. Lee, "Wideband simple cylindrical dielectric resonator antennas", *IEEE Microwave and Wireless Components Letter*, Vol. 15, No. 4, pp. 241-243, April, 2005.

[44] A. V. P. Kumar, V. Hamsakutty, J. Yohanna, and K. T. Mathew, "A sideband conical beam cylindrical dielectric resonator antenna", *IEEE Antennas and Wireless Propagation Letters*, Vol. 4, pp. 15-17, 2007.

[45] K.W. Leung, C. K. Leung, "Wideband dielectric resonator antenna excited by cavity-backed circular aperture with microstrip tuning fork", *IEEE Electronics Letters*, Vol. 39, No. 14, pp. 1033-1035, July 2003.

[46] A.A. Kishk, B. Ahn, D. Kajfez, "Broadband stacked dielectric resonator antenna", *IEEE Electronics Letters*, Vol. 25, No. 18, pp. 1232-1233, Aug. 1989.

[47] K.W. Leung, K. M. Luk, K.Y. Chow, E. K. N. Yung, "Bandwidth enhancement of dielectric resonator antenna by loading a low-profile disk of very high permittivity", *IEEE Electronics Letters*, Vol. 33, No. 9, pp. 725-726, April 1997.

[48] A Sangiovanni, J. Y. Dauvignac, C. Pichot, "Embedded dielectric resonator antennas for bandwidth enhancement", *IEEE Electronics Letters*, Vol. 33, No. 25, pp. 2090-2091, Dec. 1997.

[49] Q. Rao, T. A. Denidni, A. R. Sebak, "Broadband compact stacked T-shaped DRA with equilateral-triangle cross sections", *IEEE Microwave and Wireless Components Letters*, Vol. 16, No. 1, pp. 7-9, Jan. 2006.

[50] M. Verplanken, J. Van Bladel, "The magnetic-dipole resonances of ring resonator of very high permittivity", *IEEE Transactions on Microwave Theory Techniques*, Vol. 27, pp. 328-333, 1979.

[51] A. Ittipiboon, A. Petosa, D. Roscoe, M. Cuhaci, "An investigation of a novel broadband dielectric resonator antenna ", *Proceeding of IEEE Symposium on Antenna and Propagation*, Baltimore, MD, pp. 2038-2041, July 1996.

[52] A. A. Kishk, "Wide-band truncated tetrahedron dielectric resonator antenna excited by a coaxial probe", *IEEE Transactions on Antenna and Propagation*, Vol. 51, No. 10, pp. 469-474, Oct. 2003.

[53] G. Almpanis, C. Fumeaux, and R. Vahldieck, "Semi-trapezoid dielectric resonator antenna for wideband applications", *Proceeding of IEEE International Symposium on Antennas and Propagation*, Honolulu, Hawaii, pp. 4877-4880, June 2007.

[54] X. L. Liang, T. A. Denidni, L. N. Zhang, "Wideband L-shaped dielectric resonator antenna with a conformal inverted trapezoidal patch feed", *IEEE Transactions on Antennas and Propagation*, Vol. 57, No. 1, pp. 271-274, Jan. 2009.

[55] R. Chair, A. A. Kishk, K.F. Lee, C. E. Smith,"Wideband flipped staired pyramid dielectric resonator antenna", *IEEE Electronics Letters*, Vol. 40, No. 10, pp. 581-582, May 2004.

[56] M. Lapierre, Y. M. M. Antar, A. Ittipoboon, A. Petosa, "Ultra wideband monopole/dielectric resonator antenna", *IEEE Microwave and Wireless Components Letters*, Vol. 15, No. 1, pp. 7-9, Jan. 2005.

[57] S. Ghosh, A. Chakrabarty, "Ultrawideband performance of a dielectric loaded T-shaped monopole transmit and receive antenna/EMI sensor", *IEEE Antennas and Wireless Propagation Letters*, Vol. 7, pp. 358-361, 2008.

[58] M. N. Jazi, T.A. Denidni, "Design and implementation of an ultrawideband hybrid skirt monopole dielectric resonator antenna"', *IEEE Antennas and Wireless Propagation Letters*, Vol. 7, pp. 493-496, 2008.

[59] T. Lassen, "Long-range RF communication: Why narrowband is the de facto standard", White paper, *Texas Instrument Inc.*,pp. 1-7, March, 2014.

[60] A. Petosa, A. Ittipiboon, "Dielectric resonator antennas: A historical review and the current state of the art", *IEEE Antennas and Propagation Magazine*, Vol. 52, No. 5, pp. 91-116. October,2011.

[61] R. K. Mongia, A. Ittipiboon, M. Cuhaci, "Low-profile dielectric resonator antennas using a very high permittivity material", *IEEE Electronics Letters*, Vol. 30, No. 17, pp. 1362-1362, Aug. 1994.

[62] K.W. Leung, K. M. Luk, E. K. N. Yung, S. Lai "Characteristics of a low-profile circular disk DR antenna of very high permittivity", *IEEE Electronics Letters*, Vol. 31, No. 6, pp. 417-418, March 1995.

[63] H.Y. Lo, K.W. Leung, K. M. Luk, and E. K. N. Yung, "Low profile equilateral triangular dielectric resonator antenna of very high permittivity", *IEEE Electronics Letters*, Vol. 35, No. 25, pp. 2164-2166, Dec. 1999.

[64] K.Y. Hui, K. M. Luk, "A miniature dielectric resonator loaded patch antenna", *IEEE Transactions on Antennas and Propagation*, Vol. 53, No. 6, pp. 2118-2122, June 2005.

[65] Y. Gao, Z. Feng, and L. Zhang, "Investigation of a new radiating mode and the traditional dominant mode in rectangular dielectric resonator antenna", *IEEE Antennas and Wireless Propagation Letters*, Vol. 11, pp.909–912, 2012.

[66] Y. Gao , Z. Feng, and L. Zhang, "Experimental investigation of new radiating mode in rectangular hybrid dielectric resonator antenna", *IEEE Antennas and Wireless Propagation Letters*, Vol. 10, pp.91-94, 2011.

[67] J. I. Moon, S. O. Park, "Dielectric resonator antenna for dual-band PCS/IMT-2000", *IEEE Electronics Letters*, Vol. 36, No. 2, pp. 1002-1003, Jan. 2000.

[68] B. Amelia, S. Kamal, M. Hossein, "Compact slot and dielectric resonator antenna with dual resonance, broadband characteristics", *IEEE Transactions on Antennas and Propagation*, Vol. 53, No. 3, 1020-1027, Mar. 2005.

[69] Q. Rao, T. A. Denidni, A. R. Sebak, "A new dual frequency hybrid resonator antenna", *IEEE Antenna and Wireless Propagation Letters*, Vol. 4, 308-311, 2005.

[70] H. M. Chen, Y. K. Wang, Y. F. Lin, S. C. Lin, S. C. Pan, "A compact dual-band dielectric resonator antenna using a parasitic slot", *IEEE Antennas and Wireless Propagation Letters*, Vol. 8, pp. 173-176 ,2009.

[71] Y. Ding, K. W. Leung, "On the dual-band DRA-slot hybrid antenna", *IEEE Transactions on Antennas and Propagation*, Vol. 57, No. 3, pp. 624-630, March 2009.

[72] X.S. Fang, K.W. Leung, "Designs of single-,dual-,wide-band rectangular dielectric resonator antenna", *IEEE Transactions on Antenna and Propagation*, Vol. 59, No. 6, pp. 2409-2414, June 2011.

Chapter 3

Wideband and Miniaturized Rectangular Dielectric Resonator Antenna

An objective of this chapter is to propose a miniaturized rectangular dielectric resonator antenna (RDRA) configuration and dual mode operation employing a simple feeding scheme. It demonstrates potential advantages achieved by choosing a microstrip line feeding mechanism at the edge of the RDRA. Measurement and simulation results are both in good agreement. The fabricated antenna possesses a wide impedance bandwidth of 800 MHz (5.65 GHz to 6.48 GHz) and dimensions of RDRA are $17 \times 7 \times 3\ mm^3$. Measured radiation patterns have linear polarization over the frequency range. By adopting the proposed design, the bandwidth is enhanced more than four times as compared to a conventional way of exciting the RDRA by the microstrip line. To validate the design, a comparison of published designs are discussed.

3.1 Introduction

The rapid growth in the demand for wireless applications in the GHz range has led the research community to focus an attention on highly efficient antennas that exhibit wide bandwidth, compact size and good radiation characteristics. The dielectric resonator antennas (DRAs), introduced by Long et al. in 1983 [1], could be used for such applications due to many advantageous features they possess. These include high radiation efficiency,

compact size, light weight, and the versatility in shapes, and feeding mechanism [2]. One of the most crucial issues of DRAs is the dependence of size and impedance bandwidth on the dielectric constant of a material used in antennas. A DRA made from a low permittivity material would have a relatively large volume. It would exhibit a wide impedance bandwidth. On the other side, a high permittivity DRA would be small in size, but it would exhibit a narrow bandwidth operation [3].

Many existing and emerging wireless applications require the radiating element be as compact/low profile with wideband frequency operation as possible. Hence, a lot of research is directed towards an increase of the bandwidth of the DRAs while keeping the size low. Towards this goal, different approaches have been reported to increase the bandwidth of DRAs. For example, operating the DRA in two or more modes [4,5], stacking/embedding two DRAs of different sizes to merge their resonant bands [6], attaching parasitic metal strips on the DRA surface to incur additional resonance [7], leaving air gaps between the DRA and a ground plane [8], adjusting the aspect ratio of the DRA to reduce its Q-factor [3], modifying the basic shapes of DRAs to create discontinuities [9–14] and by an adopting new feeding structure [15] are reported.

As described in section 2.2.1, merging of dual mode in RDRA and CDRA is discussed with their structure configurations and reported performances. In [16–18], one mode is due to the RDRA, while the other is due to the feeding scheme, namely, slot, CPW inductive slot and complementary pair of the magnetic loop and the magnetic dipole. The resonance of the other mode is dependent on the physical parameters of the feeding schemes. This adds extra degree of freedom for bandwidth improvement which leads to extra complexity in designs. In [20], merging of dual modes is achieved by the RDRA itself. Here, the aperture slot uses as a feeding scheme. This shows that bandwidth improvement by merging of modes requires proper choice of physical dimensions of the DRAs, feeding schemes.

By using these methods, bandwidth ranges from 20 % to 40 % have been achieved. However, these methods suffer from complicated design structure and are not easy to fabricate. In this chapter, two nearby modes of a basic rectangular DRA are described.

Instead of a conventional way of excitation by a simple microstrip line, edge of the RDRA is placed on the open-ended line. Numerical study and field distribution of the design are presented. Measurement and simulated characteristics are presented and discussed. The reported designs around 5-6 GHz band are compared and discussed with the proposed antenna for validation of the proposed design.

3.2 Proposed Approach

Figure 3.1 shows a geometry of the conventional way of excitation by a simple microstrip line for the RDRA and Figure 3.2 shows a geometry of the proposed miniaturized and wideband RDRA. As shown in Figure 3.1 and 3.2, a 50 Ω microstrip line, having width of 4.45 mm and length of 45 mm is printed on a grounded substrate, as a feeding mechanism. The substrate with dielectric constant, ϵ_s, of 2.5, thickness (H_1) of 1.56 mm, and loss factor of 0.0017 is used. The RDRA with length a, depth d, height h, and dielectric

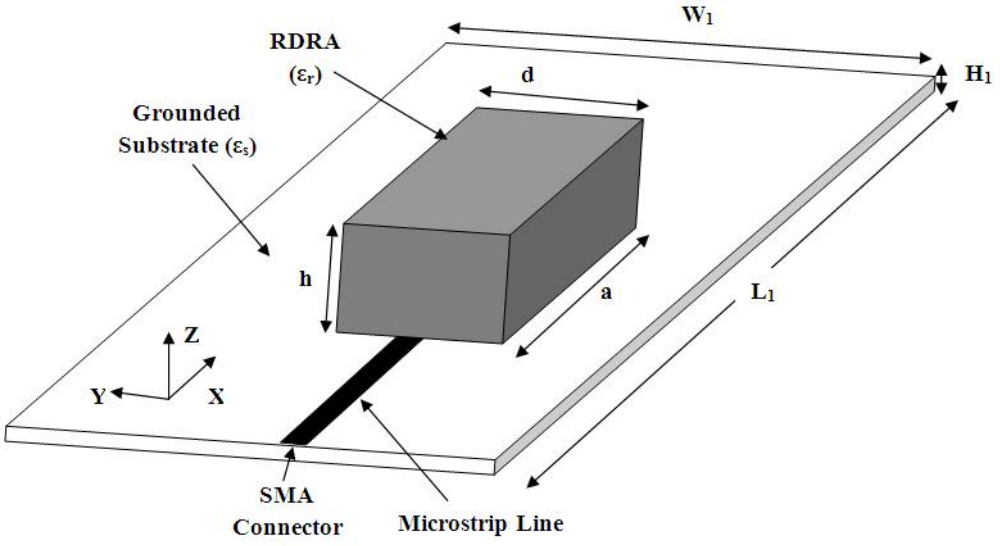

Figure 3.1: Geometry of the conventional way of excitation [2] using microstrip line.

constant ϵ_r of 32 is used. An open-ended microstrip line is placed at the edge of the rectangular DRA, as shown in Figure 3.2. The RDRA is placed above the microstrip line for coupling as shown in Figure 3.1. A ground plane structure has dimensions L_1 and W_1 as $80 \times 50mm^2$.

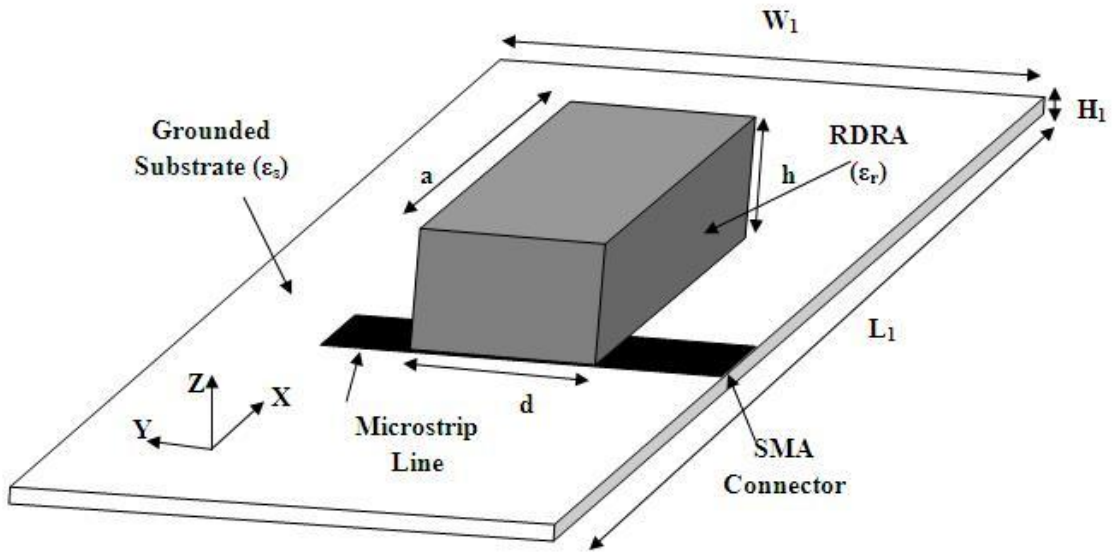

Figure 3.2: Geometry of the proposed way of excitation for miniaturized and dual mode operation using microstrip line.

3.2.1 Numerical Study

For simulation, a finite element method (FEM) based 3D electromagnetic simulator, Ansoft HFSS is used. In order to illustrate the design procedure of the proposed design, the initial dimensions of a RDRA are determined using the equations developed by magnetic wall waveguide model (MMW) with the dielectric slab and dielectric waveguide model (DWM) [3] as described in chapter 2. Parametric study has been performed on the different parameters of the proposed antenna with edge feeding. Return loss characteristics of parametric study on length, a of the proposed antenna is shown in Figure 3.3. Table

Table 3.1: Parametric study on length, d = 7 mm, h = 3 mm .

length (a) mm	Frequency Range (GHz)	BW (MHz)	% of BW
19	5.46-5.84	380	6.73
18	5.60-6.32	720	12.08
17	5.71-6.61	900	14.61
16	5.86-7.05	1190	18.44
15	6.00-7.13	1130	17.21

3.1 shows variation of resonant frequencies, impedance bandwidth, and % of bandwidth when the length (a) changes from 19 mm to 15 mm, while other dimensions are d of 7 mm, h of 3 mm. From the Figure 3.3, it is noticed that the dual resonance in the proposed

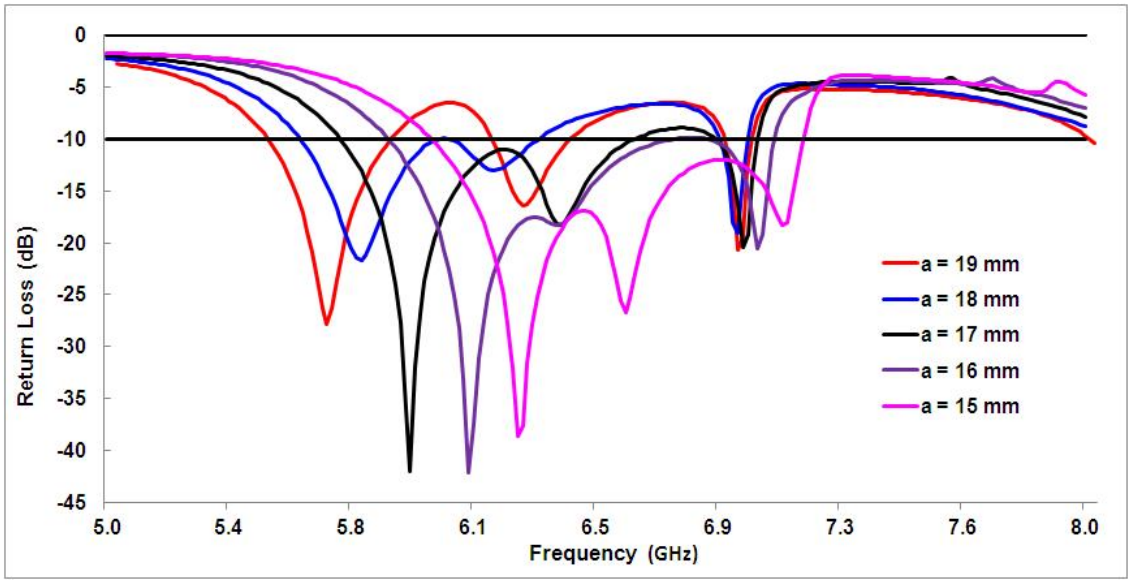

Figure 3.3: Simulated return loss for different values of length (a).

scheme is excited. For longer RDRA, only single mode is excited. By decreasing the length, resonance frequencies of both the modes are increased. The result shows that by decreasing the length, the resonant frequency and impedance bandwidth are increased. It is observed that by decreasing length from 19 mm to 15 mm, there is increase of percentage of impedance bandwidth from 6.73 % to 17.21 %. Also it is observed that for shorter length equal to 15 mm, three nearby modes have been excited with the way of feeding using microstrip line.

Parametric study on the depth of the antenna is listed in Table 3.2. Figure 3.4 shows the return loss characteristics for different values of depth while kept a of 17 mm and h of 3 mm for all cases. It is observed that by decreasing the depth (d) from 9 mm to 5 mm, the resonant frequency is increased for both the modes. For d euqal to 7 mm, the

Table 3.2: Parametric study on depth, a = 17 mm, h = 3 mm .

depth (d) mm	Frequency Range (GHz)	BW (MHz)	% of BW
9	5.46-5.82	360	6.38
8	5.61-6.24	630	10.62
7	5.71-6.61	900	14.61
6	5.84-6.32	480	7.89
5	5.96-6.46	500	8.05

impedance bandwidth is wider and it is 14.61 %. This is because of dual resonance is

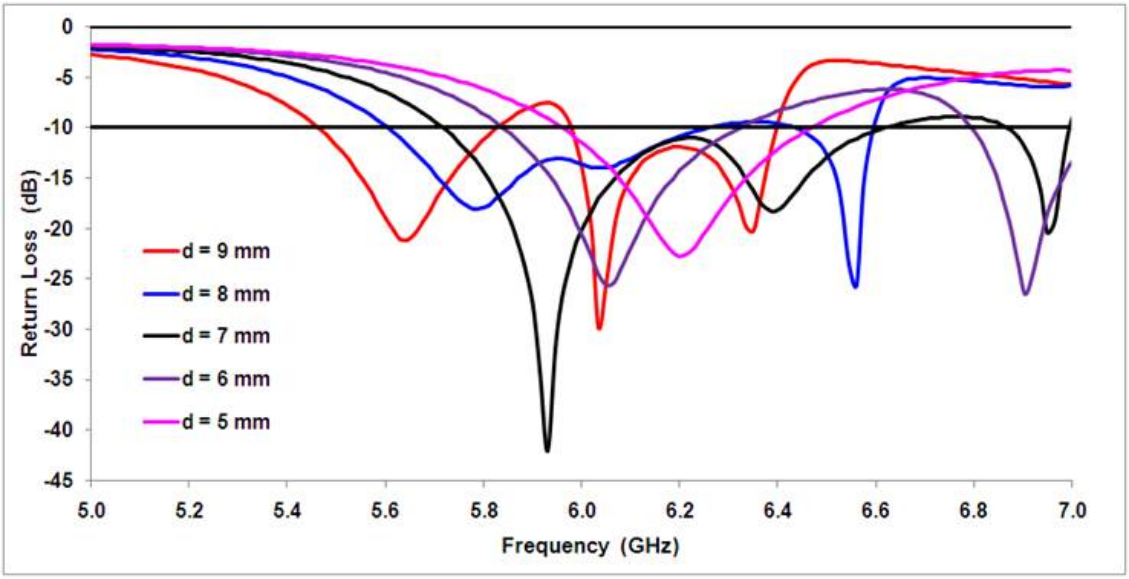

Figure 3.4: Simulated return loss for different values of d.

Table 3.3: Parametric study on height, a = 17 mm, d = 7 mm .

height (h) mm	Frequency Range (GHz)	BW (MHz)	% of BW
5	4.73-5.31	580	11.55
4	5.16-5.77	610	11.16
3	5.71-6.61	900	14.61
2	6.55-7.01	460	6.78

excited in the RDRA.

Table 3.3 shows the numerical study on resonant frequency, bandwidth when the height (h) changes from 5 mm to 2 mm. Return loss characteristics of different values of height are shown in Figure 3.5. The other dimensions are length (a) of 17 mm and depth (d) of 7 mm. The result shows that by decreasing the height, the resonant frequency of both yjr modes and impedance bandwidth are increased. For h equal to 3 mm, maximum bandwidth (900 MHz) is obtained. For thinner antenna (h equal to 2 mm), the bandwidth is narrow as single mode is excited. From these studies, it is possible to excite dual and/or three modes using the way of excitation instead of the conventional way of excitation using the simple microstrip line. From these studies, it is noticed that multiple modes by the design are due to the RDRA but not due to microstrip line. In this study, for all cases, length of the microstrip line below the RDRA is optimized for better impedance matching.

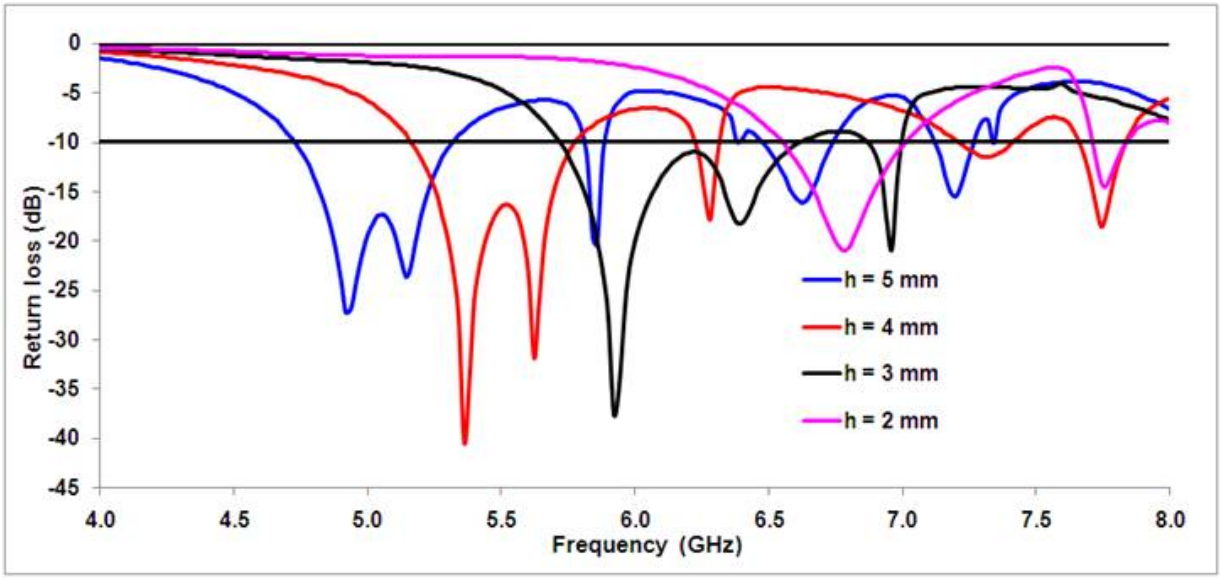

Figure 3.5: Simulated return loss for different values of h.

3.2.2 E-Field Distributions

For validation of excitation of dual modes in the design, Figure 3.6 displays the electric vector field distributions for the proposed scheme having a of 17 mm, d of 7 mm and h of 3 mm at resonant frequencies (5.93 GHz and 6.39 GHz) in three pictorial planes and within the RDRA. Arrow indicates direction of the field. Color shades represent strength of the field. The E-fields at 5.93 GHz are plotted in Figure 3.6 (a), (b), (c) and (d) for x-y, y-z, z-x plane, and within the RDRA, respectively. The E-fields at 6.39 GHz are sketched in Figure 3.6 (e), (f), (g), and (h) for x-y, y-z, z-x -plane and within the RDRA, respectively. From Figure 3.6 (b), it is seen that the E-fields are oriented in the z-axis and vary from maximum to zero as the height increases from the ground plane. They are uniformly distributed. There is a small variation $\delta < 1$ along the y-axis. From Figure 3.6 (c), it is seen that the E-fields circulate around the y-axis and vary in the x-axis and z-axis. These kind of distributions confirm the excitation of $TE^{y}_{1\delta1}$ mode at 5.93 GHz in the RDRA.

It is observed in Figure 3.6 (f) that E-fields circulate around x-axis and vary in y and z-axis. Form Figure 3.6 (g), it is noticed that E-fields vary in two half cycles variation along the x-axis. From Figure 3.6 (e), (f) and (g), it is confirmed the excitation of TE^{y}_{211} at 6.39 GHz in the RDRA. From these E-field distributions, it is confirmed that both the

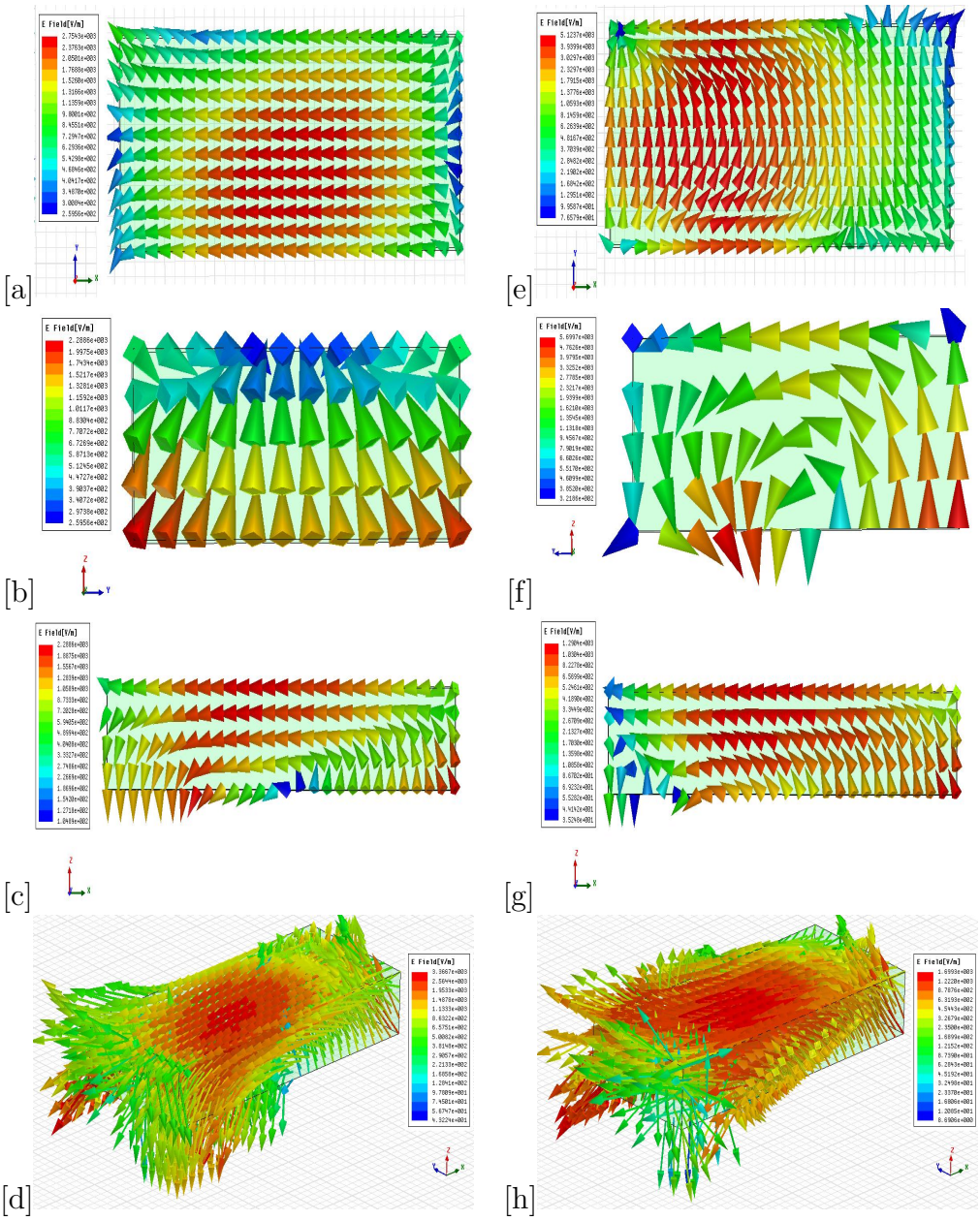

Figure 3.6: E-field distributions at 5.93 GHz (a) x-y plane, (b) y-z plane, (c) z-x plane, (d) in RDRA, at 6.39 GHz (e) x-y plane, (f) y-z plane, (g) z-x plane, (h) in RDRA.

modes are due to the RDRA itself. These dual modes are excited with the RDRA due to the way of the microstrip line placed for coupling.

3.2.3 Theoretical Analysis

Resonant frequencies of dual mode in RDRA, TE^{y}_{111} and TE^{y}_{211}, are denoted by f_1 and f_2, respectively. Looking to field distribution of both the modes, the difference between these two modes are mainly along the x-axis. The wave numbers k_{x1}, k_{x2} and k_{z1}, k_{z2}

can be written as follows:

$$k_{x1} = \frac{\pi}{a} \quad k_{x2} = \frac{2\pi}{a}, \quad k_{z1} = k_{z2} = \frac{\pi}{h}, \quad k_{y1} = k_{y2} = \frac{\pi}{d} \tag{3.1}$$

From the DWM model, the frequencies f_1 and f_2 are given by following equations

$$f_{1,2} = \frac{c}{2\pi\sqrt{\epsilon_{\mathrm{r}}}}(\sqrt{k_{x1,x2}^2 + k_{y1,y2}^2 + k_{z1,z2}^2}) \tag{3.2}$$

where,

$$k_{y1,y2}^2 = \sqrt{k_{1,2}^2 - k_{x1,x2}^2 - k_{z1,z2}^2} \tag{3.3}$$

$$k_{1,2} = \frac{2\pi f_{1,2}\sqrt{\epsilon_{\mathrm{r}}}}{c} \tag{3.4}$$

Given a dielectric constant of the RDRA, there are three degree of freedom (a,d,h) for meeting the two frequencies requirement (f_1, f_2) in (3.2). To find a unique solution, it is arbitrarily assuming that $k_{y1} = 0.59k_{x1}$ with reference to [19] and start analysis with $k_{y1} = k_{y2}$. Substituting $k_{y1} = 0.59k_{x1}$ and $k_{y1} = k_{y2}$ into (3.3), initial value of length (a_0) and depth (d_0) can be found by following equations:

$$a_0 = \pi\sqrt{\frac{c}{3(k_2^2 - k_1^2)}}, \tag{3.5}$$

$$d_0 = \frac{6.31}{\sqrt{4k_1^2 - k_2^2}} \tag{3.6}$$

The height h of the RDRA is found by using the following DWM formula [19].

$$h_{1,2} = \frac{2}{k_{y1,y2}} \arctan(\sqrt{(1 - \frac{1}{\epsilon_r})(\frac{k_{1,2}}{k_{y1,y2}})^2}) \tag{3.7}$$

Due to the initial assumption that $k_{y1} = k_{y2}$, there is no unique value exist for $h_1 = h_2$. As suggested in [20], a unique value of h_1 and h_2 can be obtained by introducing a correction factor Δa_0 for a as follows.

$$a = a_0 + \Delta a \tag{3.8}$$

The correction factor is a function of the frequency ratio f_2/f_2 in [20] valid over the range

$1 \leq f_2/f_2 \leq 2.8$.

$$\Delta a = 0.1393(\frac{f_2}{f_1})^4 - 2.3209(\frac{f_2}{f_1})^3 + 11.4422(\frac{f_2}{f_1})^2 - 23.4984(\frac{f_2}{f_1}) + 18.4437(mm) \quad (3.9)$$

A correction factor of Δd is also introduced for d_0 as follows

$$\Delta d = 10.32^{-(1-\frac{f_2}{f_1})} \quad (3.10)$$

$$d = d_0 + \Delta d \quad (3.11)$$

To balance the error, due to $k_{y1} = k_{y2}$, weighting factors are introduced for h_1 and h_2 as follows with w equal to 0.65:

$$h = wh_1 + (1 - w)h_2 \quad (3.12)$$

With above analysis, resonant frequency f_1 of TE^y_{111} mode and f_2 of TE^y_{211} mode are calculated. f_1 is 5.97 GHz whereas f_2 is 6.40 GHz have been found. Simulated resonant frequency of both modes are 5.93 GHz and 6.39 GHz. It is found that simulated and calculated resonant frequecies of both the mode are well matched. Following physical parameters are obtained based on theoretical analysis and are listed in Table 3.4. All dimensions in Table 3.4 are in mm. It is observed that there is a good agreement between

Table 3.4: Theoretical analysis of the proposed scheme

Parameters	Δa	a_0	a	Δd	d_0	d	h_1	h_2	h
Theoretical	3.7272	13.2793	17.007	1.1831	5.2921	6.4752	3.0653	2.9154	3.0128
Simulated	—	—	17.00	—	—	7.00	—	—	3.00

the calculated and simulated dimensions. With these analysis, the design of dual mode in the rectangular dielectric resonator antenna is possible.

3.3 Experimental Results

Based on extensive simulations, the RDRA is made of microwave laminate material with relative permittivity ϵ_r of 32, loss factor of 0.0011, width w, of 17 mm, depth, d, of 7 mm, and height, h, of 3 mm is fabricated with the new feeding scheme. The photograph of

fabricated the proposed RDRA is shown in Figure 3.7. The simulated and measured re-

Table 3.5: Measured and simulated parameters of the proposed antenna

Particular	Mode	Fr (GHz)	Return Loss (dB)	BW (MHz)	% of BW	Gain (dB)
Simulated	$TE^{y}_{1\delta1}$	5.93	-42.0	900	14.61	4.4
Simulated	TE^{y}_{211}	6.39	-18.3	—	—	3.4
Measured	$TE^{y}_{1\delta1}$	5.81	-51.2	800	13.27	3.9
Measured	TE^{y}_{211}	6.29	-22.2		—	3.0

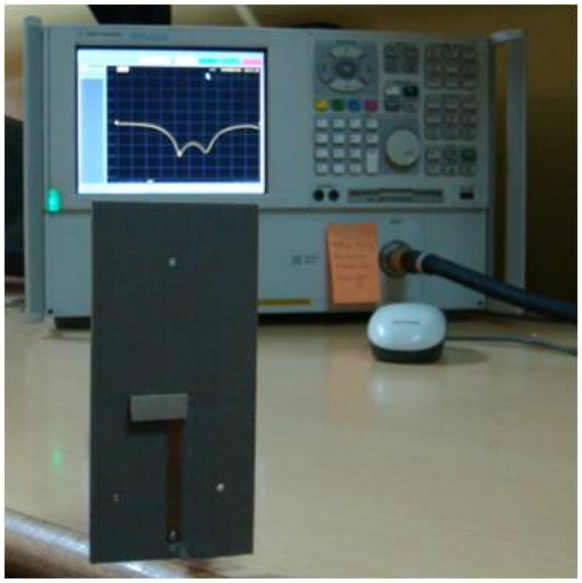

Figure 3.7: A photograph of the fabricated proposed design

turn loss characteristic are shown in Figure 3.8. The measured and simulated parameters are listed in Table 3.5. This antenna has simulated resonant frequencies at 5.93 GHz, and 6.39 GHz. The simulated 10-dB return loss impedance bandwidth is 900 MHz (5.71 GHz to 6.61 GHz – 14.61 %). The calculated resonant frequencies based on analysis presented in section 3.2 are 5.97 GHz and 6.40 GHz for mode $TE^{y}_{1\delta0}$ and TE^{y}_{211}, respectively.

The return loss characteristic of the RDRA is measured by N5230A PNA series network analyzer. By examining the results, the fabricated RDRA has a 10-dB return loss bandwidth (BW) of 800 MHz (5.68 GHz to 6.48 GHz). Resonant frequencies of the RDRA are 5.81 GHz ($TE^{y}_{1\delta1}$) and 6.25 GHz (TE^{y}_{211}). Negligible shifting of measured return loss from the simulated result may be due to unpolished side walls of RDRA, air gap and wax

between the RDRA and the microstrip line.

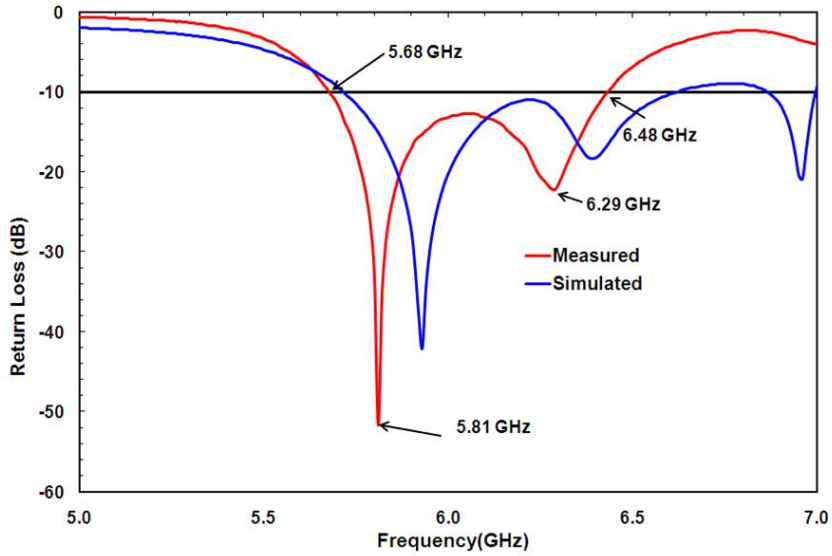

Figure 3.8: Measured and simulated return loss characteristics of the proposed antenna

Radiation patterns of antenna are measured in an anechoic chamber for four frequencies. The measured co- and cross- polarization radiation patterns at 5.81 GHz (lower limit of the BW), 5.68 GHz ($TE^y_{1\delta1}$ mode), 6.25 GHz (TE^y_{211} mode), and 6.48 GHz (upper limit of the BW) are shown in Figure 3.9. By examining the radiation patterns over the impedance bandwidth, it is observed that, as expected, they are almost of the same type i.e. broadside and linear polarization. Figure 3.9 (b) shows the radiation patterns associated with the $TE^y_{1\delta1}$ mode. The half-power beamwidth (HPBW) of the E plane and H-plane are about 92° (−34° to 58°) and 91° (−44° to 47°), respectively. Peaks of cross polarization level are close to boresight, and are about 15 dB and 10 dB below the peak of co-polarization of E-plane and H-plane, respectively for $TE^y_{1\delta1}$ mode. Figure 3.9 (c) shows the radiation pattern for the TE^y_{211} mode. The HPBW of the E-plane and H-plane are about 84° (−48° to 36°) and 89° (−45° to 44°), respectively. The cross polarization level are about 11 dB and 8 dB below the peak of co-polarization of E-plane and H-plane, respectively.

The cross polarization level for 6.48 GHz (upper limit of the bandwidth) is about 5 dB below the peak co-polarization level of both planes. This decrease of the cross-polarization level for upper limit of the bandwidth is due to the finite ground plane and

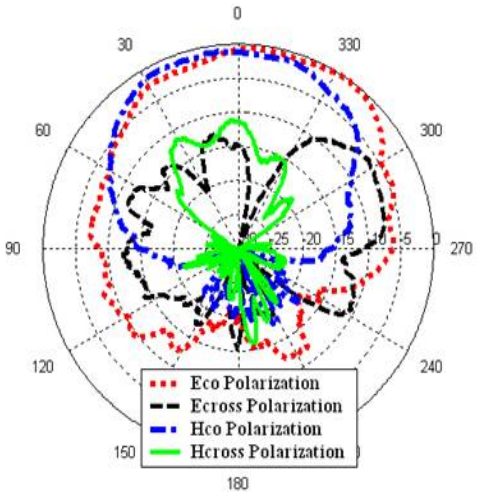

[a]

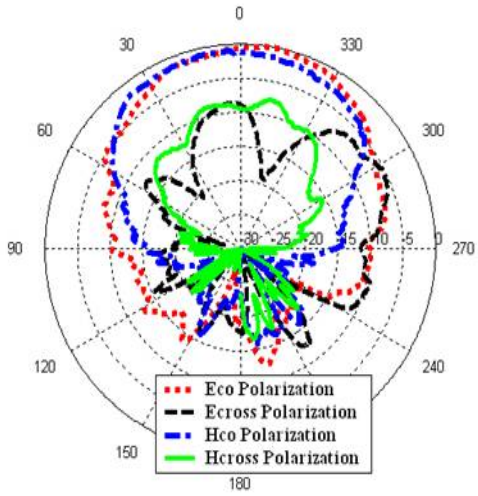

[b]

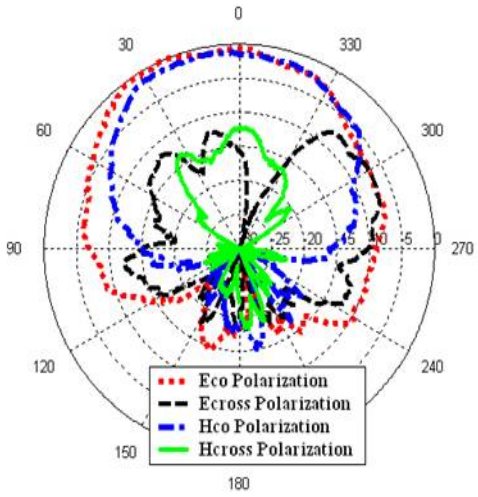

[e]

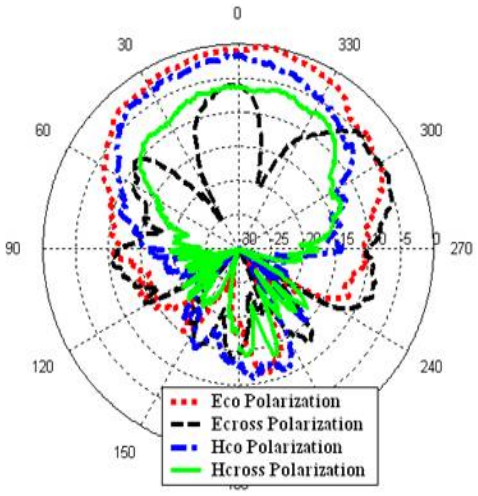

[f]

Figure 3.9: Measured radiation patterns of the proposed scheme: (a) at 5.68 GHz, (b) at 5.81 GHz, (c) at 6.29 GHz, and (d) at 6.48 GHz.

spurious radiation from the microstrip line. Figure 3.10 indicates measured gain and estimated radiation efficiency over the frequency of the proposed scheme. It is noticed that the radiation efficiency varies from 92 % to 97 % over the simulated bandwidth. The measured gain is quite good over the measured bandwidth. At 5.93 GHz, it is 3.9 dB. At 6.29 GHz, it is 3.0 dB. Figure 3.11 shows the simulated and measured return loss characteristics of the conventional RDRA (dimensions are same as the proposed RDRA) excited by the conventional way of using the microstrip line as shown in Figure 3.1. The simulated and measured resonant frequency are 5.39 GHz and 5.40 GHz, respectively. The

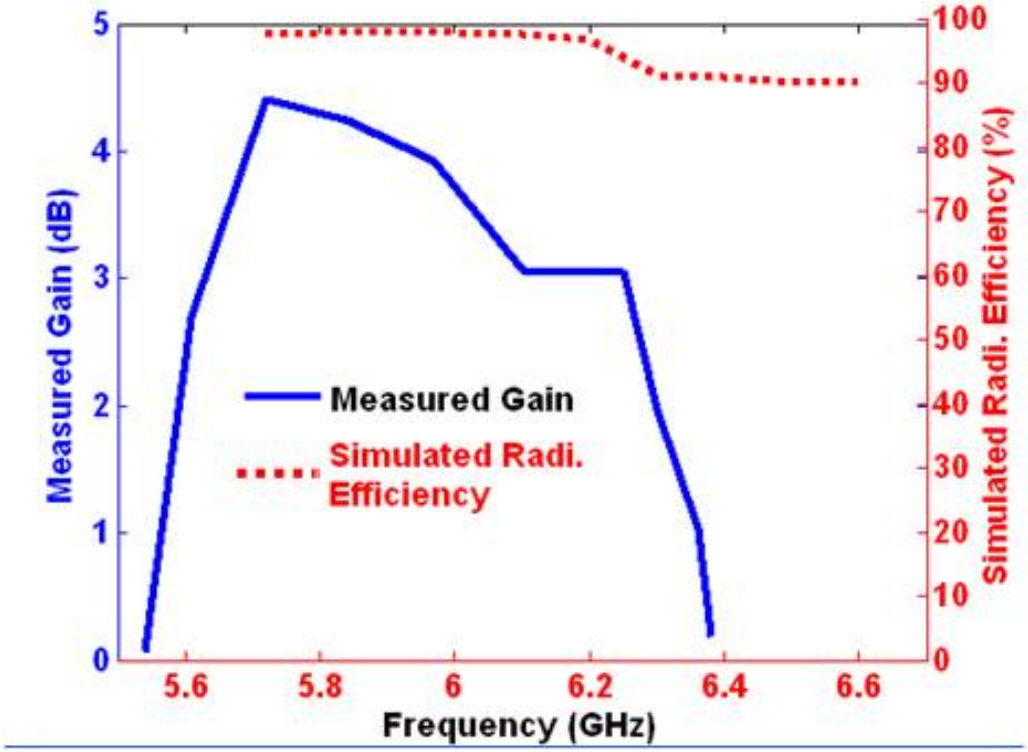

Figure 3.10: Measured gain and estimated radiation efficiency of the proposed antenna.

conventional RDRA has 3.02 % of measured impedance bandwidth. Thus the proposed feeding scheme has enhanced the bandwidth more than four times as compared to the conventional way of feeding scheme.

3.4 Discussion

Several similar antennas were reported in the literature in miniaturization form with a frequency operation over 5 GHz to 6 GHz band in [5, 9, 11–15]. A comparison of these is provided in Table 3.6 in terms of their type of structure, feeding methods, volume, dielectric constant, impedance bandwidth, % of impedance bandwidth and figure of merit (α). The figure of merit α (ratio of volume of DRA and % of impedance bandwidth) can be used for an effective comparison of the DRAs. Smaller value of α indicates that the antenna is the miniaturized and wideband DRA.

A bridge-shaped DRA has been reported with 4.58 GHz to 6.42 GHz frequency operation. It has figure of merit about 152 [9]. A hybrid dielectric-resonator-on-patch (DRoP) had

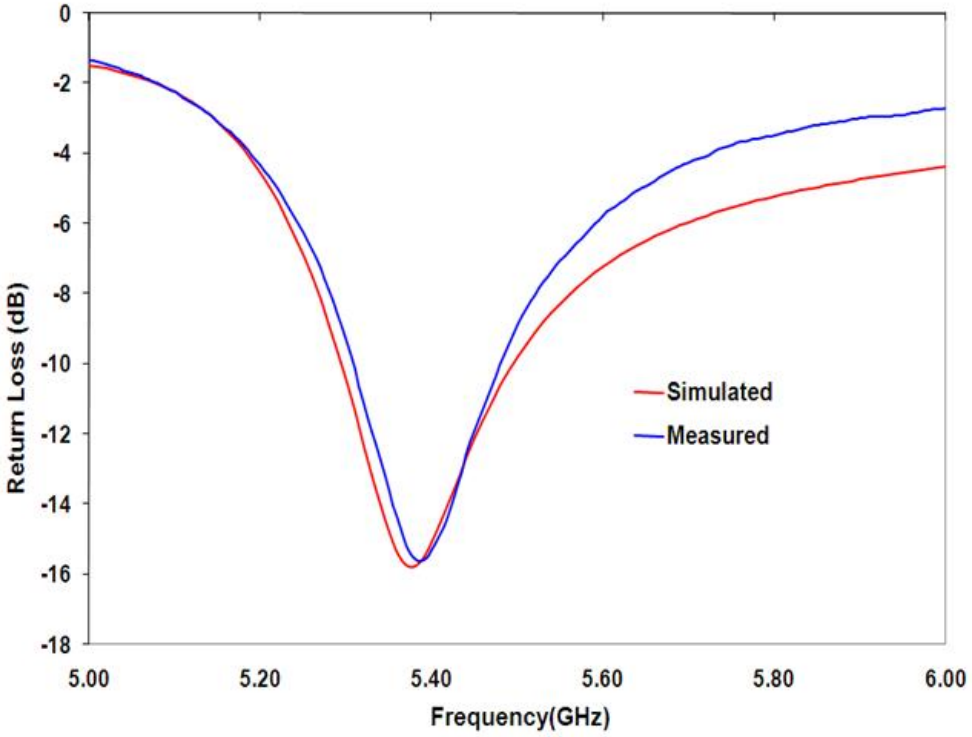

Figure 3.11: Measured and simulated return loss characteristics of the conventional antenna

been introduced for wideband operation (5.14 GHz to 6.51 GHz). The antenna has α = 80 [11]. In [12], a wideband rectangular DR with a horizontal tunnel demonstrated a 4.76-5.86 GHz band. The feeding is aperture coupled. It is observed that fabrication of this DRA is complicated. In [13], a broadband DRA with an offset well has 18 % impedance bandwidth at f_c of 5.5 GHz and a volume of 749 mm^3. It is noticed that the structure is complicated to fabricate as compared to the proposed antenna. A wideband CDRA excited by a circular aperture coupled by a microstrip tuning fork has been exhibited for 5-6 GHz band. It has figure of merit of 34 and complex design procedure [14]. A P-shaped DRA had been designed with a microstrip line with volume of 522 mm^3 and 80 % bandwidth. The structure is complicated to fabricate [14]. A L-shaped microstrip monopole is proposed as a wideband feeding technique for a dielectric ring resonator (DRR) antennas. The bandwidth is 5.09-6.47 GHz (25 % at 5.5 GHz) and $\alpha = 3$ [15].

From the [5, 9, 11–15] and Table 3.6, it is noticed that various feeding methods have been proposed to obtain 5 GHz to 6 GHz frequency band. Also various ways such as stacking, embedding, merging of modes, modifying the basic shapes, used of other structures with

Table 3.6: A comparision of the proposed scheme with other published wideband DRAs

Type of DRA	Type of Feeding	Volume (mm^3)	ϵ_r	BW (MHz)	% of BW	Figure of Merit (α)	Ref
Bridge Shaped DRA	Slot Coupled	2560	40,10	4.56-6.42	16.80	152	[9]
DRoP	Slot Coupled	1887	9.2	5.14-6.51	23.50	180	[11]
RDRA with Tunnel	Slot Coupled	1184	21	4.76-5.89	20.70	57	[12]
RDRA with an Offset Well	Slot Coupled	749	20	5.00-6.10	18.00	42	[13]
CDRA	Cavity-backed Aperture with microstrip Tuning Fork	1344	10	———	40.00	34	[5]
P-Shaped DRA	Microstrip Line	522	10	6.20-8.20	80.00	07	[14]
Dielectric Ring Resonator	L-Shaped Microstrip monopole	85.4	37	5.09-6.47	25.00	03	[15]
RDRA	Proposed Scheme	387	32	5.68-6.48	13.16	27	—

the DRA have been reported for wideband and miniaturized antenna. The reported DRA designs are complicated from structure point of view hence, not easy to fabricate as compared to simple shapes of the DRA . Figure of merit, measure of miniaturization and wide operation, is from 180 to 3. The fabricated antenna has the figure of merit of 27 and a volume of 357 mm^3. There are other the reported DRA designs [14,15] with a low figure of merit than the proposed design. But as compared to the proposed antenna, it has the complicated structure, the complex feeding network and the complex design procedure. Thus, the proposed basic RDRA design is more suitable for wideband operation existing schemes of bandwidth improvement like, without modifying the basic shape, stacking, embedding, air gap and other methods with the simple microstrip feeding line. Thus, the proposed feeding network is claimed to be more simple to design and easy to fabricate as compared to the reported feeding networks. The proposed design has less volume as compared to the reported designs.

3.5 Conclusion

In this chapter, a miniaturized rectangular DRA has been proposed for wide frequency band. A novel way is used to excite dual modes of rectangular DRA with the help of a simple microstrip line. The proposed prototype has 13 % impedance bandwidth and by means of high relative permittivity in design procedure, the size reduction is achieved. This antenna simultaneously has high radiation efficiency (due to lack of conductor loss), simple feeding mechanism, easy fabrication, and proper radiation patterns. These features make the proposed antenna as a useful element for WLAN appliances such as mobile phones, laptops, and PDAs.

References

[1] S.A. Long, M.W. McAllister and L.C. Shen , "Rectangular dielectric resonator antenna," *IEEE Electronics Letters*, Vol.19, 218–219, 1983.

[2] A. Ittipiboon, R. K. Mongia, "Theoretical and experimental investigation on rectangular dielectric resonator antennas", *IEEE Transactions on Antennas & Propagation*, Vol.45, No.9, pp. 1348-1356, 1997.

[3] A. Petosa, Dielectric resonator antenna handbook, *Artech House*, 2007.

[4] G. Almpanis, C. Fumeaux, R. Vahldieck, "Dual mode slot coupled cylindrical dielectric resonator antennas", *IEEE International Symposium on Antennas and Propagation*, pp. 2511-2514, 2006.

[5] K.W.Leung, C. K. Leung, "Wideband dielectric resonator antenna excited by cavity-backed circular aperture with microstrip tuning fork", *IEEE Electronics Letters*, Vol. 39,No. 14, pp. 1033-1035, 2003.

[6] K. W. Leung, K. M. Luk, K. Y. Chow, E. K. N. Yung, "'Bandwidth enhancement of dielectric resonator antenna by loading a low-profile dielectric disk of very high permittivity" *IEEE Electronics Letters*, Vol.33, No.9, pp. pp. 725-726, 1997.

[7] K.W. Leung ,H. K. Ng, "The slot-coupled hemispherical dielectric resonator antenna with a parasitic patch: application to the circularly polarized antenna and wideband antenna"', *IEEE Transactions on Antenna and Propagation*, Vol.53, No. 5, pp. 1762-1769, 2005.

[8] S. M. Shum, K. M. Luk, "Characteristics of dielectric ring resonator antenna with an air gap"', *IEEE Electronics Letters* ,Vol. 30, No. 4, pp. 277-278, 1994.

[9] G. Almpanis, C. Fumeaux, R. Vahldieck, "Dual mode bridge-shaped dielectric resonator antennas", *IEEE Antennas and Wireless Propagation Letters*, Vol. 9, pp. 103-106, 2010.

[10] Y. Gao, B. L. Ooi,W. B. Ewe, A. P. Popov, "A compact wideband hybrid dielectric resonator antenna", *IEEE Microwave and Wireless Component Letters*, Vol.16, No.4, pp. 227-229, 2006.

[11] K. P. Esselle, and T. S. Bird, "A hybrid-resonator antenna: experimental results", *IEEE Transactions on Antennas and Propagation*, Vol. 53, No. 2, pp. 870-871, 2005.

[12] T. H. Chang, Y.C. Huang, W. F. Su, J. F. Kiang, "Wideband dielectric resonator antenna with a tunnel", *IEEE Antenna and Wireless Propagation Letters*, Vol. 7, pp. 275-278, 2008.

[13] T. H. Chang, J.F. Kiang, "Broadband dielectric resonator antenna with an offset well", *IEEE Antenna and Wireless Propagation Letters*, Vol. 6, pp. 564–567, 2007.

[14] M. Khalily, M. K. A. Rahim, A. A. Kishk, S. Danesh, "Wideband P-shaped dielectric resonator antenna", *Radioengineering*, Vol. 22, No. 1, pp. 281-285, 2013.

[15] W. Chang, Z. Feng, "Investigation of a novel wideband feeding technique for dielectric ring resonator antennas", *IEEE Antennas and Wireless Propagation Letters*, Vol. 8, pp. 348-351, 2009.

[16] A. Buerkle, K. Sarabandi, H. Mosallaie, "Compact slot and dielectric resonator antenna with dual resonance, broadband characteristics", *IEEE Transactions on Antennas and Propagation*, Vol. 53, No. 3, pp. 1020-1027, March 2005.

[17] C.P.Chua, P.A. Pavovich, R. M. Dragos, M. S. Leung, "A compact and wideband rectangular dielectric resonator antenna", *Proceeding of the* 7^{th} *Conference on Electronic Packing Technology*, Singapore, Vol. 1, pp. 313-316, Dec. 2005.

[18] Y. Gao, B. L. Ooi, W. B. Ewe, A. P. Popov, "A compact wideband hybrid dielectric resonator antenna", *IEEE Microwave and Wireless Components Letters*, Vol. 16, No. 4, pp. 227-229, April 2006.

[19] B. Li, K.W. Leung, "Strip-fed rectangular dielectric resonator antennas with/without a parasitic patch", *IEEE Transactions on Antennas and Propagation*, Vol. 53, No. 7, pp. 2200-2207, July 2005.

[20] X.S. Fang, and K.W. Leung, "Designs of single-, dual-, wide-band rectangular dielectric resonator antennas", *IEEE Transactions on Antenna and Propagation*, Vol. 59, No. 6, pp. 2409-2414, June, 2011.

Chapter 4

Stacked Rectangular Dielectric Resonator Antenna

As described in section 2.2, stacking of DRAs is the one of the methods for improvement in the impedance bandwidth. In this method, two or more different samples of same or different dimensions and dielectric materials are stacked vertical. It is possible to have different combination of shapes, such as a dielectric disk, a rectangular DRA, and a triangle DRA in the stacked antenna. This chapter presents a design of stacked rectangular dielectric resonator antenna (RDRA) operating at 5.2 GHz with 13.56 % impedance bandwidth. A 50 Ω microstrip line is used in the proposed antenna as a feeding mechanism. The proposed stacked RDRA consists of two rectangular slabs which are made of two microwave dielectric materials with dielectric constant of 10 and 32, respectively stacked vertically to obtain improvement in bandwidth as compared to a conventional RDRA. Physical parameters of the stacked RDRA have been optimized by extensive simulations using Ansoft HFSS. The optimized parameters of the antenna are $17 \times 7 \times 4.56\ mm^3$ with a grounded substrate's size: $80 \times 50\ mm^2$. The prototype is fabricated. Measured and simulated results are both in good agreement. The proposed antenna is a suitable for wireless local area networks (WLAN) application in 5 GHz frequency band. This stacked RDRA exceeds the bandwidth requirements for IEEE 802.11a WLAN applications.

4.1 Introduction

As mentioned earlier, the rapid increase in the demand for wireless applications in the GHz range has led the research community to focus their attention on highly efficient antennas, which exhibit wide bandwidth and good radiation characteristics. The DRA introduced by Long et al. in 1983 [1], could be used for such applications due to high radiation efficiency, light weight, and versatility in their shapes and feeding mechanisms [2,3]. DRAs exhibit a wider impedance bandwidth and higher radiation efficiency, especially at millimeter-wave frequencies where the conductor losses of the MPAs are considerable.

One of the most crucial issues of conventional DRAs is the dependence of their size and impedance bandwidth on the dielectric constant of material used in antennas. A DRA made from a low permittivity material would has a relatively larger volume. This is due to the inverse proportionality between effective wavelength and the square root of the permittivity. It would, however, exhibit a low radiation Q-factor and therefore a wide impedance bandwidth. On the other side, a high permittivity DRA would be small in size, but would exhibit a narrow bandwidth operation [3]. Choice of dielectric constant of material used in the DRA is crucial important for wideband operation and compact design of the DRAs.

Applications in the wireless and mobile communication area require the development of radiating elements, which have as compact/low profile and wideband as possible. Hence, a lot of research is directed towards the increase of the bandwidth of the DRAs while keeping the size compact/low profile. Towards this goal, the technique of merging modes has proven to be very beneficial [4–6]. The basic concept relies on the excitation of multiple modes at nearby frequencies, so that an overall wide impedance bandwidth is achieved. This is done in two ways. One way is to combine the DRA modes with resonances of the feeding scheme. For instance, a simple cylindrical DRA (CDRA) is described in [4], which is fed from a microstrip line through two parallel bowtie slots. Here, the impedance bandwidth of around 33 % is obtained through the excitation of the $HEM_{11\delta}$ mode of the CDRA together with two modes from the resonant bowtie slots. The second way to achieve the merging of modes is through the design of the appropri-

ate DRA geometry that results in the excitation of higher-order DRA modes at nearby frequencies. This technique is relatively simple conceptually, but it nevertheless comes along with an important issue, which needs to be taken into account. Every mode has different radiation characteristics (radiation patterns, polarization) and therefore, a not well-controlled merging of modes technique would result in patterns of the DRA that vary with frequency. Examples of well-operating DRAs are given in [5, 6], where the excitation of the fundamental TE^x_{111} and the higher-order TE^x_{113} modes of the rectangular DRA (RDRA) or the $HEM_{11\delta}$ and $HEM_{11\Delta}$ of the CDRA result in wide impedance bandwidth and stable broadside radiation patterns. The merging of the two modes of the RDRA is achieved through the careful dimensioning of the DRA. So, if the height (h) of the RDRA is chosen to be much larger than its length, (a) and its depth (d) the TE^x_{111} and TE^x_{113} modes are excited at nearby frequencies, which is in agreement with theory [6].

It was shown experimentally in [7–10] that stacking two DRAs on the top of each can increase an impedance bandwidth. In section 2.2.2, various designs of stacked/embedded DRAs are discussed. Two disk DRAs, triangle DRAs are stacked vertically and experimentally reported impedance bandwidth around 25 % to 64 % using probe and aperture feeding schemes. These desgins use materials of different dielectric constants. However, in this method, the DRA's volume is a significant problem which may fail to maintain the major characteristic of low-profile. Fabrication is also not easy. There is a lack of closed form relation for designing the antenna. Some special geometry of DRAs can also enhance the impedance bandwidth [11–13] such as conical, biconical, notch, and triangle shaped DRA designe for broadband applications. This chapter presents that the stacked rectangular DRA offer wide bandwidth operation. Measured results are compared against the simulated results. The proposed antenna has wide impedance bandwidth. The measured co-polarization and cross polarization of radiation patterns over the impedance bandwidth (S_{11} < -6 dB) are also compared each other. The measured return loss is presented and discussed.

4.2 Proposed Approach

Figure 4.1 shows the geometry of the proposed stacked rectangular DRA. A 50 Ω microstrip line (width of 4.45 mm) is printed on top of a grounded substrate with thickness H_s of 1.56 mm, dielectric constant (ϵ_s) of 2.5 and loss tangent of 0.0017. Two DRA slabs (slab 1 & 2) having equal cross sectional area ($a \times d$), but with different permittivity ϵ_{r1} and ϵ_{r2} and different heights h_1 and h_2 to form the stacked RDRA. The slab 1 is placed above the microstrip line for coupling, and the slab 2 is placed on the top of the slab 1 for electromagnetically coupling. The total height of stacked RDRA is h = h_1 + h_2. Dimensions of the ground substrate are L_1 of 80 mm and W_1 of 50 mm. The fields equations of inside the simple rectangular DRA are as per the below (4.1 - 4.6) [2]. The initial dimensions of the RDRA were determined using equations developed by dielectric waveguide model (DWM) given in [3] as described in chapter 2.

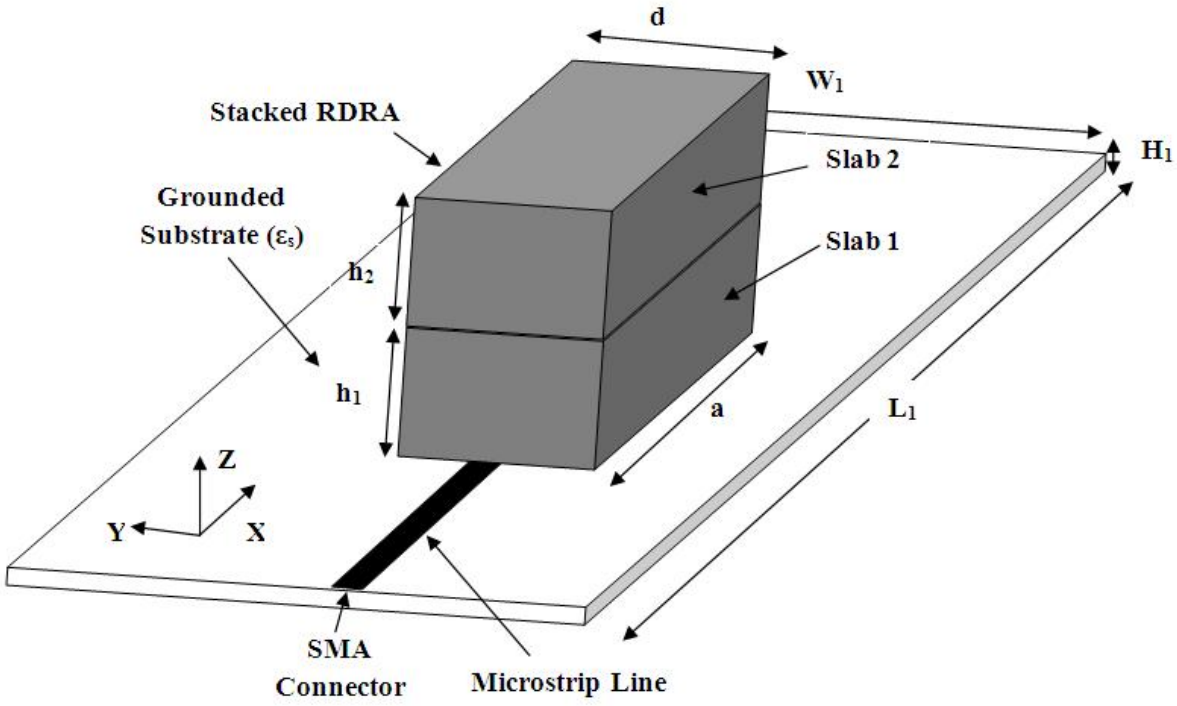

Figure 4.1: Geometry of the proposed stacked antenna.

$$E_x = Ak_y \cos(k_x x) sin(k_y y) \cos(k_z z) \tag{4.1}$$

$$E_y = -Ak_x sin(k_x x) \cos(k_y y) \cos(k_z z) \tag{4.2}$$

$$E_z = 0 \tag{4.3}$$

$$H_x = \frac{k_x k_y}{j\omega\mu_0} A\cos(k_x x) sin(k_y y) sin(k_z z) \tag{4.4}$$

$$H_y = \frac{(k_x^2 + k_y^2)}{j\omega\mu_0} A sin(k_x x)\cos(k_y y) sin(k_z z) \tag{4.5}$$

$$k_x \tan(k_x a/2) = \sqrt{(\epsilon_{r1} - 1)k_0^2 - k_x^2} \tag{4.6}$$

where,

$$k_x = \sqrt{\epsilon_{r1} k_0^2 - k_y^2 - k_y^2} \tag{4.7}$$

$$k_z = \frac{\pi}{h_1} \tag{4.8}$$

$$k_y = \frac{\pi}{d} \tag{4.9}$$

$$k_0 = \frac{2\pi f_0}{c} \tag{4.10}$$

To account for the effect of two different dielectric materials on resonant frequency of the stacked RDRA, the DWM equations are modified by a replacing slab 1's height (h_1) with an effective height (h) and dielectric constant of slab 1 (ϵ_{r1}) with effective permittivity (ϵ_{eff}) [10]. The effective height of the stacked RDRA is a simple sum of slabs' height

$$h = h_1 + h_2 \tag{4.11}$$

The effective permittivity (ϵ_{eff}) of the proposed stacked RDRA is obtained [10] as

$$\epsilon_{eff} = \frac{h}{\frac{h_1}{\epsilon_{r1}} + \frac{h_2}{\epsilon_{r2}}} \tag{4.12}$$

4.2.1 Numerical Study

Based on extensive simulation studies, design parameters of the stacked RDRA have been optimized. Slab 1 is made of a microwave material with dielectric constant of 32 and thickness, h_1, of 3 mm. Slab 2 is made of several layers of a microwave material with dielectric constant of 10.2 and thickness of each layer is 0.78 mm. Cross sectional area of slab 1 and slab 2 is a of 17 mm and d of 7 mm. Simulation studies are carried out for

different height, h_2, of the slab 2 on the slab 1 which has dimension of $17 \times 7 \times 3\ mm^3$, to form a stacked RDRA. For all cases, an open ended microstrip line is optimized for the return loss characteristic with reference to the centre of the stacked RDRA. Simulated

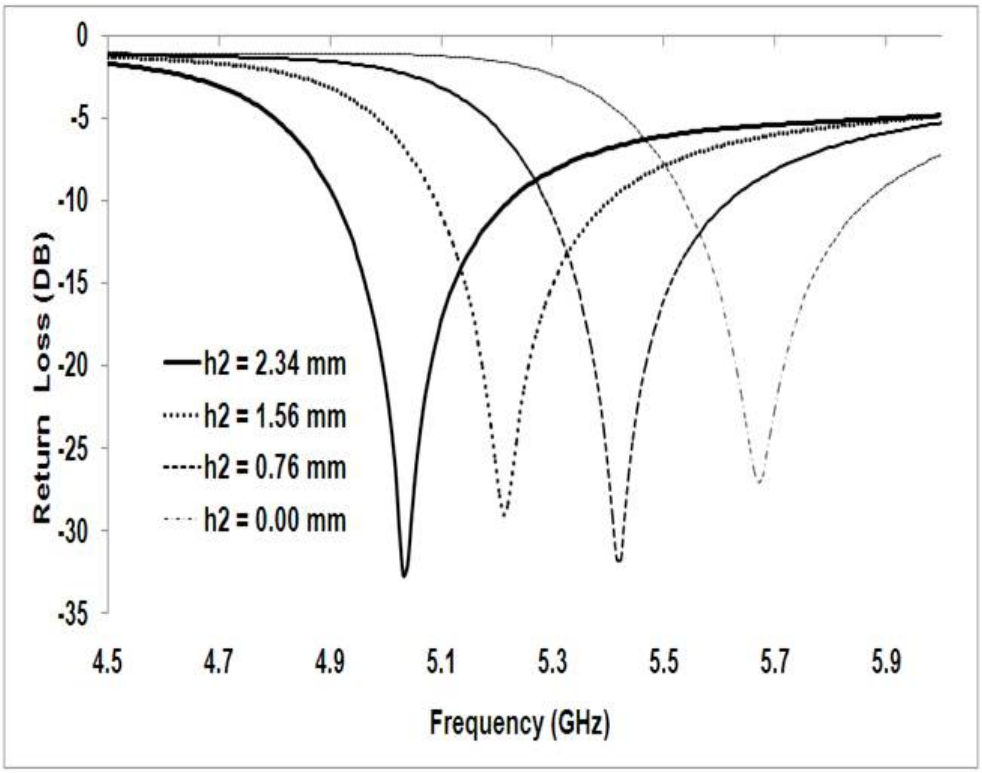

Figure 4.2: Simulated return loss for different height of slab 2.

Table 4.1: Effect of height (h_2) of slab 2 on slab 1.

h_2 (mm)	h (mm)	f_{oc} (GHz)	f_{os} (GHz)	% of Error	Return Loss (dB)	% of BW
0.00	3.00	5.341	5.68	6.36	-35.41	11.97
0.78	3.78	5.461	5.41	0.93	-30.42	12.75
1.56	4.56	5.311	5.21	1.90	-28.50	13.11
2.34	5.34	5.126	5.00	2.46	-35.52	14.00

return loss characteristics for different heights of slab 2 are shown in Figure 4.2. Table 4.1 lists calculated resonant frequency (f_{oc}) and simulated resonant frequency (f_{os}), return loss characteristics, and % of 6-dB impedance bandwidth. It is noticed that as height of slab 2 is increased from 0 mm to 2.34 mm in the step of 0.78 mm, the resonant frequency of the antenna is decreased, from 5.68 GHz to 5.00 GHz, whereas % of 6-dB impedance bandwidth is increased from 11.97 % to 14.00 %. This shows that by stacking of the low

permittivity microwave material on the conventional dielectric resonator antenna made of the high permittivity microwave material, decrease in the resonant frequency and increase in the impedance bandwidth can be achieved. Also resonant frequencies of the stacked RDRA are calculated based on equations (4.7, 4.8, 4.9, 4.10) using equations (4.11) and (4.12). Table 4.1 show that simulated resonant frequencies (f_{os}) and calculated resonant frequencies (f_{oc}) for different values of h_2. From Table 4.1, it is seen that percentage of error is in the order of 1 to 2.5 between f_{oc} and f_{os}. This show a good agreement between the calculated and simulated resonant frequencies.

Table 4.2: Optimized parameters of the stacked antenna.

Particular	Dielectric Constant (ϵ_r)	L (mm)	W (mm)	Height (mm)	Loss Tangent
Slab1	32	17.00	7.00	3.00	0.0011
Slab2	10	17.00	7.00	1.56	0.0017

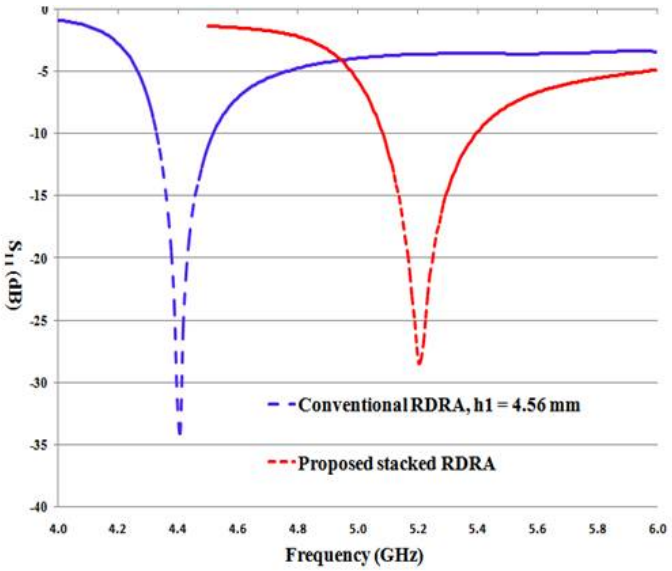

Figure 4.3: Simulated return loss characteristics of conventional RDRA and the proposed stacked RDRA.

Based on these simulation results, physical design parameters: a of 17 mm, d of 7 mm, and h of 4.56 mm have been chosen for the proposed antenna to excite at 5.2 GHz resonant frequency. Table 4.2 lists the design parameters of the proposed stacked DRA. Also simulation is carried out for the conventional rectangular DRA having length of

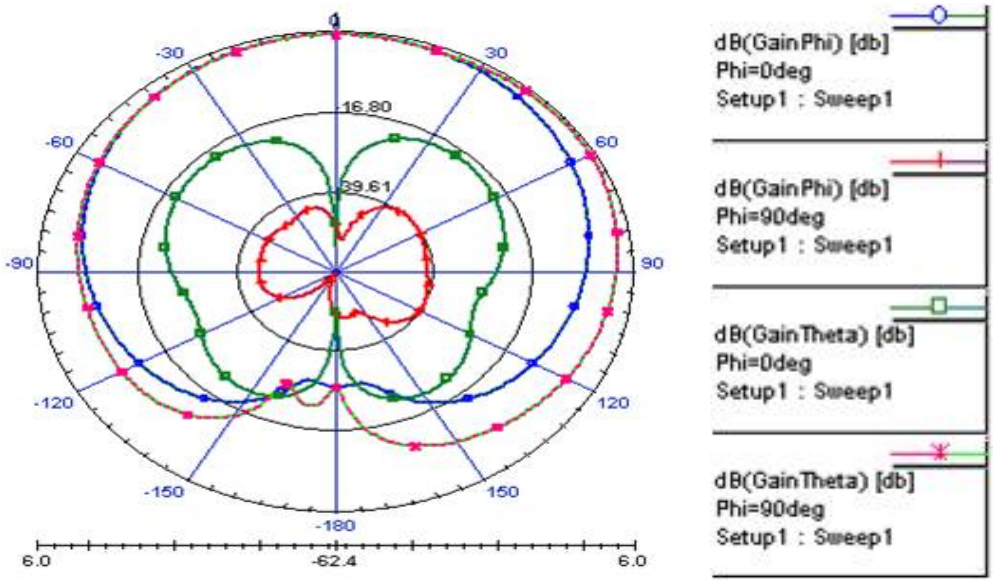

Figure 4.4: Simulated radiation pattern at 5.2 GHz of the stacked antenna.

17 mm, depth of 7 mm, height of 4.56 mm and dielectric constant, ϵ_{r1}, of 32 as same dimensions as the proposed stacked antenna has. Figure 4.3 shows simulated return loss characteristics of the conventional RDRA and the proposed stacked RDRA. It is observed that the conventional antenna is resonant at 4.41 GHz with 8.50 % of 6-dB impedance bandwidth. This shows that by stacking of different microwave materials with different permittivity, the wideband operation can be obtained. Figure 4.4 shows simulated radiation patterns of the stacked antenna at 5.2 GHz. Radiation patterns are linear and broadside.

4.3 Experimental Results

The proposed antenna is fabricated as per the pysical parameters given in Table 4.2. Figure 4.5 shows a photograph of the fabricated antenna. Return loss characteristic of the antenna is measured by N5230A PNA series network analyzer. The measured and simulated return loss characteristics of the stacked RDRA are shown in Figure 4.6. Comparison of measured and simulated performances of the proposed antenna is listed in Table 4.3. From Figure 4.6 and Table 4.3, it is noticed that measured results are in excellent agreement with simulated results. The antenna has a 6-dB return loss bandwidth of 710 MHz (5.01 GHz to 5.72 GHz) at its resonant frequency of 5.23 GHz. The co- and cross- radiation patterns of the antenna are measured in an anechoic chamber. The co-

and cross- polarization patterns in the E- plane and H- plane of the antenna are presented at resonant frequency of 5.23 GHz in Figure 4.7. There is good agreement between the simulated and measured radiation patterns as shown in Figure 4.4 and Figure 4.7. It shows that the antenna has broadside radiations. The proposed antenna has linear polarization over the said bandwidth. The proposed antenna shows the cross polarization level better than -20 dB at the resonant frequency. Measured gain is 5.23 dBi at bore site at the resonant frequency. It is in good agreement with simulated gain as listed in Table 4.3.

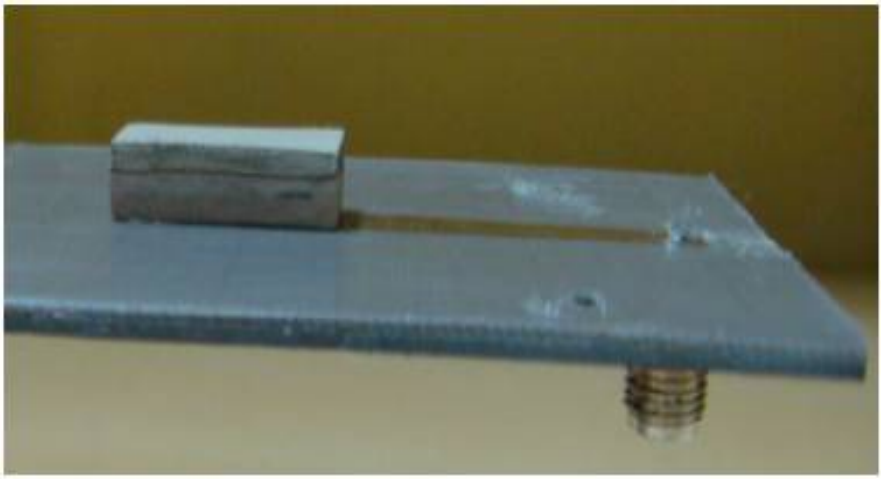

Figure 4.5: A photograph of the fabricated proposed stacked design

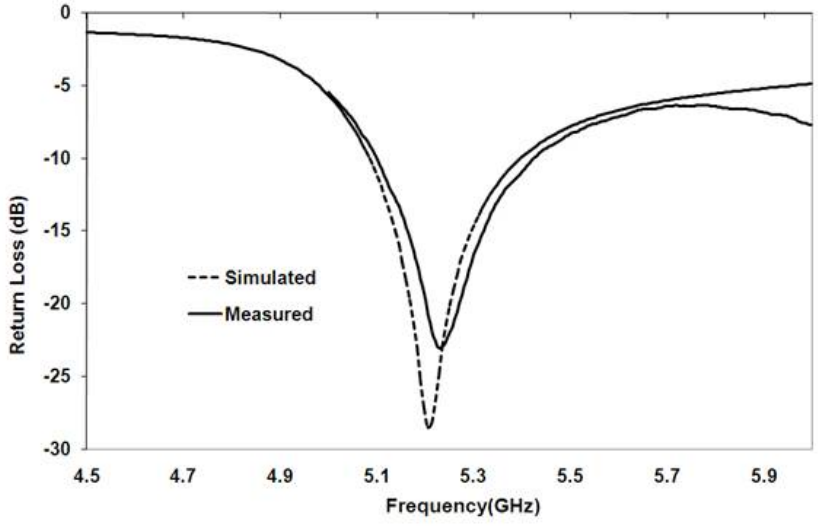

Figure 4.6: Measured and simulated return loss characteristics of the fabricated stacked antenna

Table 4.3: Performance comparison of the proposed stacked antenna.

Particular	Simulated	Measured
Resonant Freq. (GHz)	5.21	5.23
Return Loss (dB)	-28.51	-22.90
6-dB Bandwidth (MHz)	682	710
% of Bandwidth	13.11	13.57
Gain at boresite (dB)	5.25	5.23

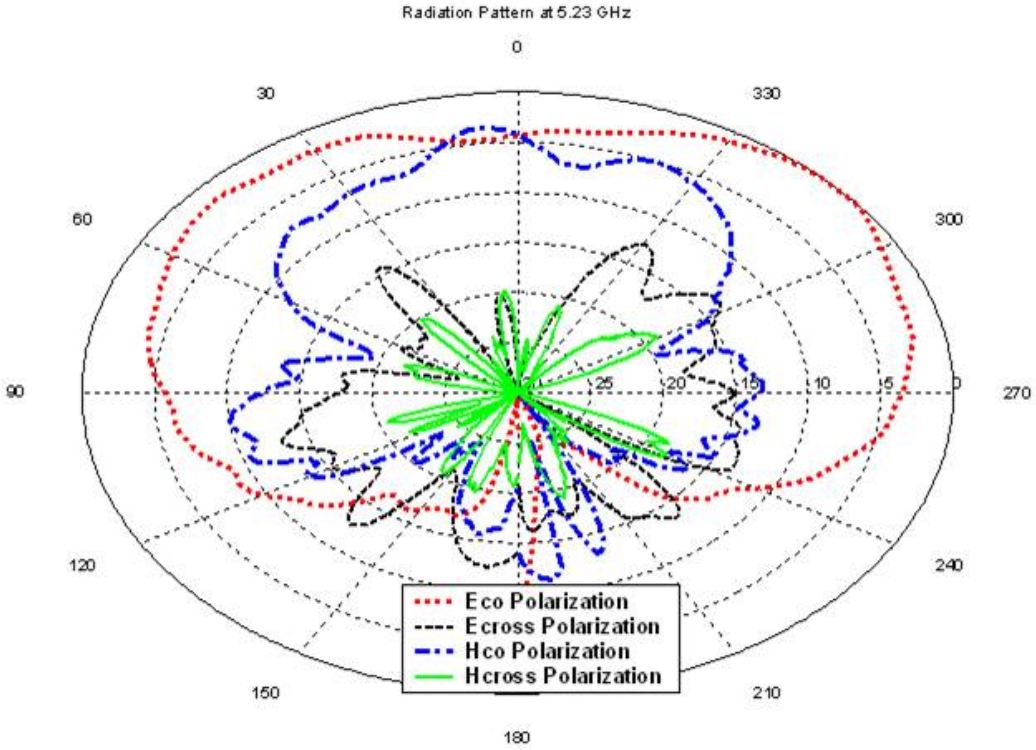

Figure 4.7: Measured radiation patterns at 5.23 GHz.

Simulation is carried out for the conventional DRA with length of 17 mm, depth of 7 mm, height of 3.44 mm, dielectric constant ϵ_{r1} of 32. These dimensions are calculated equations based on DWM analysis as given in section 4.2. It has simulated resonant frequency of 5.2 GHz and 560 MHz bandwidth. As compared to the stacked RDRA, the conventional RDRA has less volume and bandwidth at the same resonant frequency. Thus, at the cost of volume of the antenna, the wideband operation is achieved by stacking the dielectric resonator antennas. It is observed that stacking of low dielectric constant's material on the high permittivity material, the enhancement of bandwidth can be achieved. As the height of stacking material is increased, the increased in bandwidth is obtained. So there

is trade off between the bandwidth and volume of DRA.

4.4 Conclusion

In this chapter, a simple microstrip fed stacked rectangular DRA operated at 5.2 GHz has been proposed. It has 6-dB return loss bandwidth of 710 MHz with % BW of 13.57 with good radiation patterns. Antenna is made from two different materials to achieve the benefit of compact size and wider bandwidth operation. Due to absence of conductor loss, the proposed antenna has high radiation efficiency. Due to these, the antenna is proposed for WLAN applications, MIMO wireless system, WLAN, Wi-Fi, cellular phones, and GPS systems.

References

[1] Long S. A., McAllister M.W., and Shen L.C., "The resonant cylindrical dielectric cavity antenna", *IEEE Transactions on Antennas and Propagation*, Vol. 31, No. 3, pp. 406-412, 1983.

[2] Mongia R. K. and Ittipiboon A., "Theoretical and experimental investigation on rectangular dielectric resonator antennas", *IEEE Transactions on Antenna and Propagation*, Vol. 45, No. 9, pp. 1348-1356, 1997.

[3] Petosa A., Dielectric Resonator Antenna Handbook, *Artech House*, 25007.

[4] Almpanis G., Fumeaux C. and Vahldieck R., "Novel broad-band dielectric resonator antenna fed through double-bowtie-slot excitation scheme", *ACES Journal*, Vol. 22, No. 1, pp. 97-104, 2007

[5] Li B., and Leung K.W., "Strip-fed rectangular dielectric resonator antennas with/without a parasitic patch", *IEEE Transactions Antenna and Propagation*, Vol. 41, No. 10, pp. 1390-1398, 1993.

[6] Chair R., Kishk A. A., and Lee K. F., "Wideband simple cylindrical dielectric resonator antenna", *IEEE Microwave and Wireless Components Letters*, Vol. 15, No. 4, pp. 241-243, 2005.

[7] Kishk A. A., Zhang X., Glisson A. W., Kajfez D., "Numerical analysis of stacked dielectric resonator antennas excited by a coaxial probe for wideband application", *IEEE Transactions on Antenna and Propagation*, Vol. 51, No. 8, pp. 1996-2006, 2003.

[8] Kishk A. A., Ahn B., and Kajfez D., "Broadband stacked dielectric resonator antennas", *IEEE Electronics Letters*, Vol. 25, No. 18, pp. 1232-1233, Aug, 1989.

[9] Rocha H. H. B., Freire F. N. A., Sohn R.S.T.M., da Silva M.G., Santos M.R.P., Junqueria C.C.M., Cordaro T., and Sombra A.S.B., "Bandwidth enhancement of stacked dielectric resonator antennas excited by a coaxial probe: an experiment and numerical investigation", *IET Microwave Antennas Propagation*, Vol. 2, No. 6, pp. 580-587. 2008.

[10] Petosa A., Simons N., Siushansian R., Ittipiboon A. and Cuhaci M., "Design and analysis of multisegment dielectric resonator antennas", *IEEE Transactions on Antennas and Propagation*, Vol. 48, No. 5, pp. 738-742, May 2000.

[11] Almpanis G., Fumeaux C., and Vahldieck R., "Novel broadband dielectric resonator antenna fed through double-bowtie-slot excitation scheme", *ACES Journal*, Vol. 22, No. 1, pp. 97-104, 2007.

[12] Li B. and Leund K.W., "Strip-fed rectangular dielectric resonator antennas with/without a parasitic patch", *IEEE Transactions of Antenna and Propagation*, Vol. 41, No. 10, pp. 1390-1398, 1993.

[13] Chair R., Kishk A.A., and Lee K.F., "Wideband simple cylindrical dielectric resonator antenna", *IEEE Microwave and Wireless Components Letters*, Vol. 15, No. 4, pp. 241-243, 2005.

Chapter 5

Single Narrowband Rectangular Dielectric Resonator Antenna

Numerous wireless systems for consumer wireless devices require compact antenna to be integrated into small packages such as cell phones, laptop, palmtop, smart watch, and other portable devices. A key parameter for the wireless systems is a communication range which is a deciding factor in RF solution. Fundamentally, the range is dictated by a communication data rate. There are many options to increase range by reducing data rate. Two solutions are; scaling receiver bandwidth to the signal to reduce noise seen by the receiver (narrowband sytem) and adding coding gain on a higher rate signal to combat a high receiver noise in a wideband receiver. Disadvantages of coding gain system are low spectrum efficiency, reduce communication reliability, number of devices in a given area and battery lifetime. Narrowband technique for long range and reasonably low date rate is widely accepted by an industry since it gives an optimum tradeoff between range and a transmission time [1].

In section 2.3.1, the low-profile narrowband DRA is achieved by using a material of high permittivity. It is shown that the resonance of the DRA is due to waves are bouncing between the top and bottom faces of the DRAs, and hence the resonance frequency is insensitive to the radius of the circular disk DR [2], length and depth of the RDRA [3], and side length of the equilateral-triangular DRA [4]. It is observed that the low-profile narrowband DRA has no degree of freedom. The compact narrowband DRA is obtained by metallization on surfaces of the DRA. It is also observed that resonant frequency

and impedance bandwidth of the metalized DRA are decreased as compared to without metallization on the DRA. With proper metallization on the surfaces of the DRA, it is observed the new radiating mode in the RDRA [5, 6].

In this chapter, single narrowband rectangular dielectric resonator antenna (RDRA) is realized by placing single metal strip on top surface. Also, a new radiating $TE^{x}_{\delta 01}$ mode is proposed in this antenna. To validate the $TE^{x}_{\delta 10}$ mode and a conventional lowest order $TE^{x}_{\delta 11}$ mode, simple RDRA with and without a metal strip is designed, fabricated, and measured. The RDRA is mounted on the grounded substrate and fed by a simple microstrip line. Based on parametric study and electric field distributions, dimension along the y-axis is principally used to determine the resonant frequency of the proposed mode. The proposed mode has an impedance bandwidth of 35 MHz at 2.24 GHz and gain of 2.35 dB. The radiating $TE^{x}_{\delta 01}$ mode has broadside radiation patterns. As compared to the conventional mode, reduction in the resonant frequency and the impedance bandwidth by 58 % and 79 % is observed in the new mode.

5.1 Introduction

The dielectric resonator antennas (DRAs), introduced by Long et al. in 1983 [7], could be used in numerous wireless communication and sensing applications due to many advantageous features they possess. These include high radiation efficiency, compact size, light weight, and the versatility in the shapes, and feeding mechanism. There are three basic shapes available for common design, including rectangular, cylindrical, and spherical. Among these, the rectangular DRAs (RDRAs) show some advantages over other shapes. Such as, three available dimensions provide two degree of freedom (one more than the cylindrical one and two more than the spherical one), making it most flexible in designs. In practice, the rectangular DRAs are much easier to fabricate. Also, mode degeneracy can be avoided by properly choosing the dimensions. Hence it is preferred in DRA design [8].

As described in chapter 2, different modes with different antenna characteristics and radiation patterns are possible in the RDRA. TE modes are typically excited, which can

be divided into TE^x, TE^y, and TE^z modes, in the RDRA mounted on a ground plane. Depending on the relationship of the three dimensions and way of exciting mechanism, a conventional dominant mode is one of $TE^x_{\delta 11}$, $TE^y_{\delta 11}$, $TE^z_{\delta 11}$ ($0 < \delta < 1$). The mode subscripts refer to field variations along the x-, y-, and z-axes respectively. Higher-order modes can also be excited for certain aspect ratios, such as $TE^x_{\delta n1}$, $TE^x_{\delta 1n}$ modes (n = 2, 3...) as shown in Figure 2.6. However, not all higher modes have similar broadside patterns as shown by the basic mode. A $TE^x_{\delta 21}$ mode shown in Figure 2.6 has a null at broadside. Resonant frequency of these modes is a function of the three dimensions and dielectric constant, according to dielectric waveguide model (DWM) [9].

In this chapter, a rectangular DRA with and without single metal strip placed on top surface is described. The new $TE^x_{\delta 10}$ radiating mode is proposed and compared to the conventional dominant mode, $TE^x_{\delta 11}$. Parametric study has been carried out on the proposed mode. Specific field distributions of the new mode and the conventional mode are discussed. Measured return loss, radiation patterns, bandwidth, and gain are compared with simulated results of the $TE^x_{\delta 10}$ mode and show high agreement. The proposed scheme offers a narrow band as compared to the conventional RDRA.

5.2 Proposed Approach

Geometry of the conventional and proposed rectangular dielectric resonator antenna (RDRA) is shown in Figure 5.1 and 5.2 respectively. The geometry without metal patch/strip is for the conventional $TE^x_{\delta 11}$ mode, while the geometry with metal strip on top surface of RDRA is for proposed new $TE^x_{\delta 10}$ mode. A 50 Ω microstrip line is printed on a grounded substrate. The grounded substrate has dimension of $W_1 \times L_1 \times H_1$ with dielectric constant, ϵ_s of 2.5. The rectangular DRA is placed on open ended microstrip line for efficient coupling. The rectangular DRA has a depth d, a width w, and height h along x-, y- and z-axis respectively. The ceramic material with relative dielectric constant ϵ_r of 32 is used to fabricate the RDRA. A metal strip ($d \times a$) is placed on the top surface of the RDRA in the xy-plane. The metal strip could be roughly modeled an infinitely thin perfect electric conductor (PEC). As compared to the conventional RDRA, the proposed DRA has two surfaces which are roughly PEC and remaining four surfaces

are roughly perfect magnetic conductor (PMC). An interface between high dielectric and air is PMC.

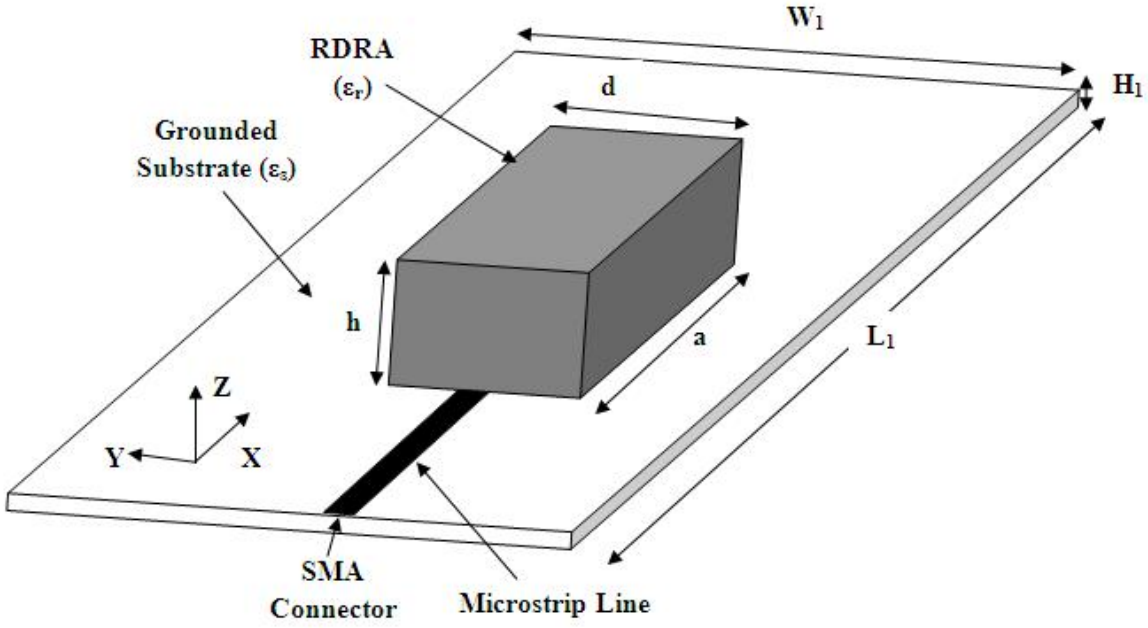

Figure 5.1: Geometry of the conventional mode in RDRA [3]

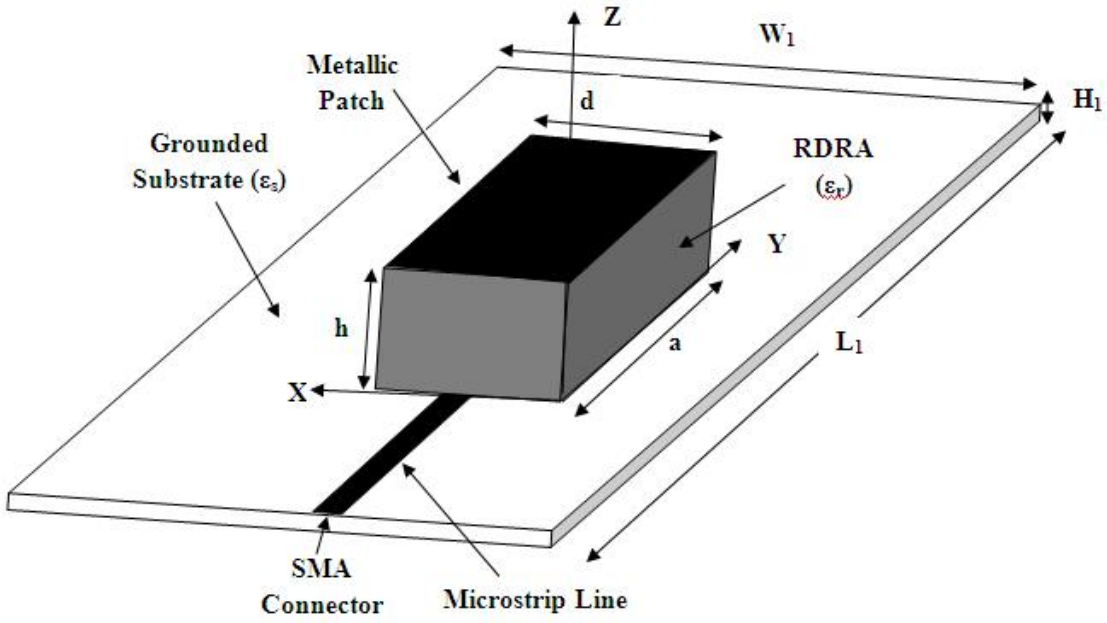

Figure 5.2: Geometry of the proposed mode in RDRA

5.2.1 E-Field Distribution

Commercial 3-D full-wave electromagnetic simulation software Ansoft HFSS, based on finite element method, is used for the numerical study. RDRA with length (a) of 17 mm, depth (d) of 7 mm and height (h) of 3 mm is simulated with the proposed geometry as well as the conventional geometry and is resonated at 2.19 GHz and 5.38 GHz, respectively. Simulated electric field distributions at resonance in the proposed antenna and the conventional antenna are shown in Figure 5.3. Arrow indicates the direction of the field. Color represents strength of the field. For the conventional $TE^x_{\delta 11}$ mode, the E-field patterns are sketch in Figure 5.3 (a), (b), (c) while for the new $TE^x_{\delta 10}$ mode, the E-field patterns are sketch in Figure 5.3 (e), (f), (g) for xy, zx and yz -plane, respectively.

For the conventional $TE^x_{\delta 11}$ mode, from the Figure 5.3 (c), the E-fields circulate around the x-axis and vary in both, along the y-axis and the z-axis. Thus, E_y and E_z are predominant whereas, E_x is uniformly distributed along x-axis. These distributions are due to boundary condition of the DRA in zx-plane. Interface between the microwave material and air in the zx-plane can be seen an imperfect magnetic wall, which could support E-field parallel to the interface and H-field perpendicular to the interface. From the Figure 5.3 (b), the E-field is oriented in the z-axis and varies from maximum to zero as the height increases from the ground plane to the top surface of the RDRA. E-fields along the x-axis are uniformly distributed and small variation, $\delta < 1$ along the x-axis. From the Figure 5.3 (a), E-fields along x-axis are uniformly distributed. The electric field is oriented along the y-axis and variation in this direction shown in Figure 5.3 (a).

For the proposed $TE^x_{\delta 10}$ mode, from Figure 5.3 (g), the E-fields circulate around the x-axis and change in along the y-axis and z-axis. This similarity is due to the same boundary condition as the conventional one in zx-plane. From the Figure 5.3 (f), E-fields are oriented along the z-axis and homogenously distributed in the same direction. There are no field variations from the ground plane to the top surface of the antenna along z-axis. Also, E-fields along the x-axis are minor δ variation. As compared to the conventional mode, different field distributions in the zx-plane are due to different boundary conditions in the xy-plane. From the Figure 5.3 (e), electric fields are along z-axis and uniformly

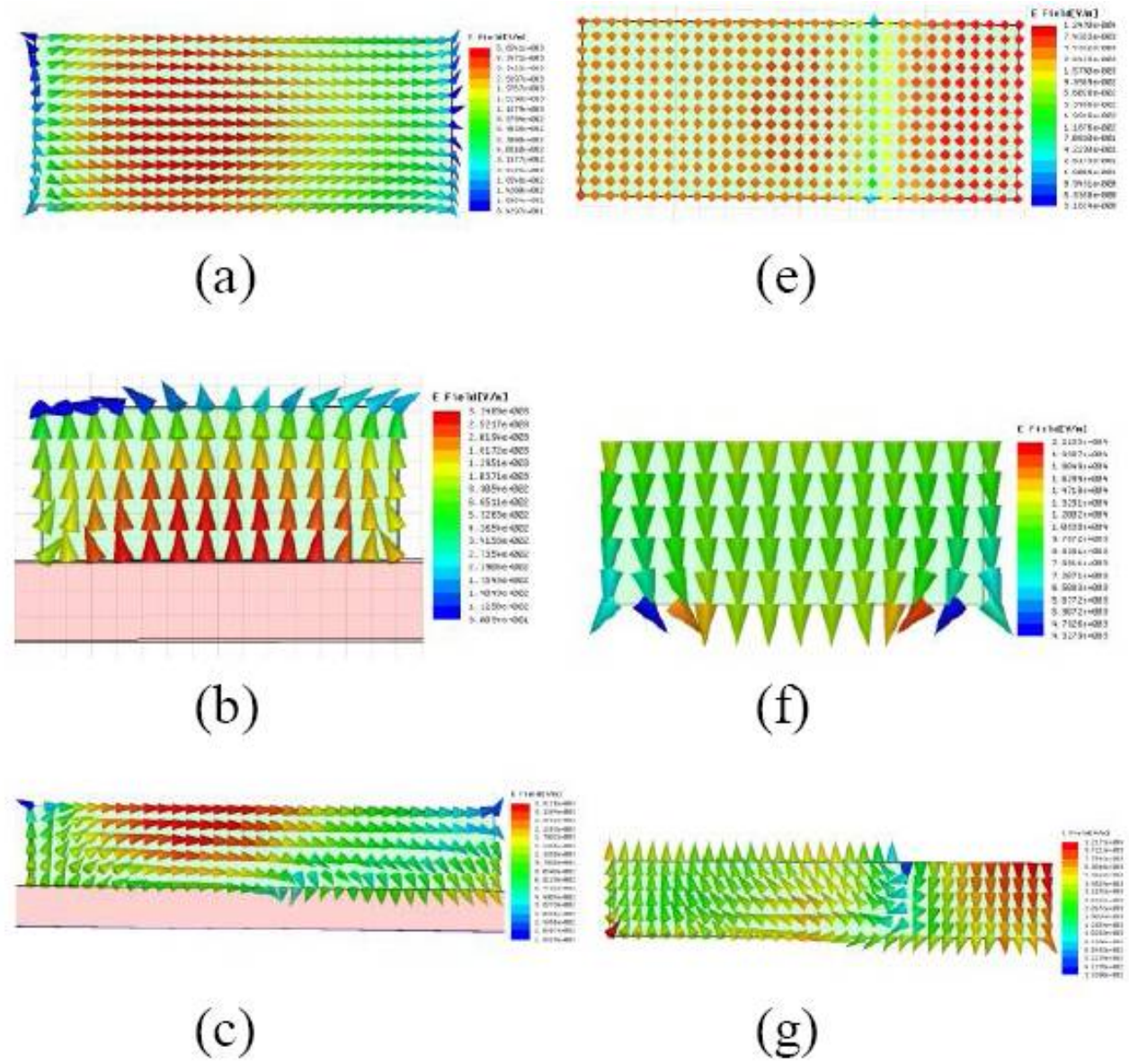

Figure 5.3: Simulated E-vector field at 5.38 GHz for the conventional $TE^x_{\delta 11}$ mode (a) x-y plane, (b) z-x plane, (c) y-z plane, at 2.19 GHz for the new mode $TE^x_{\delta 10}$ mode (e) x-y plane, (f) z-x plane, (g) y-z plane

distributed along x- and y-axis. This change of distributions as compared to the $TE^x_{\delta 11}$ mode is due to the metal strip on the top surface of the RDRA in the xy-plane. The metal strip can be modeled as an electric wall, which supports E-field component perpendicular to the surface and H-field component parallel to the interface. Figure 5.4 sketches the H-fields in the both antennas at resonance. The H_x component is dominant along center of the RDRA for both modes.

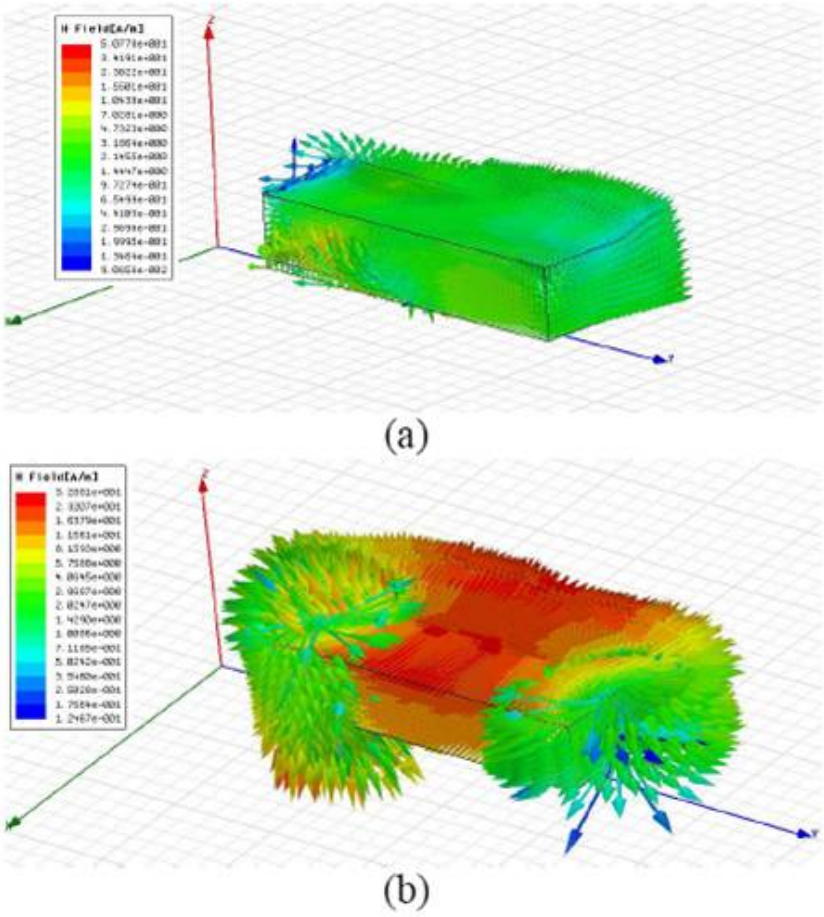

Figure 5.4: Simulated H-vector field (a) at 5.38 GHz for the conventional $TE^{x}_{\delta 11}$ mode, (b) at 2.19 GHz for the new mode $TE^{x}_{\delta 10}$ mode

5.2.2 Theoretical Analysis

The resonant frequency of the $TE^{x}_{\delta 10}$ mode can be derived by the dielectric waveguide model (DWM) and mixed magnetic wall (MMW) model in [2]. As compared to the conventional RDRA mounted on the ground plane, the proposed antenna has different boundary conditions. The PMC boundary condition $E \bullet n = 0$ is assumed at y equal to 0 and y equal to w. The imperfect PMC boundary condition is assumed at x equal to 0 and x equal to d. The PEC boundary condition at z equal to h. Because of two horizontal metal strips (one at bottom of the substrate and other at z equal to h) in the xy-plane, wave number along the z-direction is reduced to zero. Following equations are obtained for k_y and k_z:

$$k_y = \frac{\pi}{a} \qquad k_z = 0, \qquad k_0 = \frac{2\pi}{\lambda_0}, \tag{5.1}$$

Where, k_0 denotes free-space wave number corresponding to resonant frequency. The wave numbers also satisfy the following separation equation:

$$k_x^2 + k_y^2 = k_0^2 \tag{5.2}$$

The resonant frequency of the $TE_{\delta 10}^x$ mode is found by solving a following transcendental equation:

$$k_x \tan(k_x \frac{d}{2}) = \sqrt{(\epsilon_r - 1)k_0^2 - k_x^2}, \tag{5.3}$$

For given resonant frequency of the new mode, RDRA parameters such as ϵ_r, w, and d, the wave number k_x determined using (5.1) and (5.2) and also satisfies (5.3). By using DWM and MMW model, the following field components within the RDRA for the new mode are

$$H_x = \frac{k_y^2}{j\omega\mu_0} \cos(k_x x) \cos(k_y y), \tag{5.4}$$

$$H_y = \frac{k_y k_x}{j\omega\mu_0} sin(k_x x) sin(k_y y), \tag{5.5}$$

$$E_x = -k_y \cos(k_x x) sin(k_y y), \tag{5.6}$$

$$E_x = E_y = H_x = 0 \tag{5.7}$$

5.2.3 Numerical Study

To validate the new radiating mode, parametric study has been performed on different dimensions of the proposed RDRA. The study is carried out by varying one dimension, while others are invariable. The purpose of study is to see effect on resonant frequency of $TE_{\delta 10}^x$ mode. Return loss characteristics of the proposed mode due to the variation of length a, depth d, and height h of RDRA are shown in Figure 5.5, 5.6 and 5.7 respectively. Table 5.1, 5.2, and 5.3 list the calcualted and simulated resonant frequencies (f_r), % of error and return loss in dB for variation of width w, depth d, and height h respectively. There is 3 % to 9 % of error between the calculated and simulated resonance frequencies. From Figure 5.5 and Table 5.1, it is observed that when dimension along the y-axis (a) is increased from 13 mm to 21 mm, the resonant frequency is decreased from 2.70 GHz to 1.83 GHz. From Figure 5.6 and Table 5.2, it is found that when dimension along the x-axis (d) is increased from 5 mm to 9 mm, the resonant frequency of the $TE_{\delta 10}^x$ mode is

Table 5.1: Performance of parametric study on width w (d = 7 mm, h = 3 mm) of the proposed RDRA

length (a) (mm)	Calculated f_r (GHz)	Simulated f_r.(GHz))	% of error	Return Loss (dB)
21	2.0217	1.83125	9.42	-13.43
19	2.1601	2.00625	7.12	-14.64
17	2.3280	2.16250	7.10	-21.97
15	2.5371	2.45000	3.43	-10.55
13	2.8060	2.70000	3.77	-20.94

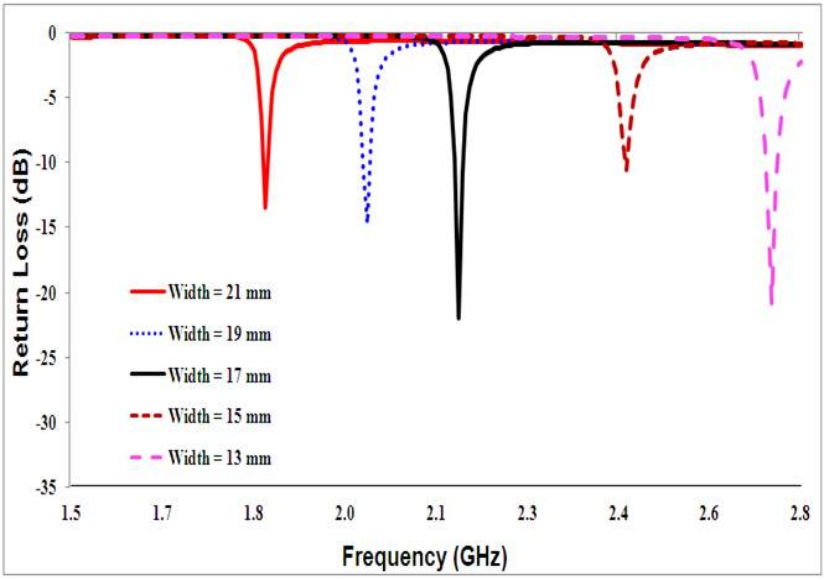

Figure 5.5: Simulated return loss of the proposed antenna with different values of length (d = 7 mm, h = 3 mm)

very minor variation from 2.23 GHz to 2.07 GHz as shown in Figure 5.6. It is % of error from 1.4 % to 14 % between calculated and simulated resonance frequencies as shown in Table 5.2. From the Figure 5.7 and Table 5.3, it is noticed that the resonant frequency of the mode almost remain stable when dimension along the z-axis (h) is increased from 2 mm to 5 mm. From Table 5.3, there are 7 to 9 % of error in simulated resonance frequency as compared to the calculated frequency. In this parametric study on dimensions of the proposed scheme, overlapping length of microstrip line between the rectangular DRA and the ground plane is optimized for better impedance matching (S_{11} < -10 dB) for all cases. In the analysis, the metalization on the top surface of the RDRA to be assumed of infinite sheet. For shorter depth, the error is more as compared to larger depth. From these characteristics, it is observed that the resonant frequency of the new mode is mainly

Table 5.2: Performance of parametric study on depth d (a = 17 mm, h = 3 mm) of the proposed RDRA

depth (mm)	Calculated Fr.(GHz)	Simulated Fr.(GHz))	% of error	Return Loss (dB)
9	2.1563	2.18750	1.44	-13.95
8	2.2329	2.08125	6.79	-15.10
7	2.3280	2.16250	7.10	-21.97
6	2.4492	2.13750	12.73	-22.20
5	2.6088	2.23750	14.23	-19.36

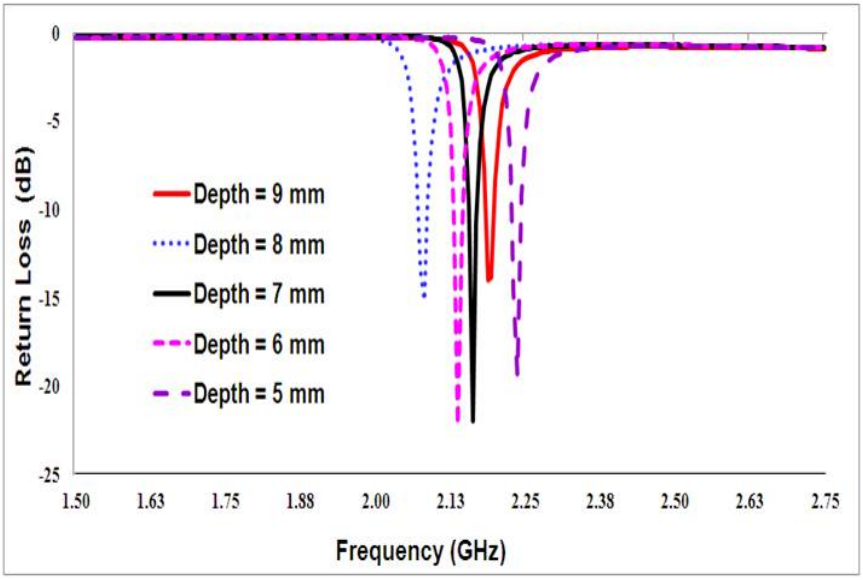

Figure 5.6: Simulated return loss of the proposed antenna with different values of depth (a = 17 mm, h = 3 mm)

depends on length a, and slightly depend on depth d. Thus, the degree of freedom for the proposed antenna design is one as compared to two degree of freedom in the conventional RDRA design. This is also confirmed by specific field distributions as given in Figure 5.3 and 5.4. This observation is also verify by equations (5.1-5.3) for determination of resonant frequency of the $TE^{x}_{\delta 10}$ mode.

The simulation is also carried out for a metal strip placed at different side walls of the RDRA. A metal strip is placed at z = h (xy-plane), x = d (yz-plane), y = a (zx-plane), and without metal strip: these four cases are simulated and return loss characteristics are shown in Figure 5.8. Resonant frequency (calculated and simulated), % of error, impedance bandwidth etc are listed in Table 5.4. It is observed that the resonant fre-

Table 5.3: Performance of parametric study on height h (d = 7 mm, a = 17 mm) of the proposed RDRA

height (mm)	Calculated Fr.(GHz)	Simulated Fr.(GHz))	% of error	Return Loss (dB)
5	2.33	2.14	7.91	-17.46
4	2.33	2.12	8.98	-20.50
3	2.33	2.16	7.10	-21.97
2	2.33	2.15	7.64	-15.02

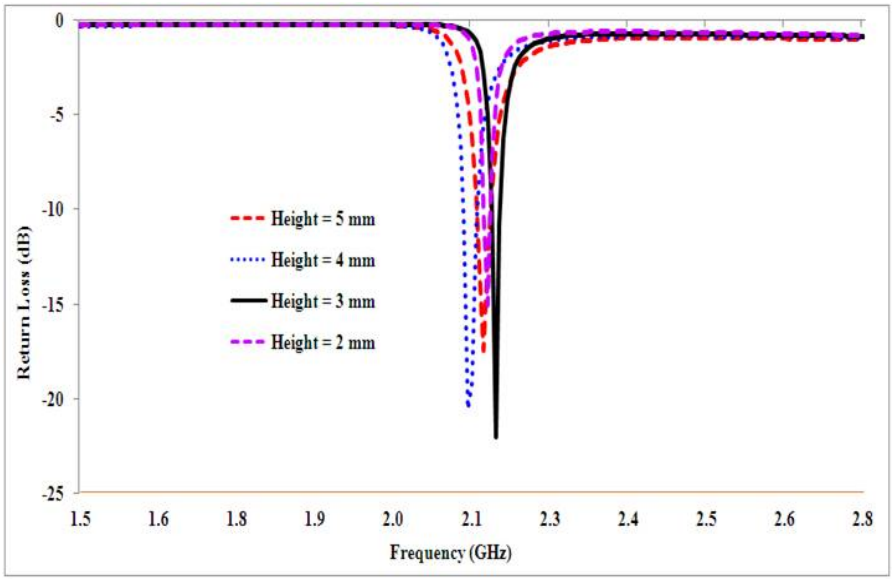

Figure 5.7: Simulated return loss of the proposed antenna with different values of height h (d = 7 mm, a = 17 mm)

quency (from 5.38 GHz to 2.19 GHz) and impedance bandwidth (from 210 MHz to 10 MHz) are drastically decreased due to the metal strip at xy-plane and zx-plane as compared to the without metal strip on RDRA, while resonant frequency is nearly same (5.38 GHz & 5.33 GHz) for the metal strip at yz-plane with increase of bandwidth (from 210 MHz to 310 MHz) as compared to the conventional RDRA. From these, it is noticed that by placing a metal strip at appropriate surface, the new radiating mode with a narrow bandwidth is possible to excite in the rectangular DRA. It is also observed that by placing a metal strip, perpenducalar surface of the ground plane, on the surface of the RDRA, impedance bandwidth can be improved.

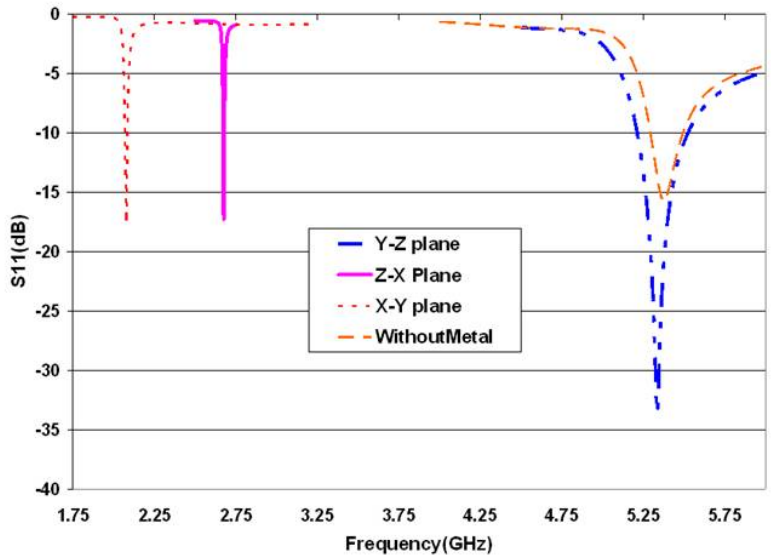

Figure 5.8: Simulated return loss for metal strip placed at different surfaces of the RDRA

Table 5.4: Performance of parametric study of metalization of the different surfaces of the RDRA

Metallic Surface	Calculated Fr.(GHz)	Simulated Fr.(GHz)	% of error	BW (MHz)	% of BW
Con. RDRA	5.34	5.38	0.92	210	3.9 %
@ z = h	2.33	2.19	6.00	20	0.9 %
@ y = d	2.45	2.68	8.36	10	0.4 %
@ x = a	5.07	5.33	5.17	310	5.8 %

5.3 Experimental Results

For further confirmation of the new radiating $TE^x_{\delta 10}$ mode, based on extensive simulation, the proposed RDRA design and the conventional RDRA design are fabricated and measured. The physical parameters of both the antennas are depth of 7 mm, length of 17 mm, height of 3 mm and ϵ_r of 32. The return loss characteristics of these prototypes are measured by an Agilent vector network analyzer. Figure 5.9 and 5.10 show the measured and simulated return loss characteristics of the proposed designs and the conventional designs respectively. A photograph of the fabricated proposed antenna shown in Figure 5.11. Measured parameters such as resonant frequency, impedance bandwidth, % of bandwidth, boresight gain, half power beam width (HPBW) and simulated radiation efficiency are listed in Table 5.5 for the $TE^x_{\delta 10}$ and $TE^x_{\delta 11}$ mode.

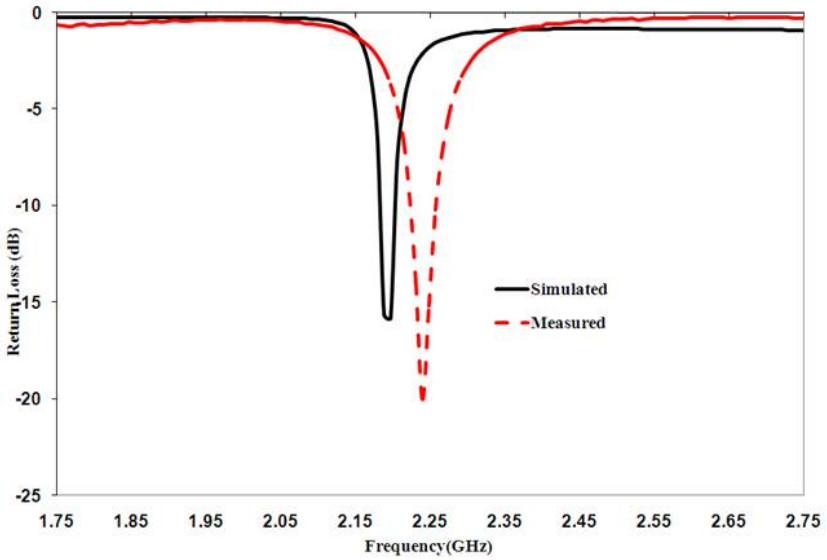

Figure 5.9: Measured and simulated return loss characteristics of the proposed narrow-band RDRA ($TE^x_{\delta 10}$ mode)

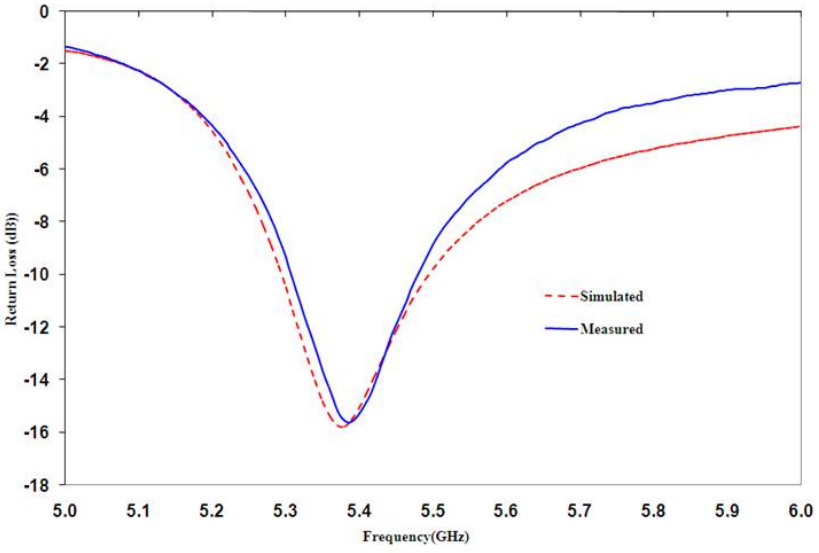

Figure 5.10: Measured and simulated return loss characteristics of the the conventional RDRA ($TE^x_{\delta 11}$ mode)

From Figure 5.9, Table 5.2, it is noticed that proposed antenna is resonated at 2.24 GHz for $TE^x_{\delta 10}$ mode with a bandwidth of 35 MHz, covering frequency band of 2.223-2.258 GHz, which are agree with the simulated results. At resonant, measured gain is 2.35 dB. The conventional $TE^x_{\delta 11}$ mode is resonated at 5.39 GHz and having bandwidth of 165 MHz as shown in Figure 5.10. With reference to the conventional $TE^x_{\delta 11}$ mode, resonant

Table 5.5: Measured parameters of the proposed and the conventional RDRA

Parameters	$TE^x_{\delta 10}$ Mode	$TE^x_{\delta 11}$ mode
Resonant Frequency (GHz)	2.24	5.39
Impedance Bandwidth (MHz)	35	165
% of Bandwidth	1.56	3.56
Gain at boresite (dB)	2.35	1.62
HPBW (Degree)	90°	92°
Simulated Radi. Efficiency	97.79 %	98.41 %
Reduction in Freq.	58.44 %	—-
Reduction in Bandwidth	78.78 %	—-

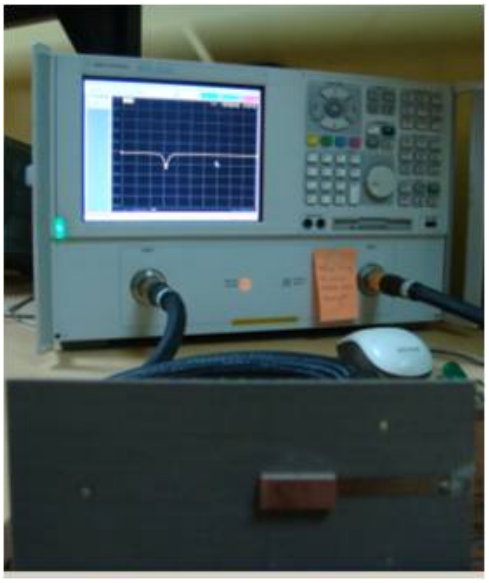

Figure 5.11: Photograph of the fabricated narrowband RDRA

frequency and bandwidth of the $TE^x_{\delta 10}$ mode are decreased by 58 % and 79 % respectively. From these results, it is concluded that by a metal strip on the top surface of the RDRA, the new mode is excited whose frequency is much smaller than the conventional mode. Also the bandwidth of the proposed mode is narrower (1.56 %) than that of the conventional one (3.56 %).

Field radiation patterns at resonant are measured in anechoic chamber for the proposed mode. For proposed mode, measured and simulated E-plane patterns are shown in Figure 5.12 (a), while measured and simulated H-plane patterns are sketched in Figure 5.12 (b). It is seen that the $TE^x_{\delta 10}$ mode has broadside radiation patterns in both principal planes. The measured cross-polar rejection is better than 20 dB in the E-plane, while it is better

than 15 dB in the H-plane. From Figure 5.12, there are good agreement between the measured and simulated radiation patterns in the both patterns. Figure 5.13 shows measured and simulated gain of the proposed mode. Simulated radiation efficiency for 0the $TE^x_{\delta 10}$ mode is around 94.79 % while for the $TE^x_{\delta 11}$ mode; it is around 98.41 %. The

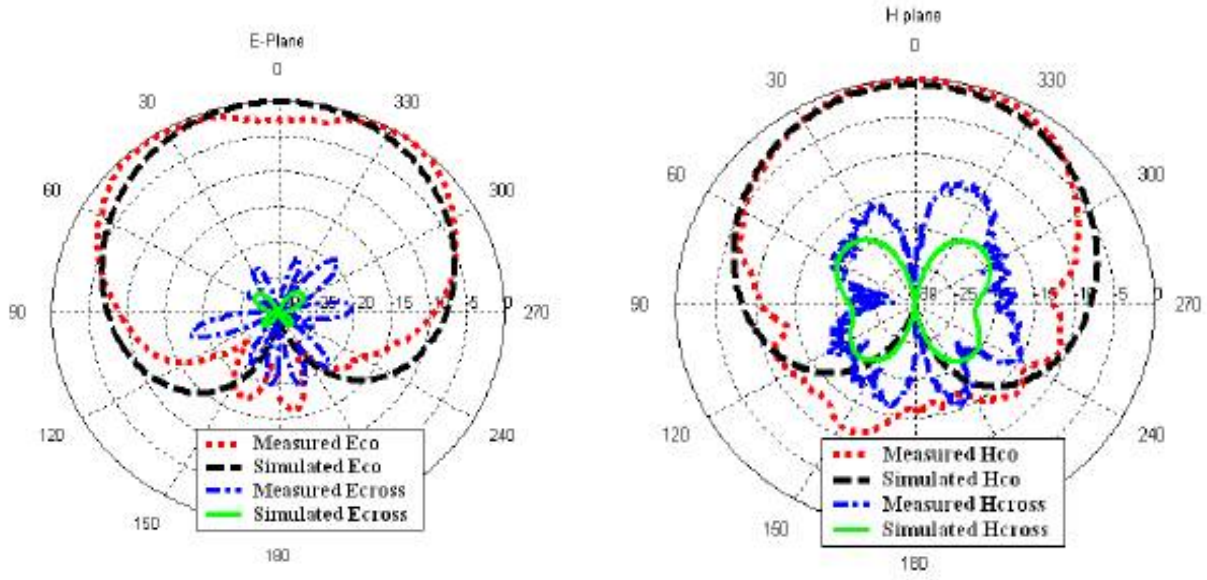

Figure 5.12: Measured and simulated radiation patterns for the proposed narrowband RDRA at resonant (a) E-plane and (b) H-plane for the proposed RDRA

reduction of efficiency in the proposed mode is due to the conductor losses in additional metal strip as compared to the conventional RDRA. The measured results of the proposed new $TE^x_{\delta 10}$ mode are compared with the published results of a $TE^x_{\delta 01}$ mode [5,6] in Table 5.6 for validation. From the Table 5.6, it is observed that proposed method of the new radiating mode is easy to fabricate due to simple structure and feeding mechanism.

To study the fabrication tolerance, numerical study on width and overlapping length of the microstrip line is carried out. Overlapping length is the length of the microstrip line between the RDRA and substrate.

Table 5.7 shows numerical study on width of microstrip line for the proposed antenna. Width of the line is vary from 4.1 mm to 4.7 mm with the step of 0.1 mm. From the Table 5.7, it is observed that resonant frequency and return loss characteristics have minor shifting as compared to optimized values of width of 4.4 mm in our fabricated narrowband

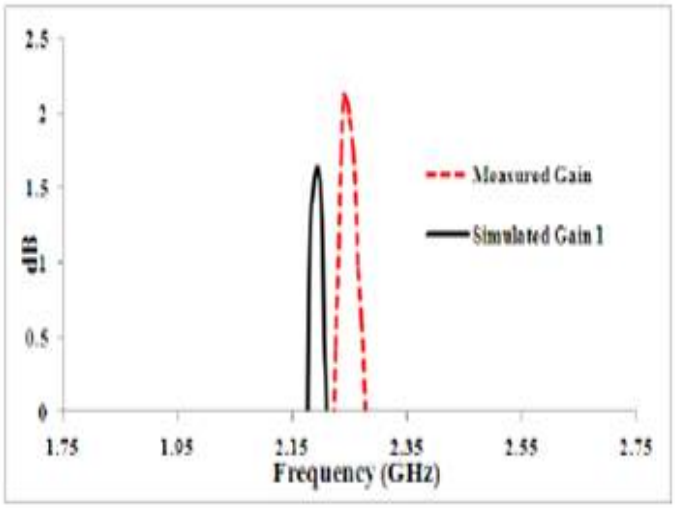

Figure 5.13: Measured and simulated gain for the proposed RDRA

Table 5.6: Comparison of the results of the $TE^x_{\delta 10}$ mode with other published new $TE^x_{\delta 11}$ mode

Particulars	$TE^x_{\delta 01}$ [5]	$TE^x_{\delta 01}$ [6]	Proposed $TE^x_{\delta 10}$
DR dimensions w x d x h mm^3	15x15x16	25x6x3.9	17x7x3
Theoretical Fr. (GHz)	2.091	—	2.330
Experimental Fr. (GHz)	1.741	3.500	2.240
Freq. Range (GHz)	1.716-1.767	3.465-3.550	2.223-2.258
BW (MHz)	51	85	35
Feeding Mechanisim Structure	Slot Coupled RDRA + 2 metal strips	T-Shaped Strip with coaxial cable RDRA + air gap + 2 metal strips	Microstrip Line RDRA + a metal strip

Table 5.7: Numerical study on width of microstrip line for narrowband RDRA

Width of Microstrip Line	Simulated f_r (GHz)	S_{11} (dB)
4.1 mm	2.16875	-21.69
4.2 mm	2.16875	-31.32
4.3 mm	2.16875	-17.37
4.4 mm	2.16250	-21.96
4.5 mm	2.15625	-18.45
4.6 mm	2.15625	-15.80
4.7 mm	2.15625	-15.29

RDRA. During the fabrication of the antenna, this show that variation in width of the microstrip line has minor variation in the resonant frequency and return loss characteristics.

Table 5.8: Numerical study on overlapping length of microstrip line for narrowband RDRA

Length of Microstrip Line	Simulated f_r (GHz)	S_{11} (dB)
12.0 mm	2.3188	-4.77
12.5 mm	2.2563	-8.25
13.0 mm	2.1938	-14.97
13.5 mm	2.1625	-21.96
14.0 mm	2.0450	-13.67
14.5 mm	2.0187	-9.26
15.0 mm	1.9688	-7.47

Numerical study is also carried out on length of overlapping microstrip line. The length is vary from 12 mm to 15 mm with the step of 0.5 mm. Table 5.8 show the variation of resonant frequency and return loss characteristics for the overlapping length of the microstrip line. From the Table 5.8, it is observed that minor variation in the length, there are significantly variation in the resonant frequency and return loss characteristics. It is concluded that variation in length of microstrip line during the fabrication, shifting of resonant frequency as well as major variation of return loss characteristics can be possible. During the fabrication, placing of RDRA on exact location of the microstrip line is very crucial. It is also noticed that the overlapping line is imperative for coupling of the RDRA with the feeding method.

5.4 Conclusion

In this chapter, a new radiating $TE^x_{\delta 10}$ mode is proposed by using a metal strip placed on top surface of the RDRA. From simulated field distributions, it is confirmed that the new mode has been excited in the proposed RDRA design. Theoretical analysis is also supported the proposed mode in the RDRA. By parametric study, resonant frequency of the $TE^x_{\delta 10}$ mode is mainly determined by width, little affected by depth, and stable with change in height. The proposed design is fabricated, measured and compared with the

$TE^x_{\delta 11}$ mode. For the $TE^x_{\delta 10}$ mode, all critical measured results are compared with the simulated results and show high agreement. From the measured results, the new mode is confirmed. It is observed that the $TE^x_{\delta 10}$ mode work at lower frequency than the $TE^x_{\delta 11}$ mode in the RDRA with the same dimensions. The $TE^x_{\delta 10}$ mode has a broadside radiation patterns as the conventional mode has. Compared to $TE^x_{\delta 11}$ mode, the proposed mode can be excited in a more compact structure, and lower impedance bandwidth, if both mode work at same frequency.

References

[1] T. Lassen, "Long-range RF communication: Why narrowband is the de facto standard", *White paper, Texas Instrument Inc.*,pp. 1-7, March, 2014.

[2] R. K. Mongia, A. Ittipiboon, M. Cuhaci, "Low-profile dielectric resonator antennas using a very high permittivity material", *IEEE Electronics Letters*, Vol. 30, No. 17, pp. 1362-1362, Aug. 1994.

[3] K.W. Leung, K. M. Luk, E. K. N. Yung, S. Lai "Characteristics of a low-profile circular disk DR antenna of very high permittivity", *IEEE Electronics Letters*, Vol. 31, No. 6, pp. 417-418, March 1995.

[4] H.Y. Lo, K.W. Leung, K. M. Luk, and E. K. N. Yung, "Low profile equilateral triangular dielectric resonator antenna of very high permittivity", *IEEE Electronics Letters*, Vol. 35, No. 25, pp. 2164-2166, Dec. 1999.

[5] Y. Gao, Z. Feng, and L. Zhang, "Investigation of a new radiating mode and the traditional dominant mode in rectangular dielectric resonator antenna", *IEEE Antennas and Wireless Propagation Letters*, Vol. 11, pp.909–912, 2012.

[6] Y. Gao , Z. Feng, and L. Zhang, "Experimental investigation of new radiating mode in rectangular hybrid dielectric resonator antenna", *IEEE Antennas and Wireless Propagation Letters*, Vol. 10, pp.91-94, 2011.

[7] S.A. Long, M.W. McAllister, and L.C. Shen, "Rectangular dielectric resonator antenna," *IEEE Electronics Letters*, Vol. 19, pp. 218-219,1983.

[8] A. Ittipiboon, R. K. Mongia, "'Theoretical and experimental investigation on rectangular dielectric resonator antennas", *IEEE Transactions on Antennas and Propagation*, Vol. 45, No. 9, pp. 1348-1356,1997.

[9] A. Petosa, Dielectric Resonator Antenna Handbook, *Artech House*, 2007.

Chapter 6

Dual Narrowband L-Shaped Dielectric Resonator Antenna

Nowsday, there are great demands of dual services such as IEEE 802.11 standards in personal and commercial wireless devices. For example, Wi-Fi and WLAN services are gradually expanding in the area of modern wireless communication. To provide both the services, it is required to have an antenna which covers both the frequency band, i.e. the antenna to be a wideband antenna. As discussed in chapter 2, design of the wideband antenna is not simple and straightforward. A dual band antenna provides an alternative to the wideband planar antenna for applications in which large bandwidth is needed for operating at two separate transmit-receive bands. The dual band antenna exhibits a dual resonant behavior in a single radiating structure or combine multiple radiating elements to create antennas that operate in two separate bands. In the applications where, an increased bandwidth is needed for operating at two separate sub-bands, a valid alternative to the broadening of total bandwidth is represented by the dual narrowband antennas. Indeed, the optimal antenna for a specific application is one that ensures the matching of the bandwidth of the transmitted and/or the received signal. When the two operating bands are far apart, the dual band antenna can be conceived to avoid use of two separate antennas. The antennas that operate in dual- or multi-bands that can be integrated on a package for mass production are in high demand. Many applications have additional requirement that the antennas to be compact and conformal.

Dielectric resonator antennas are widely accepted for these requirements due to their im-

portant characteristics, as mentioned in chapter 1. Dual-frequency and multi-frequency operation of dielectric resonator antennas have been studied by many researchers. The dual- or multi- frequency DRAs exhibits a multi resonance behavior in a single or multiple radiating structures. A variety of designs for dual band operations have been reported by using hybrid DRAs. As discussed in secion 2.3.2, various DRA designs are reported and discussed earlier for dual narrowband operation. Conical DRA [1], circular disk DRA [2], and RDRA [3] are reported dual narrowband designs. In these, one band is achieved by the DRA, whearas second band is achieved by a feeding mechanism such as eccentric rings [1], parasitic C-slot [2] and zonal slot [3]. Recently, two different modes of the RDRA are excited such that dual band operation is achieved. This is due to proper selection of physical parameters of the RDRA [4]. In principle, the dual narrowband antenna should operate with similar features, both in terms of radiation and impedance matching at two separate frequencies. Obtaining these features by using non planar technologies is not a straightforward matter, particularly when an intrinsic structural and technological simplicity of DRAs are to be preserved.

Motivation:

- As described in chapter 5, in our work of an investigation of new mode in a RDRA, narrow band is achieved by placing a conducting plate on the surface of the RDRA. To achieve dual band operation, two RDRA are merged in L-shaped and placed a metallic conductor on the surface. The one arm of the L-shaped DRA excite one narrow band, while the other arm of the L-shaped DRA excite second narrow band.

- Objective is to design a compact DRA on a wrist watch (rectangular) for human identification system using RFID technology. Optimum position is to place the DRA at corner of the wrist watch. Thus, a L-shaped DRA is better choice for the system.

L-shaped dielectric resonator antenna with metalization on surface is introduced in this chapter. The proposed antenna is operated on dual frequency bands. Simple microstrip line is used as a feeding mechanism. It is operated at 2.4 GHz and 5.8 GHz frequency

band. It has circular polarization radiation patterns. Simulation results are presented on various parametric studies on the L-shaped DRA.

6.1 Introduction

Radio frequency Identification (RFID) solution is a revolutionary applications of automatic identification and data capture technology that is contactless and does not require line of sight. RFID tags will be embedded in all kinds of consumer products and scanned from several meters away (The distance lies on types of the tag, operation frequency and type of technology), revealing the information about the product and (potentially) its owner. By attaching tags to products, an automated inventory will be easily maintained. Tags also allow customers to pay a reader. Postal services will equip shipped goods with tags for tracking purposes and read-write storage, integrated sensors, or more gates for computation purposes. In a word, RFID system is a common and useful tool in manufacturing, supply chain management, and inventory control [5]. Nowadays, it can be applied into some pretty new applications, like human identification. This application has wide use in military purpose to fight against terrorisms, border movement of troops, and hidden movement of criminals around the nation.

A typical radio frequency identification system is made up of three components: 1) an electronic data carrying device called RFID tag is combined with an antenna. The tag is usually a microchip and contains the item to be identified 2) a reader that communicates with the tag antenna by means of electromagnetic waves 3) a host data processing system embodies the information of the identified item and communicates with other remote data processing systems [6]. The RFID system [6, 7] covers frequency bands of low-band range 100-500 KHz, high frequency 13.56 MHz, ultra high frequency (UHF) 860-960 MHz, and microwave band range 2.4 GHz and 5.8 GHz. The most highlighted applications that utilize the UHF and microwave band. Owing to its long reading range and high reading speed, there has been more and more research into design of microwave RFID tag antenna [8]. Most applications require that the tags to be compact in size, low cost, easy fabrication, circular polarization, multiple bands, single feed, single layer, good matching, high directivity, high radiation efficiency, and easy to integrate with microwave

circuits.

Various RFID antennas were reported in literature namely folded printed dipole antenna [6], patch antenna [9], two layered patch antenna [10], half-ring folded-slot antenna [11], slot-loaded patch antenna [12], loop antenna, spiral antenna [13], and other modified patch antennas with different feeding mechanism for various characteristics of RFID. There are various issues on printed patch antennas such as wide beam width, narrow bandwidth, surface wave excitation, radiation efficiency and radiation characteristics. Due to these, dielectric resonator antenna proposed for the RFID antenna in this chapter.

The DRA introduced by Long et al. in 1983 [14], could be used for such application due to higher radiation efficiency, versatility in their shape and feeding mechanism, and wide bandwidth at millimeter-wave frequencies where the conductor losses of metallic patches are considerable. The DRA is a resonant antenna, fabricated from a high-permittivity microwave material mounted on a ground plane and fed by a coaxial probe, aperture coupling, coplanar waveguide, and direct microstrip line. Various geometries of the DRA such as cylindrical, rectangular, hemispherical, spherical, and triangular are possible. The resonant frequency of the DRA is a function of size, shape, and permittivity of material used in DRA [15].

In this chapter, dielectric resonator antenna (DRA) is proposed as a RFID antenna for human identification system with dual mode, circular polarized, compact in size, single layered, single feed, high radiation efficient, and easy to integrate and to fabricate. Simulation is carried by Ansoft HFSS simulation tool. Various characteristics of the antenna are studied and discussed.

6.2 Proposed Approach

Figure 6.1 shows a geometry of a proposed L-shaped dielectric resonator antenna. L-shaped DRA with metallic plate (patch) is placed on one of corner of a wrist watch. A 50 Ω microstrip line is used, which is printed on top of a grounded substrate with thickness (h) of 0.76 mm length (L_s), width W_s, dielectric constant (ϵ_r) of 10.2 and loss tangent of

0.0017. The L-shaped DRA is characterized by arm lengths L_1 and L_2, width W, height

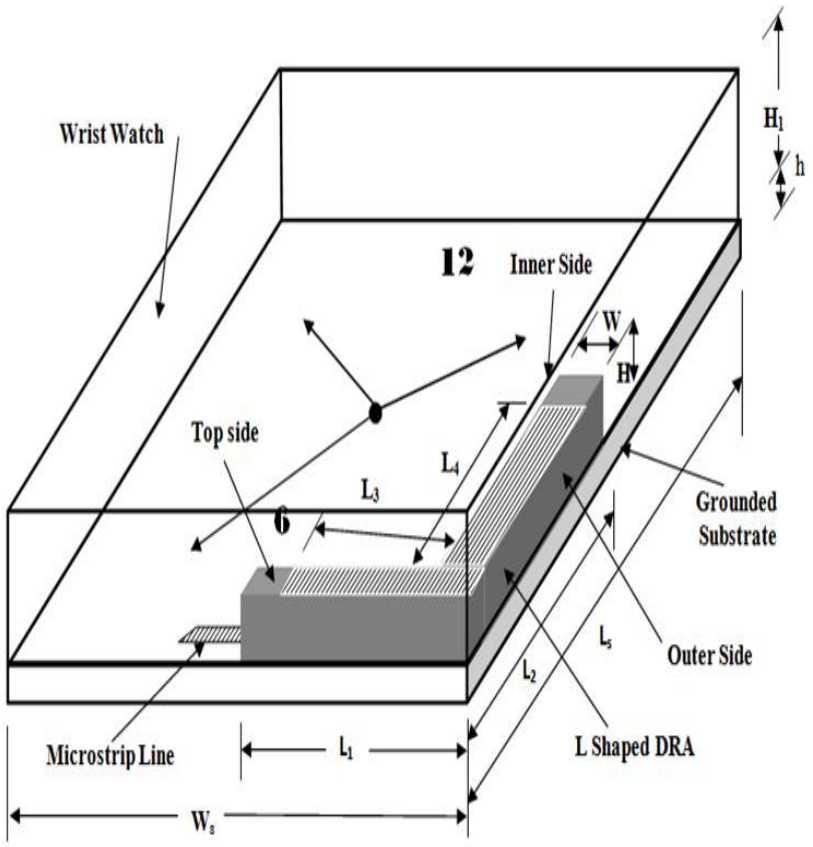

Figure 6.1: Geometry of the proposed dual narrowband L-shaped DRA

H, and dielectric constant ϵ_r. The metallic conducting plate, which is characterized by arm lengths L_3 and L_4 and width W, is placed on the L-shaped DRA. The wrist watch is made of plastic material with dimension of $L_s \times W_s \times H_1 + h$. The field equations of the antenna and initial equations of resonant frequency are given in [16] for rectangular DRAs as decribed in chapter 2.

6.2.1 Theoretical Analysis

The resonant behavior of the simplified case of an isolated conventional rectangular RDRA is analyzed here. The antenna is characterized by height b, width d, and length w, as shown in Figure 6.2 and is made of microwave material with dielectric constant ϵ_r. This geometry is equivalent to a RDRA of the same material placed over an infinite ground plane with dimensions a, d, and height h equal to b/2. If the smallest dimension of the rectangular DRA is in x direction, then the dominant lowest order mode will be the TE^x_{111}

mode [16]. The equations for calculating the resonant frequency are

$$k_x^2 + k_y^2 + k_z^2 = \epsilon_r k_0^2 \tag{6.1}$$

Where, k_0 denotes free-space wave number corresponding to resonant frequency [16].

$$k_0 = \frac{2\pi}{\lambda_0}, k_y = \frac{\pi}{a}, k_z = \frac{\pi}{b} \tag{6.2}$$

$$k_x \tan(k_x \frac{d}{2}) = \sqrt{(\epsilon_r - 1)k_0^2 - k_x^2}, \tag{6.3}$$

The cross sectional view of a compact rectangular DRA with metallic plates on top and

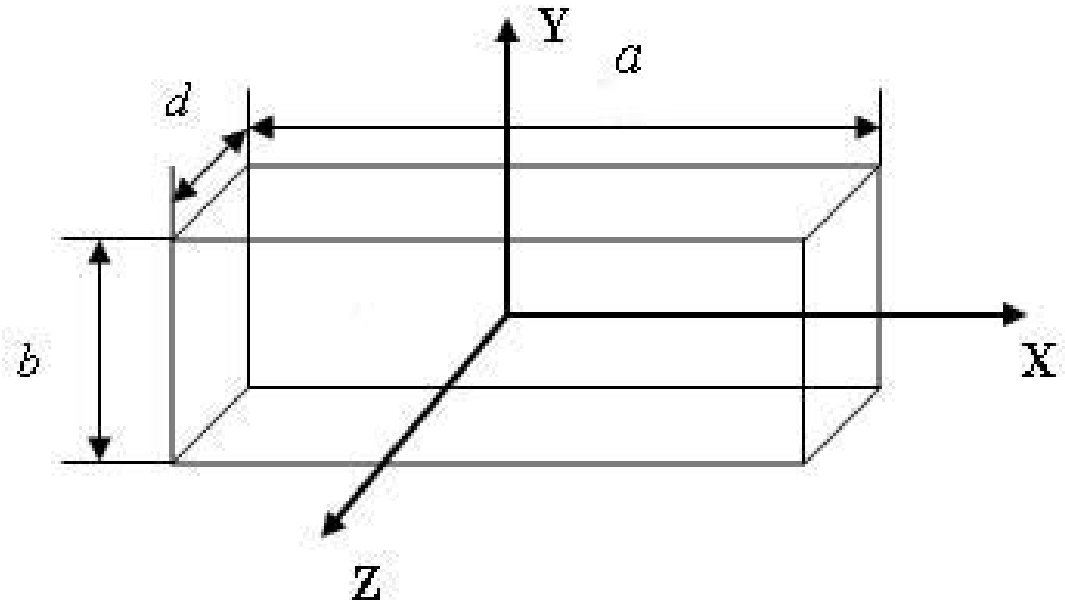

Figure 6.2: Geometry of an isolated conventional RDRA

bottom surfaces is shown in Figure 6.3. Image theory to be used to replace the geometry with an isolated RDRA of height equal to four times of original height i.e. b equal to 4h. The above equations can therefore be uses for calculating the resonant frequency of this antenna geometry also. It may however be noted that this model does not include the effects of the top metal layer being finite. Similarly the effects of dimensions of the feed microstrip line and the presence of the dielectric laminate beneath this are not considered here [17]. It was investigated that drastically decreased in volume, resonant frequency, impedance bandwidth achieved for patch on DRA [17, 18], while impedance bandwidth

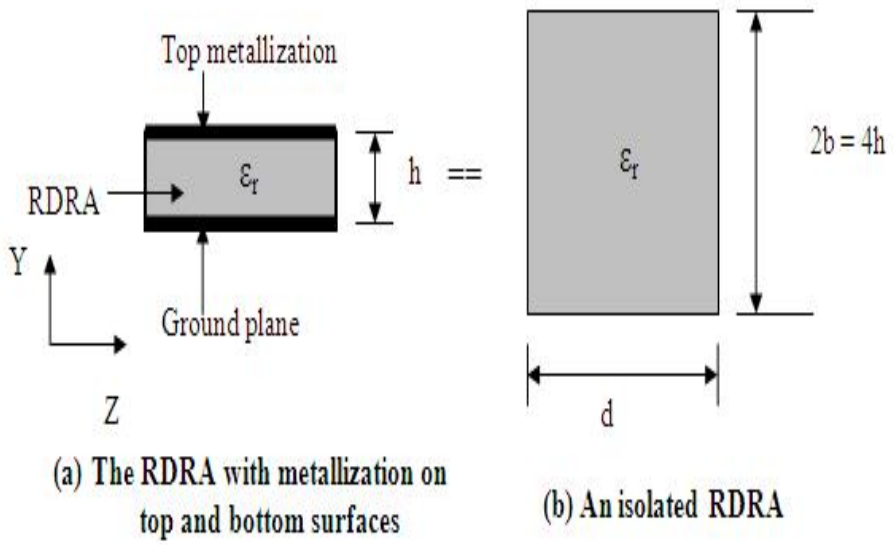

Figure 6.3: A compact DRA with metallic layer and its equivalent DRA in free space

improved for a DR on patch [19].

6.2.2 Numerical Study

Based on extensive numerical studies, design parameters of the proposed antenna have been optimized. The L-shaped DRA is made of a microwave material with dielectric constant of 32 and loss tangent of 0.0017. Dimension of one arm are L_1 of 10 mm, W of 2 mm, H of 3 mm, while second arm are L_2 of 12 mm, W of 2 mm, H of 3 mm used. A 50 Ω microstrip is placed on the grounded substrate which has dimension L_s of 25 mm, W_s of 25 mm and h of 0.76 mm. The dimensions of wrist watch are L_s of 25 mm mm, H_1 + h equal to 5.76 mm with a plastic material. Copper foil as a L-shaped patch is placed on top side of the L-shaped DRA. Initial dimensions of patch is L_3 of 12 mm, L_4 of 10 mm, W of 2 mm are used.

Simulations are carried out for placing the L-shaped patch on top , outer, top + inner, top + outer, top + inner + outer sides of the L-shaped DRA, and without patch (only the L-shaped DRA). For each case, a length of the microstrip line is optimized for better return loss characteristics. Return loss characteristics of patch on DRA for all five cases are shown in Figure 6.4. Resonant frequency, return loss characteristics, impedance bandwidth (S_{11} -10 dB) and % of bandwidth for all cases are tabulated in

Table 6.1: Parametric study of patch placed on sides of DRA

Patch on the L-Shaped DRA	Fr.(GHz)	Return Loss (dB)	BW (MHz)	% of BW
Outder Side	2.30	-10.50	—	—
Top + Outer Sides	2.55	-18.25	16	0.62
Top Side	2.67	-23.84	20	0.70
Top + Outer + Inner sides	2.72	-26.41	18	0.64
Top + Inner sides	2.77	-33.93	20	0.70
Without Patch	7.56	-12.95	240	3.17

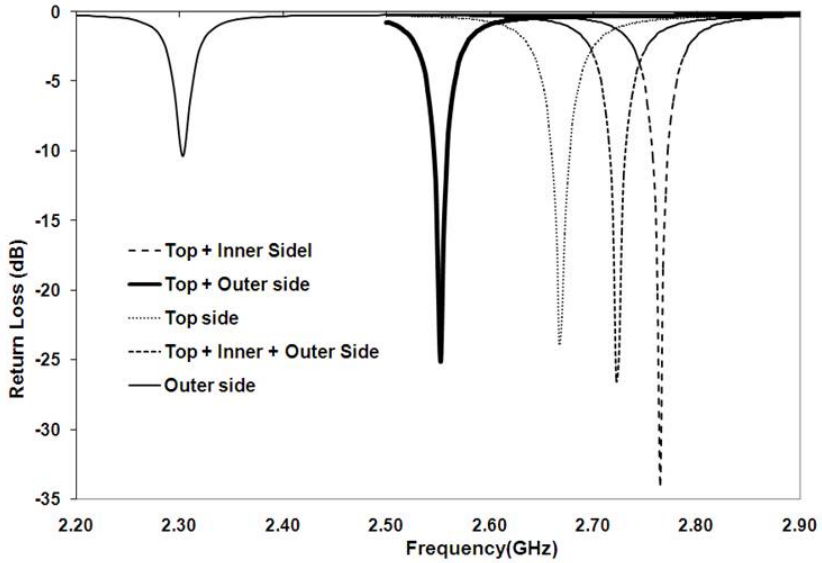

Figure 6.4: Return loss characteristics of patch placed on different combination of sides of the antenna

Table 6.1. From Figure 6.4 and Table 6.1, it is observed that the L-shaped DRA without patch is resonanted at 7.56 GHz with 240 MHz impedance bandwidth and has 3.17 % of impedance bandwidth. By placing the L-shaped patch on outer side of the antenna, resonant frequency drastically decrease to 2.30 GHz with narrow bandwidth operation are observed as compared to without metalization of the L-shaped DRA. This kind of observation is also noticed for the L-shaped patch is placed on top, top + inner, top + outer and top + inner + outer side of the L-shaped DRA. From these study, it is noticed that by metalization on the top surface of the L-shaped DRA, there is decreased of resonance frequency from 7.56 GHz to 2.55 GHz and decreased of impedance bandwidth from 240 MHz to around 16 MHz. Figure 6.5 shows the co- and cross- right handed circular polarization (RHCP) and left handed circular polarization (LHCP) radiation patterns at 2.30 GHz for the L-shaped patch placed on the outer side of the L-shaped DRA.

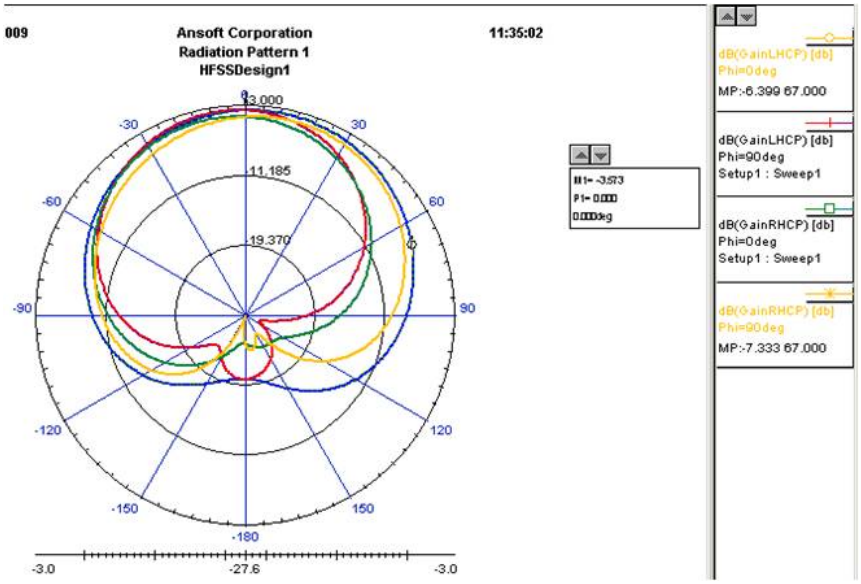

Figure 6.5: Circular Polarized radiation pattern at 2.30 GHz for metallic layer on outside wall

Table 6.2: Parametric study of different arm length of patch on inner side of the antenna

L_3, L_4 (mm)	Fr.(GHz)	Return Loss (dB)	BW (MHz)	Gain (dB)
3	5.45	-17.42	80	6.60
4	4.72	-21.95	40	2.34
	6.77	-12.31	80	2.33
5	4.13	-21.72	35	1.33
	6.23	-13.12	50	2.18
6	3.63	-25.44	25	0.39
	5.74	-18.64	60	2.32
7	3.29	-18.05	25	0.32
	5.34	-27.76	60	2.28
8	3.00	-29.46	20	-0.8
	4.96	-21.28	45	1.92

Simulations are carried out for different values of length of arm (L_3 and L_4) of the L-shaped patch which is placed on the inner side of the L-shaped DRA while keeping other dimensions of the L-shaed DRA invariable. Both the arm length (L_3 and L_4) of the L-shaped patch are vary from 3 mm to 8 mm. The return loss characteristics are shown in Figure 6.5 for differetn values of length of arms of the L-shaped patch. Various parameters of the antenna are listed in Table 6.2. By increasing the length of both the arms of the L-shaped patch from 3 mm to 8 mm, the antenna is operated in dual band. From

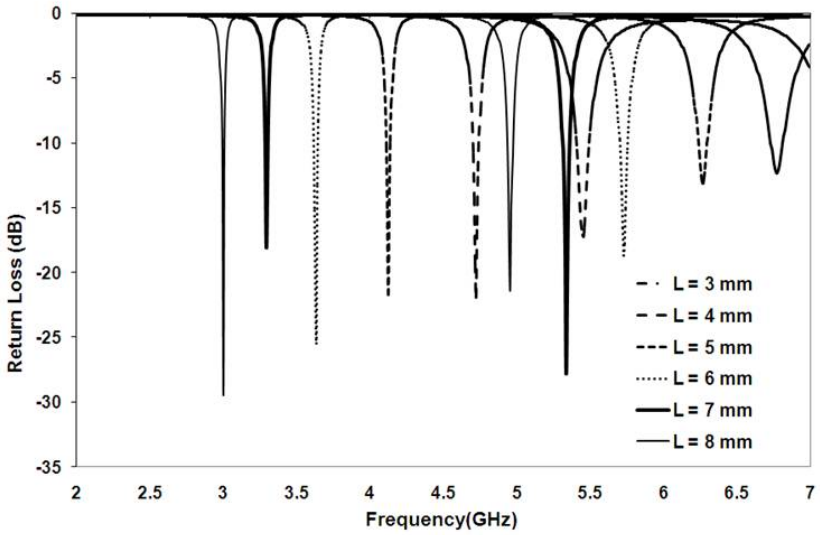

Figure 6.6: Return loss characteristics for different arm length of patch placed on inner side of DRA

Figure 6.5 and Table 6.2, It is observed that resonant frequency of first and second band, impedance bandwidth and gain at boresite are decreased as increased in arm length. For all case, length of the microstrip line is optimized for better return loss. It is concluded that by placing the L-shaped patch of shorter length compared to full length of L-shaped patch on the inner side of the L-shaped DRA, two different resonant are excited with higher impedance bandwidth as compared to full length of the patch.

Table 6.3: Parametric study of different arm length of the L-shaped patch placed on the outer side of the L-shaped DRA

L_3, L_4 (mm)	Fr.(GHz)	Return Loss (dB)	BW (MHz)	Gain (dB)
2	7.30	-12.00	150	5.57
3	5.77	-22.39	60	3.17
4	4.72	-20.31	30	2.11
5	4.11	-17.00	20	1.11
6	3.60	-20.68	20	-0.28
	6.45	-10.00	–	2.64
7	3.19	-23.03	20	-1.15
	5.90	-11.16	40	2.75

Also, simulations are carried out for different values of length of both arms of the L-shaped patch which is placed on an outer side of the antenna while other dimensions of

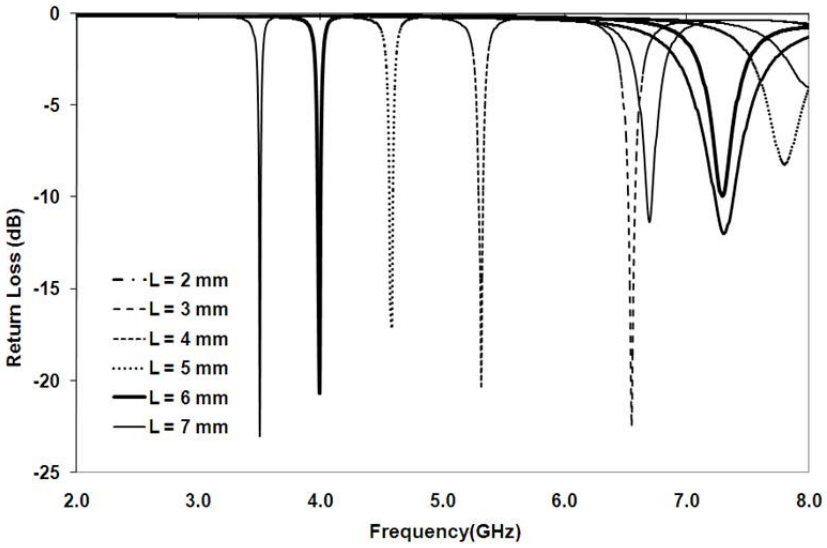

Figure 6.7: Return loss characteristics for different arm length of L-shaped patch placed outer side of L-Shaped DRA

the antenna are unchanged. Length of both the arms of the L-shaped patch are vary from 2 mm to 7 mm. The return loss characteristics for different values of length (L_3 and L_4) of both arms of the patch are shown in Figure 6.6. Various required parameters are listed in Table 6.3. Based on numerical studies carried out by varying the arm length of the patch on the outer side of the L-shaped DRA, it is noticed that dual band operation is observed with proper selection of arm length of the patch. From Table 6.3 and Figure 6.6, it is seen that by an increasing arm length of the L-shaped patch, there are decreased in resonant frequency, impedance bandwidth and gain. It is observed that arm length is increased from 2 mm to 7 mm, the resonant frequency is decreased from 7.30 GHz to 3.19 GHz as compared to without metalization of the L-shaped DRA at cost of decreased in impedance bandwidth from 150 MHz to 20 MHz. For L_3 and L_4 equal to 6 mm and 7 mm, two resonances are excited . Thus, dual narrowband is achieved by partial metalization on the outer side of the L-shaped DRA. It is also noticed that for shorter length of the both arms of the L-shaped patch, only single band is excited in the antenna.

Extensive numerical study has been carried out on the L-shaped patch which is placed on the different surfaces of the L-shaped DRA. As compared to without metalization of the L-shaped DRA, there are drastically decreased in resonant frequency and impedance bandwidth are observed when, the fully metalization on the any surfaces of the L-shaped

DRA. Simulation is carried out for different vlaues of length of both the arms of the L-shaped patch, which is planced on the inner and outer surface of the L-shaped DRA. From these simulations, it is observed that by proper selection of the length of the arm of the patch, dual band is excited in the antenna. It is noticed that by increasing the length of arm of the patch, there is decreased on resonant frequency of the both bands. This indicates that both the resonance are due to DRA itself. It is noticed that both the band have a narrow impedance bandwidth. Thus, the partial metalization on the L-shaped DRA leads a dual narrowband DRA. Also the radiation patterns of the proposed antenna are circular polarized at the both resonance. As described in chapter 5, the metalization on the top surface of the rectangular DRA, the linear and broadside radiation patterns are obtained, whereas, by metalization on the top surface of the L-shaped DRA, the circular polarized radiation patterns are achieved. Volume of the dual band L-shaped DRA is 132 mm^3. Thus, the proposed antenna has dual naroowband operation, circular polarized radiation patterns and compact in size, single feed, single layer and high radiation efficiency.

With proper selection of dimensions, the proposed antenna can be resonated at 2.4 GHz and 5.8 GHz free ISM bands for RFID applications. The proposed antenna has circular radiation pattern, high radiation efficiency, dual mode operation and enough bandwidth. It is easy to fabricate and integrate with microwave circuits. The proposed antenna has single feed, single layer technology. The size of the antenna is very small. In [20], rectangular dielectric resonator antenna (dielectric constant of 37) as a RFID tag is reported with $18 \times 18 \times 9$ mm^3 with a planar area of 324 mm^2 and volume of 2916 mm^3 operated at 2.4 GHz. The proposed L-shaped DRA with metalization has dimensions $22 \times 2 \times 3$ mm^3 with a planar area of 44 mm^2 and volume of 132 mm^3. As compared to the reported RDRA RFID tag, volume of the proposed antenna is decreased by a factor of 95 %, whereas the planar area is decreased by a factor of 86 %. Thus, the proposed antenna is miniatruzed as compared to the reported DRA. These features of the proposed antenna make major candidate in the field of RFID application to work as reader and tag.

6.3 Conclusion

In this chapter, a L-shaped patch on L-shaped dielectric resonator antenna (DRA) has been proposed around 2.4 GHz and 5.8 GHz free ISM bands. A simple microstrip line is used as a feeding mechanism. Metallic patch is placed on side of the L-shaped DRA to achieve compact in size. By properly choosing arm length of the L-shaped patch, dual band operation can be achieved. And also improvement in impedance bandwidth is observed. Radiation patterns of the proposed antenna are circular polarization. Due to absent of conductor loss in proposed antenna, high radiation efficiency can be achieved. Volume of the antenna is 132 mm^3 with a planar area of 44 mm2 which is miniaturized as compared to the reported RFID antennas as a dielectric resonator antenna in literature. Thus the proposed antenna has all require characteristics of RFID reader and tag antenna. This type of antenna has a potential in RFID application such as human identification for military use.

References

[1] Q. Rao, T. A. Denidni, A. R. Sebak, "A new dual frequency hybrid resonator antenna", *IEEE Antenna and Wireless Propagation Letters*, Vol. 4, 308-311, 2005.

[2] H. M. Chen, Y. K. Wang, Y. F. Lin, S. C. Lin, S. C. Pan, "A compact dual-band dielectric resonator antenna using a parasitic slot", *IEEE Antennas and Wireless Propagation Letters*, Vol. 8, pp. 173-176 ,2009.

[3] Y. Ding, K. W. Leung, "On the dual-band DRA-slot hybrid antenna", *IEEE Transactions on Antennas and Propagation*, Vol. 57, No. 3, pp. 624-630, March 2009.

[4] X.S. Fang, K.W. Leung, "Designs of single-,dual-,wide-band rectangular dielectric resonator antenna", *IEEE Transactions on Antenna and Propagation*, Vol. 59, No. 6, pp. 2409-2414, June 2011.

[5] L. Zhang, H. Zhou, R. Kong, F. Yang,"An Improved approach to security and privacy of RFID application system", *IIEEE International Conference on Wireless Communication, Networking and Mobile Computing*, pp. 1149-1152, 2005

[6] X. Li, L. Yang, S. X. Gong, Y. J. Yang, and J. F. Liu, " A compact folded printed dipole antenna for UHF RFID application", *Progress in Electromagentics Research Letters*, Vol. 6, pp. 47-54, 2009.

[7] Z. G. Fan, S. Qiao, J. T. Huangfu, and L. X. Ran, "A miniaturized printed dipole for 2.45 GHZ RFID readers", *Progress In Electromagentics Research*, Vol. 71, pp. 149-158, 2007.

[8] Y. C. Lee, and J. S. Sun, "A fractal dipole tag antenna for RFID dual-band application", *Microwave and Optical Tech. Letter*, Vol. 50, pp. 1963-1966, 2008.

[9] J. M. Lee, N. S. Kim and C. S. Pyo, " A circular polarized metallic patch antenna for RFID reader ", *Proceeding of Asia-Pacific Conference on Communication*, pp. 116-118, 2005.

[10] X. Zhishu , and L. Xiuping, "Aperture coupling two-layered dual band RFID reader antenna design", *Proceeding of ICMMT*, 2008.

[11] D. Ma, W. X. Zhang, "Broadband CPW-fed RFID antenna at 5.8 GHz", *IEEE Electronics Letters*, Vol. 42, No. 22, pp. , 2006

[12] S. Maci, G. Biffi Gentill, P. Piazzesi, C. Saivador, "Dual-band slot-loaded patch antenna", *IEEE Proceeding Microwave antenna propagation*, Vol. 142, No. 3, pp. 225-232, 1995.

[13] L. W. Mayer and A. L. Scholtz, "A dual band HF/UHF antenna for RFID tags", *Proceeding of IEEE Vehicular Technology Conference*, pp. 1-5, 2008.

[14] S. A. Long, M.W. McAllister, and L. C. Shen, "Rectangular dielectric resonator antenna", *IEEE Electronics Letters*, Vol. 19, pp. 218-219, 1983.

[15] A. Petosa, "Dielectric resonator antenna handbook", *Artech house*, 2007.

[16] R. K. Mongia, and A. Ittipiboon, "Theoretical and experimental investigation on rectagnular dielectric resonator antenna, "*IEEE Transactions on Antennas and Propagation*, Vol. 45, No. 9, pp. 1348-1359, 1997.

[17] G. D. Makwana, and K. J. Vinoy, "Design of a compact rectangular dielectric resonator antenna at 2.4 GHz", *Progress In Electromagentics Research C*, Vol. 11, pp. 69-79. 2009.

[18] Nasimuddin, and K. P. Esselle, "A low profile compact microwave antenna with high gain and wide bandwidth",*IEEE Transactions on Antennas and Propagation*, Vol. 55, No. 6, pp. 1880-1883. 2007.

[19] Nasimuddin, and K. P. Esselle, "Antennas with dielectric resonators and surface mounted short horn for high gain and wide bandwidth", *IET Microwave, Antennas and Propagation*, Vol. 1, No. 3, pp. 723-728, 2007.

[20] L. Z. Thamae, Z. Wu, W. Konard, "Rectangular dielectric resonator antenna for RFID application", *Proceeding of the 2nd European Conference on Antenna and Propagation*, pp. 1-5, 2007.

Chapter 7

Conclusion and Future Research Work

7.1 Conclusion

In this thesis, bandwidth consideration in a RDRA is addressed. Two aspects of bandwidth namely, wideband and narrowband in the RDRA are considered. At the same time, the RDRA has to be miniaturized. Objective of the thesis is to validate experimentally proposed designs of the miniaturized RDRAs. Two designs of the RDRAs are for wideband operation, whereas, two designs of the RDRAs are for narrowband operation. Theoretical analysis, numerical study and experimental validation are performed and discussed for all the designs of the RDRA. For the numerical study, a 3-D FEM based electromagnetic simulation tool, HFSS, by Ansoft is used. These designs are compared with other reported DRA designs to claim miniaturization of the designs.

It is seen that, the resonance frequency of the RDRA depends predominantly on physical parameters such as length, depth and height, dielectric constant, aspect ratios (length/depth and width/depth). It is also noticed that impedance bandwidth depends on the dielectric constant, and aspect ratios. It is seen that maximum bandwidth is possible for a longer and wider RDRA, whereas, minimum bandwidth is possible for a square DRA. From this, it is concluded that at specific resonance frequency and dielectric constant, a design of miniaturized and wideband and /or narrowband RDRA is a challenge for the researcher.

A literature survey is conducted on various designs of DRA for wideband and narrowband operation. Survey is conducted on various methods of bandwidth improvement such as merging of modes, stacking/embedding of DRAs, modified shaped of DRAs, and hybrid DRAs with various feeding schemes. From this, it is seen that there is a need of optimization of various parameters of feeding schemes and DRAs to achieve a specific wide bandwidth. This leads to extra degree of freedom, difficulty in fabrications and complex design methodology. From the literature survey on the single narrowband DRA designs, it is seen that narrowband can be achieved by metallization on the surfaces of the DRA and using high dielectric constant material (of the order of 82-100). From the survey on dual narrowband DRA designs, it is seen that one of the dual band is due to the feeding method. Thus, the feeding method works as a feed for the DRA as well as the radiator. It is also noticed that to achieve a dual narrowband in the DRA, various physical parameters of the DRA and feeding method have been optimized. Thus, it is very complex and hard-to-design for dual narrowband DRA. Recently, dual band are achieved by the RDRA itself.

In this thesis, the 50 Ω microstrip line is used as feeding scheme in all proposed RDRAs. A dual mode and miniaturized RDRA had been proposed using the novel way of excitation by the microstrip line. After the parametric study, the optimized and fabricated RDRA had 13 % impedance bandwidth in the range of 5.68 GHz to 6.48 GHz. It is seen that the both modes, $TE^{y}_{1\delta1}$ and TE^{y}_{211}, are of the RDRA. Measured gain of 3.9 dB and 3.0 dB is observed for $TE^{y}_{1\delta1}$ and TE^{y}_{211}, respectively. It is also seen that over the bandwidth, measured radiation patterns are broadband and linear polarized with HPBW of 90° and 92° in E- and H- plane, respectively. The measure of compactness and wideband bandwidth, the figure of merit of the proposed RDRA is 27. As compared to the reported designs, the proposed design is miniaturized, easy to fabricate and simple to design.

The stacked RDRA, made of two different materials with dielectric constants of 32 and 10.2, operated at 5.2 GHz has been proposed. It has 6-dB return loss bandwidth of 710 MHz with broadband radiation patterns. Measured gain is 5.23 dB of the antenna. It is seen that the conventional RDRA operated at 5.2 GHz has less impedance bandwidth

(560 MHz) and low profile.

A narrowband antenna is proposed by metallization on top surface of the RDRA. A new radiating $TE^x_{\delta 10}$ mode is observed in the proposed antenna. From simulated field distributions, it is confirmed that the new mode has been excited in the proposed RDRA design. Theoretical analysis also confirms the new mode in the RDRA. By parametric study, resonant frequency of the $TE^x_{\delta 10}$ mode is mainly determined by length, little affected by depth, and stable with change in height. The proposed design is fabricated, measured and compared with a conventional $TE^x_{\delta 11}$ mode. For the $TE^x_{\delta 10}$ mode, all critical measured results are compared with the simulated results and show good agreement. From the measured results, the new mode is confirmed. It is observed that the $TE^x_{\delta 10}$ mode works at lower frequency (2.24 GHz) than the $TE^x_{\delta 11}$ mode which works at higher frequency (5.39 GHz) in the RDRA with the same dimensions. The proposed antenna has 35 MHz (1.56 %) bandwidth, whereas, the conventional antenna has 165 MHz (3.56 %) bandwidth. $TE^x_{\delta 10}$ mode has a broadside (HPBW equal to 90°) radiation patterns similar to the conventional mode. Compared to $TE^x_{\delta 11}$ mode, the proposed mode can be excited in a more compact structure, and lower impedance bandwidth when both the modes work at the same frequency.

An L-shaped patch on an L-shaped DRA has been proposed around 2.4 GHz and 5.8 GHz ISM bands. Metallic patch is placed on side of the L-shaped DRA to achieve compactness. By properly choosing arm length of the L-shaped patch, dual narrowband operation can be achieved. Radiation patterns of the proposed antenna show circular polarization. Volume of the antenna is 132 mm^3 with a planar area of 44 mm^2 which is miniaturized as compared to the reported RFID antennas as a DRA in literature. Thus, the proposed antenna has all required characteristics of RFID reader and tag antenna. The proposed antenna has a potential in RFID application such as human identification for military use.

7.2 Future Research Work

During this research work, several research studies were conducted to understand the effect of several modifications to the RDRAs, with regard to their resonance frequency, impedance bandwidth, and radiation patterns using the simulation tool. Yet due to limitation of time, some aspects have been left for more investigations, some of them are listed below.

- By using a novel way of placing a microstrip line beneath the RDRA, dual mode and miniaturized RDRA has been investigated. It has potential to excite three modes in the RDRA with other possible dimensions. This may provide larger bandwidth and miniaturized RDRA.

- As of today, the tri-narrowband DRA is not reported yet. By using the same concept of the dual narrowband L-shaped DRA, it is possible to design tri-narrowband with some other shapes of DRA with metallization.

- In this work, four RDRAs are used with the microstrip line feeding. It is suggested to explore idea of these designs with other possible feeding schemes, namely, coaxial probe, CPW, aperture, etc. By these, it is possible to have different aspect on bandwidth of the RDRA.

- In this work, rectangular cross section of DRA is taken for all designs. It is suggested that these concepts can be applied to other basic shapes as well as modified shaped DRA. It may have more compact and wide bandwidth DRA.

Appendix A

Simulation Tool and Experimental Setup

A.1 Simulation Tool

A 3-D finite element method (FEM) electromagnetic simulation tool, High Frequency Structure Simulator (HFSS), by Ansoft, is used to determine optimum dimensions of the DRA. HFSS is a high-performance full wave electromagnetic (EM) field simulator for arbitrary 3-D volumetric passive device modeling. It integrates simulation, visualization, solid modeling, and automation in an easy-to-learn environment where solution to 3-D EM problems are quickly and accurately obtained. Ansoft HFSS employs adaptive meshing and brilliant graphics to give performance and insight to all of 3-D EM problems. The Ansoft HFSS can be used to calculate parameters such as S-, Z-, Y- parameters, resonant frequency, fields, radiation patterns, gain, directivity. It includes package modeling, printed circuit board (PCB) modeling, electromagnetic compatibility / interference (EMC/EMI), antennas/mobile communication, connectors, waveguides and filters [1].

HFSS is an interactive simulation system whose basic mesh element is a tetrahedron. This allows to solve any arbitrary 3-D geometry, especially those with complex curves and shapes in a fraction of the time. HFSS uses tangential vector finite elements, adaptive meshing, and adaptive Lanczos-Pade Sweep (ALPS). HFSS offers multiple state-of the-art solver technologies based on finite element, integral equation or advanced hybrid

methods to solve a wide range of microwave, RF and high-speed digital applications. The software includes a linear circuit simulator with integrated optimetrics for input and matching network design [1].

Each HFSS solver incorporates a powerful, automated solution process, so there is need only to specify geometry, material properties and the desired output. From there, HFSS automatically generates an appropriate, efficient and accurate mesh for solving the problem using the selected solution technology. With HFSS, the physics defines the mesh; the mesh does not define the physics. Engineers rely on the accuracy, capacity, and performance of HFSS to design high-speed components including on-chip embedded passives, IC packages, PCB interconnects and high-frequency components such as antennas, RF/microwave components and biomedical devices [2].

With HFSS, engineers can extract matrix parameters (S,Y, Z parameters), visualize 3-D electromagnetic fields (near- and far-field) and generate ANSYS Full-Wave SPICE models that link to circuit simulations. Signal integrity engineers use HFSS within established EDA design flows to evaluate signal quality, including transmission path losses, reflection loss due to impedance mismatches, parasitic coupling and radiation [2].

ANSYS HFSS software contains the technology, solvers and capabilities needed to model RF and microwave as well as signal- and power-integrity issues. HFSS includes following main features: - Automatic Adaptive Meshing - Solver Technologies - Advanced Finite Array Simulation Technology - Mesh Element Technologies - Advanced Broadband SPICE Model Generation - Optimization and Statistical Analysis - EDA Design Flow Integration - High-Performance Computing - Powerful Post-Processing Capabilities [1, 2]

Within the context of HFSS, boundaries exist for two main purposes: 1) to either create an open or a closed electromagnetic model or, 2) to simplify the electromagnetic or geometric complexity of the electromagnetic model. A closed model simply represents a structure, or a solution volume, where no energy can except through an applied port. For an Eigen mode simulation, this could be a cavity resonator. For a driven modal or terminal solution, this could be a waveguide or some other fully enclosed structure.

An open model represents an electromagnetic model that allows electromagnetic energy to emanate or radiate away. Common examples would be an antenna, a PCB, or any structure that is not enclosed within a closed cavity.

While most HFSS simulations deals with models that are open, by default, HFSS initially assumes that any given model is closed. HFSS assumes all outer surfaces of the solution space are covered, or coated, by a perfect electric conductor boundary. In order to create an open model, a user will need to specify a boundary on the outer surfaces that will overwrite the default perfect electric conductor boundary.

The second reason why boundaries are used within HFSS is to decrease the geometric/electromagnetic complexity of a given structure or model. These boundaries should only be used internally to a model or possibly on a symmetry plane. A user should exercise caution when using boundaries as they can create unintended results if applied incorrectly. Every HFSS model, a user creates will use boundaries on the outer surfaces of the solution space. This is direct result of the fact that a user must specify whether a given model is open or closed. As a result, any given HFSS model will always either have Conducting, Radiation or Perfectly Matched Layer boundary (PML) on all outer surfaces.

Conducting boundaries are the PEC, finite conductivity, or impedance boundary. Radiation boundaries are used to create an open model. PML boundaries are used to create an open model and preferred for antenna simulation.

A radiation boundary is used to simulate an open problem that allows waves to radiate infinitely far into space, such as antenna designs. HFSS absorbs the wave at the radiation boundary. Radiation boundaries must be applied to outer faces of a model. If modeling an antenna, these faces must be at least a quarter wavelengths away from any radiating surface.

At the radiation boundary surfaces, the second-order radiation boundary condition is

used:

$$(\nabla \times E)_{tan} = jk_0E_0 - \frac{j}{k_0}\nabla_{tan} \times (\nabla_{tan} \times E_{tan}) + -\frac{j}{k_0}\nabla_{tan}(\nabla_{tan} \bullet E_{tan}) \quad (A.1)$$

where, E_{tan} is the component of the E-field that is tangential to the surface, k_0 is the free space phase constant $\omega\sqrt{\mu_0\epsilon_0}$. The second-order radiation boundary condition is an approximation of free space. The accuracy of the approximation depends on the distance between the boundary and the object from which the radiation emanates.

Radiation boundaries, also referred to as absorbing boundaries, enable you to model a surface as electrically open: waves can then radiate out of the radiation boundary, essentially ballooning the boundary infinitely far away from the structure and into space. Radiation boundaries may also be placed relatively close to a structure and can be arbitrarily shaped. This condition eliminates the need for a spherical boundary. For structures that include radiation boundaries, calculated S-parameters include the effects of radiation loss. When a radiation boundary is included in a structure, far-field calculations are performed as part of the simulation. The radiation boundary needs to be placed at least $\lambda/4$ from radiating devices. In our simulation setup, A radiation box, whose height from the ground plane is more than $\lambda/4$ distance for all proposed RDRAs, is created with radiation boundary conditions [3].

A.2 Experimental Setup

Various parameters such as return loss, scattering parameters, standing wave ratio, reflection coefficient, impedance, radiation patterns, gain, directivity, radiation efficiency are measured for validation of fabricated RDRAs. Two-port vector network analyzer (VNA) shown in Figure A.1 is the most powerful kind of a measuring device and can measure frequencies from 5 Hz up to 110 GHz. It measures and display complete amplitude and phase characteristics of an electric network. These characteristics include scattering parameters, magnitude and phase, standing wave ratio, insertion loss, gain, attenuation, group delay, return loss and reflection coefficient. Dynamic range is generally defined as the maximum power the receiver can accurately measure minus the

Figure A.1: Agilent Technologies: N5230A (10 MHz to 50 GHz), PNA series vector network analyzer

receiver noise floor. There are many applications requiring large dynamic range. One of most common is measuring cross polarization performance of the antenna. At least 80 dB dynamic range is needed to properly characterize the antenna performances. Before measurement, calibration of the VNA is necessary, because accuracy of measurement is greatly influenced by sources of errors such as systematic, random, and drift. Systematic errors are due to imperfections in the analyzer and test setup. Random errors, instrument noises, are unpredictable and vary with time in a random process. They cannot be removed by calibration. Drift errors are primarily caused by temperature variation. For antenna measurements, one-port calibration is required. The calibration is carried out with standard load, open and short circuit load at desired frequency range [4]. Reflection coefficient , Γ is defined as ratio of reflected voltage divided by incident voltage. Return loss is defined as - $20\log(\Gamma)$ in dB [5]. Return loss measurement of the fabricated antenna can be obtained by the VNA after proper calibration. [4]

Practical antenna do not radiate uniformly in all directions. Radiation pattern is a graphical representation of the distribution of radiation energy as a function of angle about the antenna in the 3-D space and is generally measured in far field region. Strength

of radiation is usually measured in terms of field strength, power density or decibels (dB). Thus a complete radiation pattern gives relative field strength (or power radiated) at all angles elevation (ϕ) and azimuthal (θ) in spherical coordinate system and requires a 3-D presentation. However, in practice, it is common to present cross sections of the radiation patterns in two principal planes of interest. For linearly polarized antennas, these planes are E- and H-planes. E-plane is the plane passing through the antenna in the direction of beam maximum and parallel to the far-field E vector. H-plane is the plane passing through the antenna in the direction of beam maximum and parallel to the far-field H vector. The far field region is defined as that region of space where angular field distribution of the antenna is essentially independent of the distance from the antenna. If maximum dimension of the antenna is D, then the far field region is commonly taken to exist at distance greater than $2D^2/\lambda$ from the antenna where, λ is the wavelength [6]. As mentioned in Chapter 4, the proposed stacked RDRA is resonated at 5.23 GHz. Wavelength (λ) is 0.057361 m. The largest dimension of the stacked RDRA (D) is 80 mm. For the stacked RDRA, the far-field region is 0.223 m. During measurement of radiation patterns of the stacked RDRA, the separation between the horn antenna and the stack RDRA is 3.48 m. This ensures that the radiation patterns are measured in far-field region.

Radiation patterns are measured in an in-house anechoic chamber (shown in Figure A.2.) by a swept frequency measurement using the vector network analyzer. Setup of radiation patterns measurements is shown in Figure A.3. Where, an antenna under test (receiving antenna) will be placed in front of a standard wideband horn antenna (transmitting antenna). The transmitting antenna is fixed for each polarization (E- and H- planes) and the receiving antenna is rotated from -180° to 180° in azimuth direction with the help of stepper position controller. The horn antenna is connected to one port of the VNA and the testing antenna is connected to second port of the VNA. The VNA acquires data for each degree step of rotation and store in the computer. Polar plot is obtained using a MATLAB program.

Most important figure of merit that describes performance of an antenna is the gain. Gain of the antenna is defined as "the ratio of the intensity, in a given direction, to

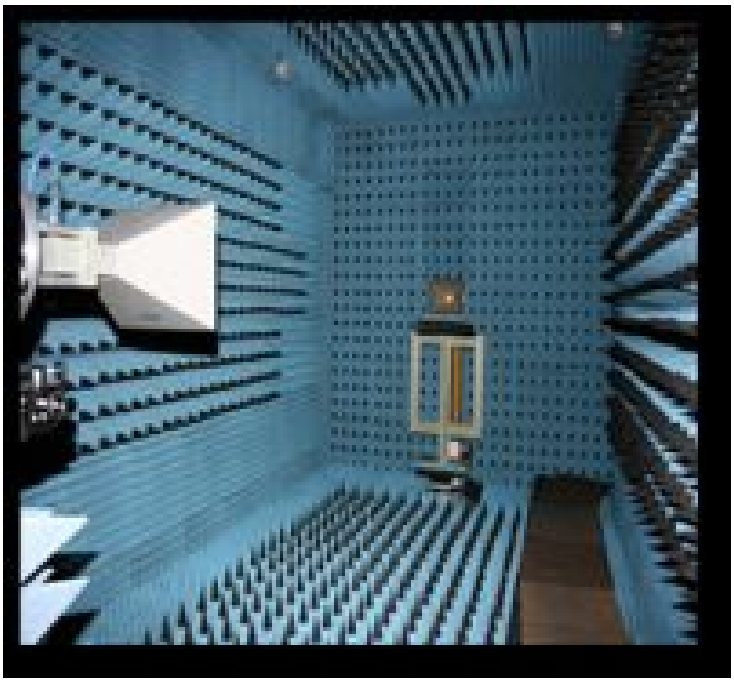

Figure A.2: A photograph of an anechoic chamber

the radiation intensity that would be obtained if the power accepted by the antenna were radiated isoropically". Usually, there are two basic methods that can be used to measured the gain of the antenna: absolute-gain and gain-transfer (or gain-comparison) measurements. The absolute-gain method is used to calibrate antennas that can then be used as standards for gain measurements, and it requires no a priori knowledge of the gains of the antennas. Gain-transfer methods must be used in conjuction with standard gain antennas to determine the absolute gain of the antenna under test. The two antennas which are most widely used and universally accepted as gain standard are a resonant $\lambda/2$ dipole and pyramidal horn antenna. All of these methods are based on Friss transmission formula as given below [6]:

$$\frac{P_r}{P_t} = (\frac{\lambda}{4\pi R})^2 G_t Gr \tag{A.2}$$

where, P_r and P_t are received power and transmitted power in watt, respectively. G_r and G_t are gains of the receiving antenna and transmitting antenna, respectively. R is separation between the two antennas in meter. λ is operating wavelength in meter. Equation (A.1) can be written in a logarithmic decibel form as

$$(G_t)_{dB} + (G_r)_{dB} = 20\log(\frac{4\pi R}{\lambda}) + 10\log(\frac{P_r}{P_t}) \tag{A.3}$$

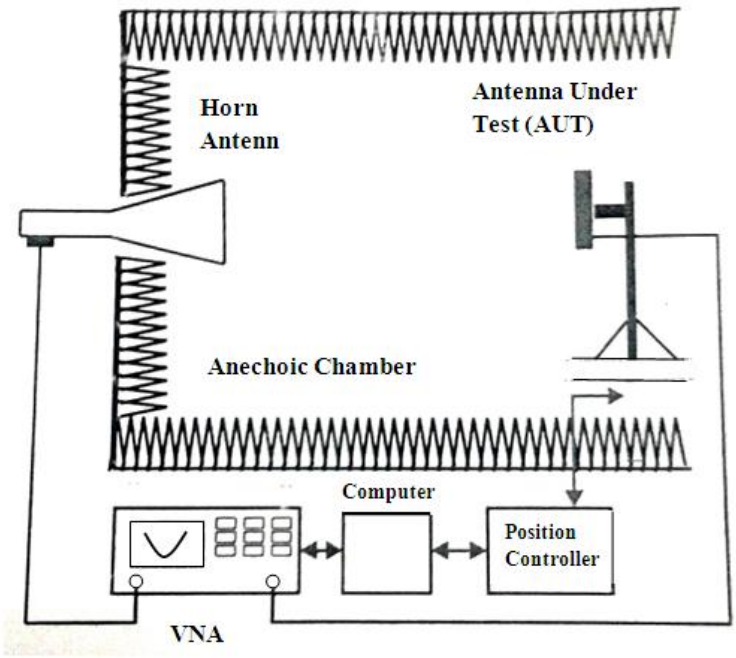

Figure A.3: Setup of radiation patterns measurement

Following care must be utilized to avoid error in gain measurement. 1) The system is frequency stable. 2) The antennas meet the far field criteria. 3) The antennas are aligned for boresight radiation. 4) All the components are impedance and polarization matched. 5) There is a minimum of proximity effects and multipath interference [6]. Gain transfer method is used for gain measurement of the RDRAs. Two identical horn antennas and the test antenna are used to measure gain of the test antenna. Two almost identical horn antennas are placed in anechoic chamber and separated by a distance of 3.48 m. One horn antenna works as a transmitting antenna, whereas, the other one works as a receiving antenna. The VNA is used to measured S_{21}, ratio of received power (P_r) and transmitted power (P_t). For identical two horn antennas, equation (A.2) reduces to

$$(G_t)_{dB} = (G_r)_{dB} = \frac{1}{2}[20\log(\frac{4\pi R}{\lambda}) + 10\log(\frac{P_r}{P_t})] = (G_{Horn})_{dB} \tag{A.4}$$

After obtaining gain of the horn antenna, $(G_{Horn})_{dB}$, at given frequency, the receiving horn antenna is replaced with the antenna under test. Then, equation (A.2) becomes

$$(G_{UT})_{dB} = [20\log(\frac{4\pi R}{\lambda}) + 10\log(\frac{P_r}{P_t})] - (G_{Horn})_{dB} \tag{A.5}$$

where, $(G_{UT})_{dB}$ is gain of the antenna under test. $(G_{Horn})_{dB}$ is gain of horn antenna which

is obtained from equation (A.3). Again, S_{21} is measured and gain of the antenna under test is obtained using equation (A.4). As desribed in Chapter 4, gain measurement result at resonant frequency of 5.23 GHz for a stacked RDRA is mentioned below. Wavelength (λ) is 0.057361 m. Distance (R) between the transmiting antenna and receiving antenna in the anechoic chamber is 3.48 m. Path loss (PL) in dB is defined as below,

$$(PL)_{dB} = 20\log(\frac{4\pi R}{\lambda}) \tag{A.6}$$

Measured S_{21} is -39.42 dB at resonant frequency when two identical horn antennas are connected to the VNA. From (A.3), gain of the horn antenna is 9.11 dB. When the receiving antenna is replaced with the stacked RDRA, measured S_{21} is -43.91 dB. From (A.4), gain of the stacked RDRA is 4.61 dB.

Beamwidth is a parameter associated with the radiation pattern of the antenna. The beamwidth of the pattern is defined as the angular separation between two identical points on opposite side of the pattern maximum. In the antenna, there are a number of beamwidth such as half-power beamwidth (HPBW) and first-null beamwidth (FNBW). One of the most widely used beamwidth is the HPBW, which is defined by IEEE as: "In a plane containing the direction of the maximum of a beam, the angle between the two directions in which the radiation intensity is one-half value of the beam". The beamwidth of the antenna is a very important figure of merit. Beamwidth is used a tradeoff between it and side lobe level; that is, as the beamwidth decreases, the side lobe increases and vice versa. It is also used to describe resolution capabilities of the antenna to distinguish between two adjacent radiating sources or radar targets. From Figure 4.7, HPBW is 90° and 70° for E-plane and H-plane, respectively [6].

Another important parameter of the antenna is directivity. The directivity is defined as "the ratio of the radiation intensity in a given direction from the antenna to the radiation intensity averaged over all directions". Directivity of the antenna can be computed using measurements of its radiation patterns. Simplest, but least accurate, method requires the following steps : 1) Measure the two principal E- and H- plane patterns of the test antenna. 2) Determine the HPBW (in degrees) of the E- and H- plane patterns. 3)

Compute the directivity using following equation:

$$D_0 \cong \frac{4\pi(180/\pi)^2}{\Theta_1\Theta_2} = \frac{41253}{\Theta_1\Theta_2} \tag{A.7}$$

where, Θ_1 and Θ_2 are HPBW (degree) in E- and H- plane, respectively. The method is usually employed to obtain rough estimates of directivity [6]. It is more accurate when the pattern exhibits only one major lobee, and its minor lobes are negligible. From (A.6), directivity is 6.54 dB for the stacked RDRA.

Radiation efficiency (η) is defined as the ratio of the total power radiated by the antenna to the total power accepted by the antenna at its input terminals during radiation. System factor, such as impedance and/or polarization mismatches, do not contribute to the radiation efficiency because it has very small contribution [6]. One of popular technique to estimate radiation efficiency is the Wheeler Cap method [7]. This method is based on the Q-factor of the antenna. The total power lost (P) can be divided into two components: radiated power (P_{rad}) and power dissipated (P_{dis}):

$$P = P_{rad} + P_{dis} \tag{A.8}$$

The Q-factor (Q_0) can be decomposed into a radiation Q-factor (Q_{rad}) and a dissipation Q-factor (Q_{dis}):

$$\frac{1}{Q_0} = \frac{P_{rad} + P_{dis}}{\omega W} = \frac{1}{Q_{rad}} + \frac{1}{Q_{dis}} \tag{A.9}$$

where, ω and W are radian frequency and average energy stored. The radiation efficiency of the antenna is the ratio of the radiated power to the total power which can also be expressed in terms of Q-factors as

$$\eta = \frac{P_{rad}}{P_{rad} + P_{dis}} = 1 - \frac{Q_0}{Q_{dis}} \tag{A.10}$$

The values of Q_0 and Q_{dis} can be determined experimentally by measuring the return loss of the antenna with and without a metallic radiation shield also known as a Wheeler Cap. Without the shield, the measured bandwidth represents Q_0. When the shield is placed over the antenna, the radiation of the antenna is suppressed and the measured

bandwidth represents Q_{dis}.

The radiation efficiency is also given by following equation [6],

$$\eta = \frac{G}{D_0} \tag{A.11}$$

where, gain and directivity are measured in the direction of maximum radiation. In our study, radiation efficiency is calculated by using (A.10). The radiation efficiency of the stacked RDRA is 71 %.

References

[1] HP85180A High-Frequency Structure Simulator (HFSS): User's Reference, *Hawlett-Packard Company*, 1994.

[2] High-Frequency Structure Simulator (HFSS), *Ansoft Corporation*, Pittsburgh, PA

[3] An Introduction to HFSS: Fundamental Principles, Concept and Use,*ANSYS Inc*, Canonsburg, PA, USA.

[4] Agilent 10 hints for making better network analyzer measurements - Application note 1291-B, *Agilent Technologies Inc.*, USA, Oct. 2001.

[5] D.M. Pozar, "Microwave Engineering", *Addison-Sesley Publishing Co, New York*, 1990.

[6] C.A. Balanis, "Antenna Theory: Analysis and Design", Second edition, *John Wiley and Son, Inc., New York*, 1982.

[7] H. A. Wheeler, "The radian sphere around a small antenna", *Proceeding of IRE*, Vol. 47, pp. 1325-1311, Aug. 1959.

List of Publications

International Journals

- G.D. Makwana, Deepak Ghodgaonkar, Sanjeev Gupta, "Dual mode and miniaturized rectangular dielectric resonator antenna with a simple feeding scheme", *International Journal of RF and Microwave Computer-Aided Engineering*,(Impact Factor:0.845), published by John Wiley and Sons Inc. (Wiley Blackwell), Vol. 25, No. 3, pp. 229-235, March, 2014.

- G.D. Makwana, Deepak Ghodgaonkar, Sanjeev Gupta, "Investigation of a New Radiating Mode in Rectangular Dielectric Resonator Antenna: Experimental Validation", *International Journal of Microwave and Optical Technology*, Vol. 9, No. 4, pp. 309-316, July, 2014 (Impact factor: 0.229) indexed by SCOPUS, Google, EI-Compendex, EBSCO, ISI and Media Finder.

- 3. G.D.Makwana, Deepak Ghodgaonkar," Dielectric Resonator Antenna as a RFID Tag for Human Identification System in Wrist Watch" *International Journal on Smart Sensing and Intelligent Systems*, Vol.6, No.3,1153-1166, June 2013.

- 4. G.D. Makwana, Deepak Ghodgaonkar, "Wideband Stacked Dielectric Resonator Antenna at 5.2 GHz", *International Journal of Electromagnetics and Application*, published by Scientific and Academic Publishing, USA, Vol.2, No. 3, pp. 41-45, May 2012. http://article.sapub.org/10.5923.j.ijea.20120203.04.html

International Conference

- 1. G. D. Makwana, Deepak Ghodgaonkar. "Dielectric Resonator Antenna as a RFID Tag for Human Identification System in Wrist Watch" *Proceeding of 6th International Conference on Sensing Technology (ICST-2012)*, 18-21, December, 2012, pp. 238-242 organized by Massey University, New Zealand and C-DAC, Kolkatta, published in IEEE Explore with an IEEE catalog number (CFP1218E-CDR) and ISBN (978-1-4673-2254-4).